Fall 2018

Synthesis and comprehensive studies of nanogels for enhanced oil recovery

Jiaming Geng

Department: Geosciences and Geological and Petroleum Engineering

SYNTHESIS AND COMPREHENSIVE STUDIES OF NANOGELS FOR ENHANCED OIL RECOVERY

by

JIAMING GENG

A DISSERTATION

Presented to the Faculty of the Graduate School of the

MISSOURI UNIVERSITY OF SCIENCE AND TECHNOLOGY

In Partial Fulfillment of the Requirements for the Degree

DOCTOR OF PHILOSOPHY

in

PETROLEUM ENGINEERING

2018

Approved by:

Dr. Baojun Bai, Advisor
Dr. Thomas P. Schuman
Dr. Ralph E. Flori Jr
Dr. Shari Dunn-Norman
Dr. David J. Wronkiewicz

PUBLICATION DISSERTATION OPTION

This dissertation consists of the following four articles, formatted in the style used by the Missouri University of Science and Technology:

Paper I: Pages 28-53 was published in Fuel.

Paper II: Pages 54-79 was published in Energy & Fuels.

Paper III: Pages 80-103 was published in SPE Asia Pacific Oil and Gas Conference and Exhibition.

Paper IV: Page 104-127 is in preparation for Chemical Engineering Journal.

ABSTRACT

Nanomaterials have been developed and applied for enhanced oil recovery (EOR) in oil industry. Among the developed nanomaterials, nano-sized crosslinked polymeric gel particles (nanogels) have shown the potential in improving both the macro- and micro-displacing efficiency. This dissertation focuses on the synthesis and the potential EOR mechanisms of nanogels. Nanogels with positive, negative, and neutral charges were synthesized through suspension polymerization. The morphology, size distribution, and zeta potential of nanogels were elucidated by corresponding technologies, such as scanning electron microscopy and dynamic light scattering. The ability of nanogels in oil-water interfacial tension (IFT) reduction and oil-in-water (o/w) emulsion stabilization was studied at various nanogel concentrations, temperatures, and salinities. Moreover, nanogels showed an electro-interaction controlled adsorption on the rock surface, which could modify the wettability of rock surface and reduce the permeability of porous medium. The core flooding results demonstrate that nanogels with proper charges can easily transport through the porous medium and reduce the water permeability by forming multilayer adsorption on the rock surface. The residual oil was produced in o/w emulsion state during the nanogel flooding and in isolated oil drops during the post water flooding, which indicated the abilities of nanogels in increase the displacing efficiency and sweeping efficiency, respectively.

ACKNOWLEDGEMENTS

Completion of this Ph.D. dissertation was possible with the support of my advisor, my committees, my family, and my friends.

Firstly, I would like to express my sincere gratitude to my advisor, Dr. Baojun Bai, for his continuous support throughout the course of my doctoral research. I would also like to thank my committee members, Dr. Thomas Schuman, Dr. Ralph Flori, Dr. Shari Dunn-Norman, and Dr. David Wronkiewicz, for their insightful comments and help throughout the research.

The work was supported by Dr. Baojun Bai's fund from Department of Energy (DOE). I am thankful for their financial support.

I would like to express my thanks and respect to Dr. Jianmin Wang and Dr. Lizhu Wang for their help and guidance.

At last, I am deeply and sincerely grateful to my family and my friends, especially my wife, Sisi Chen. Without their support, help, and encouragement, I would have never been successful in pursuing a Ph.D. degree.

TABLE OF CONTENTS

LIST OF ILLUSTRATIONS

PAPER II

PAPER III

LIST OF TABLES

1. INTRODUCTION

1.1. STATEMENT AND SIGNIFICANCE OF THE PROBLEM

The global demand of energy is expected to increase as much as 53% over the next 20 years[1]. Fossil fuels, such as crude oil and natural gas, are expected to supply much of the energy consumption worldwide continually. To meet the future energy demand, the oil industry need either find new fields or increase the oil recovery from the existing fields, including enhance the production of unconventional resources like shale oil and tight oil. Currently, the low effective circulations of injecting fluid through high permeable area have become one of the most important problems in mature reservoirs because they lead to excessive water production and a rapid decline in the productivity[2]. The tiny oil droplets trapped in pores and the thin oil film adhered on the rock surface in swept zones results in a low displacement efficiency (Figure 1.1). The distribution of residual oil is depended on the wettability of rock surface.

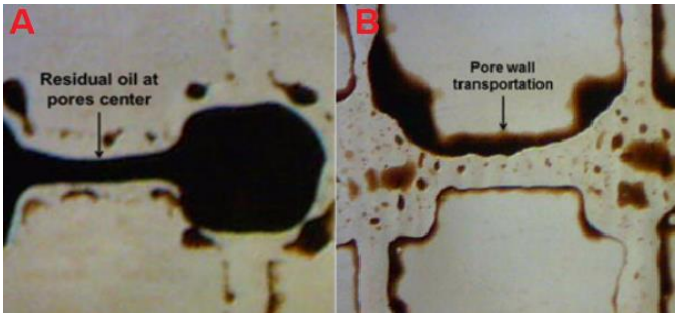

Figure 1.1. Residual oil at the pore center of water-wet transparent model and spread along the surface of oil-wet transparent model[3].

Water would like to flow along the rock surface and leave the residual oil as oil droplets in the pore center in water-wet formations while residual oil tends to form oil film and spread along the rock surface in oil-wet formations. Either the bypassing of unswept oil or the insufficient displacement of residual oil lead to a low oil recovery. Nanofluids are expected to bring an effective, economic, and environmental-friendly method to the oil industry for enhanced oil recovery. The resistivity to salt, temperature, and shear promises the ultilization of nanomaterials in harsh reservoir conditions. In addition, the small size endows nanomaterials with the ability to inject into and transport through the porous medium. Many researchers have dedicated to the studies of nanoparticles for enhanced oil recovery. The inorganic nanoparticles, including but not limit to nanosilica, nano-metallic oxide, and nano-clay, preder to adsorb at the oil-water interface and reduce the surface energy irreversibly. In addition, the nanosilica could form wedge-like aggregations between oil and rock surface, which helps to displace the residual oil adhered to rock surface. Nano-sized polymeric hydrogel is one kind of nanoparticles that has not only the properties of nanoparticles, but also the properties of hydrogels like stimuli-reponsive behavior, visco-elastic 3D network. However, no publications have been reported on the enhanced oil recovery mechanisms of nano-sized polymeric hydrogels and the charge effect of nano-sized polymeric hydrogels on their corresponding behaviors. The main objective of this dessertation is to investigate the charge effect of nano-sized polymeric hydrogels on their interactions with the rock, and oil-water interface and the potential EOR mechanisms of nano-sized polymeric hydrogels. The obtained knowledge will help to understand the EOR mechanisms of

nano-sized polymeric hydrogels and optimizing their physicochemical properties for better performances in a certain reservoir.

1.2. RESEARCH OBJECTIVES AND SCOPE

This research work systematically investigated the charge effect of nano-sized polymeric hydrogels on the interactions with the oil-water interfaces and the rock surfaces. Five specific tasks are:

a. Synthesize nano-sized polymeric hydrogels with positive, negative, and neutral charge through suspension polymerization;
b. Study the adsorption processes of nano-sized polymeric hydrogels at the oil-water interfaces and the charge effect on the stability of corresponding oil-in-water (o/w) emulsions;
c. Study the dynamic and static adsorption processes of nano-sized polymeric hydrogels at the sandstone surface and discuss the potential EOR mechanisms of nano-sized polymeric hydrogels;
d. Investigate the effect of salinity on the physicochemical properties of nano-sized polymeric hydrogels, the oil-water interfacial tension, and the stability of corresponding emulsions;
e. Evaluate the effect of physical factors on the stability of produced nano-sized polymeric hydrogel-stabilized emulsions.

Various technologies were applied to elucidate and characterize the morphology, rheology, size distribution, and zeta potential of synthesized nano-sized polymeric hydrogels. Nano-sized polymeric hydrogel samples with various monomer to crosslinker

ratios, sodium acrylate to acrylamide ratios were prepared to study the dependence of emulsion stability on the strength and charge density of nano-sized polymeric hydrogels.

Four journal/conference articles in the following section were written to address the specific tasks:

a. In the first paper, nano-sized polymeric hydrogels with positive, negative, and neutral charge were synthesized through suspension polymerization. The dynamic interfacial tension between decane and nanogel dispersions was calculated based on the shape of oil droplets using goniometer. The o/w emulsions stabilized by nano-sized polymeric hydrogels were prepared using ultrasonic homogenizer. The average diameter of oil droplets and the equilibrium emulsion volume were used to characterize the stability of the o/w emulsions. Concentration and charge of nano-sized polymeric hydrogels that influence the oil-water interfacial tension and the stability of o/w emulsions were investigated. The emulsion stabilization ability of nano-sized polymeric hydrogels was compared with commercial nanosilica at the end of this task.

b. In the second paper, Berea sandstone that has negative surface charge was used to understand the importance of electro-interactions in the adsorption kinetics of nano-sized polymeric hydrogels on sandstone surface and investigated the potential EOR mechanisms of nano-sized polymeric hydrogels. The wettability modification ability of nano-sized polymeric hydrogels was characterized by the contact angle before and after adsorbing nano-sized polymeric hydrogels. In addition, the thickness of adsorption layer inside the pores and throats was calculated based on the assumption of parallel capillary tube model. The potential

EOR mechanisms of nano-sized polymeric hydrogels was analyzed based on the improvement of both the displacing and sweeping efficiency.

c. In the third paper, the influence of salinity on the size and zeta potential of nano-sized polymeric hydrogels was investigated. The decane-water and crude oil-water interface behavior were characterized at various salinities. The oil-water interfacial tension in the presence of nano-sized polymeric hydrogels and stability of corresponding emulsions were studied at various salinities and the interfacial tension behavior was analyzed based on the stimuli-responses of nano-sized polymeric hydrogels.

d. In the fourth paper, several physical factors, such as crosslinking density and charge density of prepared nano-sized polymeric hydrogels, the salinity and pH of surrounding solutions, the ultrasound time, the oil type, and the oil to water ratio, were controlled during the preparation of o/w emulsions. The influences of the physical factors on the properties of produced emulsions were illustrated by the appearance, the size distribution from optical microscopy, and the structure from scanning electron microscopy. After understanding the influence of the physical factors on the emulsion stability, the destabilization of stimuli-responsive emulsions was investigated.

In this dissertation, “nanogel” refers to the crosslinked polymeric gel particle with an original diameter less than 100 nm that is able swell in water.

2. LITERATURE REVIEW

Microgels/nanogels are crosslinked polymeric particles that considered as hydrogels when they are composed of water soluble/swellable polymer chains. The size of microgels and nanogels is given as 0.1-100 μm and 1-100 nm under dried condition, respectively. The classification of microgels/nanogels based on the homogeneity/heterogeneity of the composed monomers/polymers and the architecture of particles are taking into account in this review. Microgels/nanogels are mainly synthesized through the polymerization of monomers and the crosslinking of polymers. Generally, the structures and functional groups of microgels/nanogels determined the environmental responsive behavior of gel particles like thermal, pH, and salt responsive behavior. Furthermore, the properties of microgels/nanogels, such as size distribution, swelling, rheology, mechanical strength, and thermal stability, markedly affect their applications in oil industry. Microgels/nanogels are able to transport in the porous media and form strategic plugging to divert flooding fluid to the relatively unswept zones for enhanced oil recovery. In addition, the microgels/nanogels reduce oil-water interfacial tension and modified rock wettability to improve the recovery of residual oil. The applications of stimuli-responsive microgels/nanogels in conformance treatment and acid stimulation are also discussed in this review.

2.1. CURRENT STATUS

Microgels/nanogels are crosslinked polymeric particles that considered as hydrogels when they are composed of water soluble/swellable polymer chains. Microgels/nanogels have high water content, deformability, stimuli-responsive

properties, and adjustable chemical and mechanical properties. Moreover, the tunable size from tens of nanometers to hundreds and the large surface area for the functional groups of macrons of microgels/nanogels offer great potential for the utilization of microgels/nanogels in petroleum engineering.

Generally, the microgels, which have been of intense research interest for many decades, comprise covalent and/or coordinate bonds to maintain their polymeric networks at the reservoir condition. Such microgels are wide variedly used in the oil industry, including near wellbore and in depth conformance control; temporary plugging during the acidizing; and water shutoff and sand control. Until recently, the nanogels have been studied for the wettability modification of rock surface and oil-water interfacial tension reduction. Additionally, the stimuli-responsive microgels/nanogels, such as poly(N-isopropylacrylamide) (PNIPAM) and polyacrylic acid-based gel particles, are able to swell/shrink with the environmental stimulation and consequently change the rheology of their dispersion and/or the rock surface/oil-water interface behavior.

With regard to the preparation of microgels/nanogels in recent decades, particular attention has been devoted to the synthesis of microgels/nanogels with robust mechanical strength, specific response to the environmental stimuli, unique interfacial properties, as well as to the synthetic methods[4-9]. Although many review papers have given an excellent overview of the synthetic methods and the basic understanding of the properties of the microgels/nanogels, the focus of these publications are mostly on the utilization in the moderate environment, like drug delivery and controllable release in human body.

This review is attempt to compile the comprehensive microgels/nanogels researches published in the last decade for enhanced oil recovery (EOR), including but

not limited to conformance control and acid stimulation. This review will describe the classification of microgels/nanogels based on their architectures and functionalities. The synthetic strategies based on chemical crosslinking will be introduced in this review, including micromolding and microfluidic method, membrane method, spray drying method, emulsion polymerization, mini-emulsion and microemulsion polymerization, suspension polymerization, and dispersion/precipitation polymerization. In addition, this review will describe the various methods to characterize and evaluate the physicochemical properties and the applications of microgels/nanogels for conformance correction and acid stimulation.

2.2. CLASSIFICATION OF MICROGELS/NANOGELS

Microgels/nanogels can be classified into homopolymeric microgels/nanogels and copolymeric microgels/nanogels based on the number of monomer contained in the polymeric network. In addition, the copolymeric microgels/nanogels can be further classified based on their structures: the interpenetrating network (IPN) microgels/nanogels, the core-shell microgels/nanogels, and the Janus microgels/nanogels.

For the applications in oil industry, various functional microgels/nanogels have been developed, such as the thermal-responsive, pH-responsive, self-healing, and fluorescent microgels/nanogels. In this section, the basic properties of microgels/nanogels classified by structures and functionalities will be introduced.

Homopolymeric microgels/nanogels are referred to polymeric network derived from a single species of monomer[10]. The polymer chains in homopolymeric microgels/nanogels would be crosslinked through physical and/or chemical crosslinking

to form the three dimension networks. Copolymeric microgels/nanogels are comprised two or more different monomers, arranged in a random, block, or alternating configuration along the chains consisting in the polymeric network[11]. To obtained specific physicochemical properties, copolymeric microgels/nanogels are prepared in some unique structures, like interpenetrating network, core-shell, and anisotropic structures. For example, the agar/polyacrylamide (PAM) IPN gel was prepared in a heating-cooling-photopolymerization process to eliminate the uncontrollable swelling and unnecessary diffusion process in the two-step synthesis of IPN gel. The agar/PAM IPN gel exhibits excellent mechanical and recoverable properties ascribe to the interpenetrated agar and PAM networks[12]. Another method to prepare IPN microgels/nanogels is using the seed polymerization: the precursor of the second network is absorbed into the microgels/nanogels containing the first network and polymerized to give the IPN microgels/nanogels[13]. The IPN microgels/nanogels commonly have better the swelling and mechanical properties than the neat microgels with one network. In addition, the stimuli-response behavior might be largely different ascribe to the interactions between two networks[14, 15].

Core-shell microgels/nanogels have a well-defined solid core made from a polymer or rigid colloid, which the stimuli-responsive shell is affixed to. The functional colloids such as superparamagnetic iron oxide particles may be included in the core resulting in the magnetic responsive of core-shell microgels/nanogels[16]. Core-shell microgels/nanogels can be prepared in a two-step synthesis. The core gel particles was dispersed into the monomer solution and polymerized to obtain the core-shell microgels/nanogels[17]. In addition, the core-shell microgels/nanogels can be prepared

through the association of block polymers. Generally, the block polymers with both hydrophilic and hydrophobic segments turn to form micelles in a proper solvent. By crosslinking the functional groups in the block polymers leads to the formation of core-shell microgels/nanogels[18]. The stimuli-responsive behaviors of core-shell microgels/nanogels are more complex than the homopolymeric ones. For example, a core-shell microgel composed of two temperature-sensitive polymers with different low critical solution temperatures (LCSTs) showed a doubly temperature-sensitive behavior[19]. The core and shell in the core-shell microgel were shrinking based on their LCSTs, respectively. Moreover, the hematite-PNIPAM core-shell microgels have both the thermal responsive behavior of the PNIPAM shell and the magnetic responsive behavior of hematite core[20].

Janus microgels/nanogels are the gel particles have two or more distinct physical properties on the surface. The simplest case of a Janus microgel is achieved by dividing the microgel into two distinct parts, each of them either made of a different materials or bearing different functional groups[21]. There are many methods to generate Janus microgels/nanogels: self-assembly using two kinds of block polymers; masking by functionalizing partial surface of the microgels/nanogels; and phase separation by combining two or more different phases in a microgel/nanogel. Janus microgels/nanogels are able to form self-assembles by controlling their asymmetric functionalities. The poly(acrylic acid) (PAA) and PNIPAM Janus nanogels formed self-assembled cluster at the temperature above 31 °C and dispersed when cooled down[22]. The stimuli-responsive aggregating and dispersing behavior of Janus nanogels can also be triggered

by pH[23]. Recently, it was found that amphiphilic Janus microgels/nanogels can adsorb at the oil-water interface to achieve an ultra-low interfacial tension[24].

Generally, most of the microgels/nanogels used in oil industry are polyacrylamide-based gel particles. Although the hydrophilic property of acrylamide groups promise the swelling ratio of corresponding microgels/nanogels, the sensitivity of polyacrylamide-based microgels/nanogels to salinity, pH, and temperature limited their applications under the harsh reservoir conditions. In addition, it is essential to develop some "smart" microgels/nanogels that can responsive to the surrounding environments to deal with the complex situations in oil reservoirs.

Poly(N-isopropylacrylamide) (PNIPAM) microgels/nanogels are sensitive to the surrounding temperatures that their polymeric network shrinks at temperature above the LCST. The PNIPAM microgels shrink and form agglomeration at temperature above their LCST, which may be promising for enhanced oil recovery[25]. Although the large size of microgels agglomeration could plugging the throats, the uncertainty brings by the complex reservoir condition limits the applications of PNIPAM microgels. To apply microgels/nanogels in complex reservoirs, the microgels/nanogels that can further swell stimulated by the reservoir temperature were developed[26]. These microgels/nanogels are able to transport through the porous medium and second swell at reservoir temperature to form plugging in depth. A stable crosslinker and a labile crosslinker are subjected into the polymeric network to ensure the thermal responsive property to the microgels/nanogels. After the labile crosslinker, such as polyethylene glycol dimethyl acrylate (PEGDMA), degrade at reservoir temperature, the microgels/nanogels will further swell. At such cases, the stable crosslinker should not degraded at reservoir

temperature. N,N'-methylene bisacrylamide (MBAA) is widely used as the stable crosslinker for the applications at reservoir temperature less than 100 °C. To further improve the resistance ability of the stable crosslinkers with higher temperatue, tetraallylammonium chloride (TAAC) was subjected to the microgels/nanogels. Zhang et al. have demonstrated the TAAC crosslinked gel can stand as high as 250 °C without any degradation[27].

The pH responsive microgels/nanogels are the gel particles that use the pH change as their activation trigger. The microgels/nanogels prepared with certain polyelectrolytes, such as PAA, and PDMAEMA, are sensitive to the pH of surrounding environments, capable of swelling by several orders of magnitude due to pH change. For example, the carboxylic groups (COOH) in the PAA networks are ionized and repelled each other in alkaline environments. The electrostatic repulsion leads to the swelling and diameter increment of PAA microgels/nanogels, which results in the effective viscosity increasing of the corresponding dispersions. In order to utilize the PAA microgels/nanogels, an acid pre-flush is required to tune the reservoir pH below the pKa of the carboxylic groups. Since the microgels/nanogels exhibit low viscosities at shrinking state, the microgels/nanogels dispersions are fairly easy to propagate through the porous medium. As a result of geochemical reaction between the pre-flushed acid and mineral components in the rock, the pH increases and triggers the swelling of PAA microgels[28]. Besides triggered by alkaline, the microgels/nanogels are able to be stimulated by CO_2 and swell under acidic conditions. For instance, the tertiary amine in the PDMAEMA microgels/nanogels is protonated in acidic solution so as to induce the increment of microgel/nanogel diameter. The PDMAEMA microgels/nanogels can be applied in CO_2

flooding reservoirs and control their conformance. The PDMAEMA microgels/nanogels are brought by injection water to the target zone without any pre-flush slugs. The interaction between chasing CO_2 and tertiary amine induced the swelling of PDMAEMA and plugging in the high permeable zone.

In comparison with traditional microgels/nanogels, self-healing microgels/nanogels display the extraordinary ability to self-healing/self-associating. So far, the self-healing microgels/nanogels are cauterized into two classes on the basis of chemistry of the activate composites: autonomic and nonautomonic self-healing materials[29]. The development of self-healing in microgels/nanogels is based on the concept of constitutional dynamic chemistry that comprises of non-covalent chemistry as well as dynamic covalent chemistry. For instance, the nanocomposite gel particles consisted of a unique poly(N,N-dimethylacrylamide) (PDMAA) and PNIPAM/clay network structure[30]. These gels exhibited comprehensive self-healing together with extraordinary mechanical properties. The self-healing in these gels was attributed to the autonomic reconstruction of crosslinks across the damaged interface in the nanocomposites gels. The in situ polymerization of polydopaamine was used to coat the clay under basic condition to prepare clay gels. The self-assembled three dimensional networks was attribute to the reformation of damaged catechol-ferric ions complexes[31]. Carbon nanotubes and graphene oxide were also used in the preparation of self-healing nanocomposited hydrogels in addition to clay nanoparticles[32, 33]. Besides using the nanocomposition method, molecular interdifusion, recombination of chain ends, living polymerization have been utilized in the preparation of self-healing

microgels/nanogels[34]. The self-healing microgels/nanogels could be used to efficiently control the conformance for the abnormal features[35].

The fluorescent microgels/nanogels are mainly prepared by subjected the fluorescent monomers in the polymeric network of gel particles. Allyl rhodamine B (RhB)[36, 37], nitrobenzofurazan (NBD-NHMe)[38, 39], and fluorescein o-acrylate[40] fluorescent monomer have been used to elucidate the distribution of microgels/nanogels in the porous medium and/or at the oil-water interfaces.

2.3. SYNTHETIC METHODS

A variety of approaches for the synthesis of microgels/nanogels have been investigated in the past several decades. We categorized these synthetic methods into four major themes: micro-molding and microfluidic-based synthesis, emulsion and suspension polymerization, dispersion polymerization, and atomization route. The formation of the microgels/nanogels is based on either the polymerization and crosslinking of monomer or the crosslinking/association of preformed polymers using small molecules and/or metallic ions. The synthesis routes will be introduced and discussed in the literature.

Micro-molding and microfluidic devices are very small scale systems for producing monodispersed microgels. The microgels with defined shape, structure, and morphology can be precisely produced using micro-molding and microfluidic-based synthesis.

In microfluidic synthesis, two or more streams of immiscible fluid containing various reagents are injected and the precursor droplets are formed at the intersection of the immiscible fluids. Commonly, photopolymerization or polycondensation are utilized

to prepare microgels in the continuous microfluidic synthesis. The most frequently applied microfluidic droplet generates with various geometric configurations, including “T-junction”, “Flow Focusing”, and “Co-flow”[41]. Confinement of droplets, flow rate of liquids, reaction rate are key factors affecting the dispersity, shape, and morphology of resulting microgels[42]. Recently, the microgels with complicated microstructures like Janus and core-shell microgels have been successfully synthesized using microfluidic devices[43-45]. As an example of microfluidic synthesis, monodisperse polyacrylamide microgels are prepared from a water-in-oil emulsion made in a polydimethylsiloxane (PDMS)-based microfluidic device with rectangular 25*25 μm channels. The aqueous solution of acrylamide (AM), N,N’-methylenebisacrylamide (MBAA), and ammonium persulfate (APS) was co-injected at 700 μL/h with the oil phase at 1200 μL/h. Thermal gelation of the droplets was achieved at 65°C for 1 h[46]. Although it is unlikely that microfluidics can be up scaled appropriately and economically for industrial production, the microfluidics can obtain valuable insights into controlling parameters necessary for the design of large scale processing equipment[42].

Membrane emulsification involves the use of a membrane through which an aqueous solution permeates under adequate pressure into oil phase. The resulting monodispersed droplets are stabilized by the surfactants in the oil phase and polymerized by physical or chemical crosslinking. Membrane techniques offer same advantages to the microfluidic techniques with additional benefits of energy efficiency[47].

Micro-molding of microgels has been examined as a potential method to fabricate submicron-sized microgels. By controlling the features on the mold stamp, the size and shape of microgels can be precisely designed. To produce microgels through micro-

molding method, a precursor solution is placed into a mold, which is fabricated by hydrophilic chemicals such as PDMS. The gelation is then induced by UV-light or changing temperature. The formed microgels are then taken out from the mold after gelation[48].

A top-down method called “Particle Replication In Nonwetting Templates (PRINT)” was developed to fabricate submicron-sized microgels[49]. A photocurable perfluoropolyether (PFPE) replica was used as the molding material. The nonwetting nature of fluorinated materials confines the liquid precursor inside the features of the mold, which allowing the generation of isolated microgels. Using PRINT, monodispersed microgels of poly(ethylene glycol diacrylate) (PEGDA), polylactic acid (PLA), and polypyrrole were prepared with sizes ranging from 200 nm to micron-scale[5].

The emulsion and suspension polymerizations are commonly two-phase systems that starting monomer(s) and/or the resulting gel particles are in the form of a fine dispersion in an immiscible liquid. The polymerization initiator is soluble in the monomer phase for suspension polymerizations whereas soluble in the immiscible phase for emulsion polymerizations. Emulsifier(s) or stabilizer(s) are used in addition to monomer and immiscible phase during the polymerization process to stabilize the monomer droplets and resulting particles. Microgels/nanogels with average size from 50 nm to 2 mm can be made from emulsion and suspension polymerizations.

According to the diameter of dispersed monomer droplet in a continuous phase, the emulsion polymerization with stable and pseudo-stable dispersed droplets is named as microemulsion polymerization and miniemulsion polymerization, respectively. Generally, the emulsion polymerization using a w/o emulsion is called inverse emulsion

polymerization. For a typical emulsion polymerization, 10 g of heptane, 1.12 g of laureth-3, and 0.4 g of monomer stock solution were added to the glass vial and vigorously shook until a one-phase optical transparent solution was obtained. Then 100 μL of initiator stock solution was added to the 4.61 g microemulsion and kept at ambient temperature for 12 h. The average diameter of produced nanogels is 55 nm[50]. Another example of emulsion polymerization is 2 g of N-vinylcaprolactam (VCL), 0.08 g of chain transfer agent, 0.06 g of tris(hydroxymethyl)aminomethane hydrochloride, 0.13 g of 1,3,5-trioxane, and 0.08 g of ethylene glycol dimethacrylate (EGDMA) were dissolved in 190 g of water. The cationic initiator was added under nitrogen purging at 70 °C and subsequently cooled to 25 °C. The diameter of resulting microgels is from 154 to 769 nm[51]. The emulsion polymerization is one of the most common but promising processes for the microgels in industrial scale but require a very high level of control of all the operating variables[52].

In suspension polymerization, the volume ratio of the monomer phase to the polymerization medium is usually kept within 10`50%, but in principle, the volume ratio can be as high as unity or even higher. The monomer phase is suspended in the polymerization medium in the form of small droplets by means of a stirrer and a suitable stabilizer. Under a certain temperature condition, the “monomer capsules” are converted directly to the corresponding microgels/nanogels of approximately the same size. The average size of the monomer droplets can be readily controlled by varying the stirring speed, volume ratio of monomer to polymerization medium, concentration of stabilizer, and the viscosities of monomer phase and polymerization medium[53].

In dispersion polymerization, the monomer, crosslinker, and initiator are all soluble in the polymerization medium, which is a poor solvent for the resulting microgels. Accordingly, the dispersion polymerization system is homogeneous at the starting point. Depending on the solvency of the medium for the resulting macromolecules, phase separation occurs at an early stage that leads to nucleation and the formation of primary gel particles. The polymerization proceeds largely within the individual particle and consequently, leads to the formation of spherical microgels. A typical example of dispersion polymerization is 1-vinyl-2-pyrrolidone (VP) and 4,4'-azobis(4-cyanopentanoic acid) were added to the cyclohexane containing polystyrene-hydrogenated polybutadiene-polystyrene block polymers and reacted at 70 °C for 2 h. Ethylene dimethacryalte (EDMA) was added to the mixture and continued the reaction for an additional 6 h[54]. The polymerization medium need to be precisely designed to obtain microgels/nanogels with narrow size distribution. Moreover, supercritical carbon dioxide ($scCO_2$) has been utilized as the polymerization medium to prepare microgels/nanogels whose monomer is soluble in $scCO_2$[55]. The diameter of resulting microgels through dispersion polymerization is in the range of 100 nm to 10 μm.

The production of microgels/nanogels through atomization involves forming small precursor droplets in air/liquid. The gelation of microgels/nanogels can be initiated by the temperature of surrounding environment. Breaking up of the liquid streams in laminar flow occurs through a Rayleigh instability that the small waves formed along the interface of the liquid stream propagate along the stream and eventually break the stream into small drops[56]. These droplets turn to spherical configuration to minimizing the surface energy.

Spinning disk atomization utilizes precursor fluid flowing across the spinning disk and breaking into small isolated droplets through Rayleigh instabilities at the edge of the disk. The gel particles with defined size distribution can be obtained by controlling the disk wettability, spinning rate, and flow rate. The diameter of the droplet exiting from the edge of spinning disk decreased with the rotational speed whereas increased with the liquid flow rate[57]. The teeth of the spinning disk are regarded as the forming site of drops that the tooth width should be adjusted to the intended drop size to produce gel particles with desired size[58]. An active ingredient can be encapsulated into the microgels by concurrent flow of the active ingredient and the encapsulating materials across the disk[59]. The Janus microgels can be synthesized by spinning disk atomization wherein a bi-layered jet of two precursors are ejected off the edge of a spinning disk and broken down into Janus droplets at the edge of disk[60]. This method has the advantage that it has very high productivity[61]. However, the gel particles synthesized via spinning disk method generally have high polydispersity and large particle size. To get the monodisperse microgels, the standard spinning disk is modified by adding a slope surface, and teeth at the edge of spinning disk; controlling the wettability of the spinning disk; and the collection method based on the flight distance of different sized particles[59, 62]. The liquid properties, including fluid density, viscosity, and surface tension, are found to determine the size distribution of produced microgels as well as the liquid flow rate, spinning speed, and disk diameter[63]. Spinning disk atomization is a simple, efficient, and cost effective method commonly used in industrial scale for producing spherical microgels with an average diameter in the range of 40 μm to several mm[64].

Spray drying method produces microgels by pass a flow of precursor and air concurrently through a nozzle at a relatively high flow rate and atomized into a stream of hot air to remove the solvent[65]. The breaking of droplets is caused by the fluid jet instabilization and can be controlled through adjusting air and precursor flow rates, nozzle size, viscosity and surface tension of precursor fluid[66]. Generally, the spray drying method is used to made microgels in industrial scale, the monodispersed microgels with diameter as low as ~350 nm were prepared for small sample amount (50-500 mg) using well designed spray dryer[67]. To process multiple separate solvent streams, a microfluidic spray dryer with an array of two-focusing cross junctions was developed[68]. In comparison with other atomization methods, the size distribution of produced microgels through the spray drying method is much narrower with an average diameter from 20 nm to 15 μm.

2.4. EVALUATION METHODS

The physicochemical properties of microgels/nanogels, such as size, mechanical strength, surface charge, etc., markedly influence their applications for enhanced oil recovery. A variety of evaluation methods and screening criteria have been developed to select the candidates for a specific reservoir condition. In this section, a brief introduction to the basics of evaluation methods that is related to the applications for enhanced oil recovery will be provided.

The diameter and size distribution of microgels/nanogels is an important parameter that determined their transport behavior in porous medium. Size matching between the pore size of formation rocks and the diameter of microgels/nanogels

dominates the plugging performance. By simulating the plugging performance of microgels in the nuclear-pore membrane, only the microgels with a diameter 1/3-1/2 times of the pore size can plug the membrane effectively[69]. The steric hindrance of pore access by neighboring microgels prevents the occlusion of pore[70]. However, such size matching behavior of microgels was only observed in the pore occlusion experiments using a nuclear-pore membrane[2]. In the pore-throat simulate model, microgels with an average diameter of 55 μm are able to plug the 200 μm throat[71].

Currently, static and dynamic light scattering, optical microscopy, scanning electron microscopy (SEM), and transmission electron microscopy (TEM) are applied to measure the size of microgels/nanogels. Among these size measuring methods, static and dynamic light scattering are used to measure the size distribution of microgels/nanogels in good solvent. Ultrasound is commonly applied to re-disperse agglomerated microgels/nanogels before size measurements. SEM is commonly used to elucidate the morphology and microsctructures of microgels/nanogels. However, the diameter of microgels/nanogels in dehydrated state can be obtained by SEM.

The surface charge of microgels/nanogels generally dominates the stability of corresponding gel particle dispersions. The high absolute value of surface charge renders microgels/nanogels with electrostatic hindrance, which helps to prevent the gel particles from agglomerating. Salt ions are able to shield surface charge of microgels/nanogels by screening effect. Zeta potential, which reflected the stability of gel particle dispersion, is the electric potential in the interfacial double layer at the location of the slipping plane.

The microgels/nanogels are able to swell several to hundreds times in water due to the hydrophilic moieties consisting in the polymeric network. Swelling ratio plays an

important role on the size and mechanical strength of microgels/nanogels, which influence the transport behavior of microgels/nanogels in porous medium. In general, the swelling ratio of microgels/nanogels is significantly influenced by the salt ions dissolved in the formation water. However, the swelling response was modified by embedded chromium (Cr3+) ions in the polymeric network of microgels[72].

The flow properties of microgel dispersions were strongly dependent on the salt concentration due to decreased particle size and the formation of microgel aggregation[73]. The storage and loss modulus of microgels/nanogels latex (solid content~5%) reflect the interactions among the swollen microgels/nanogels. For example, for the PNIPAM latex, the storage modulus continuously increased with the frequency whereas the loss modulus almost independent to the frequency, which demonstrate the strong interactions among the swollen microgels[74]. For the microgels/nanogels dispersions transport in a restricted environment, the slip phenomena cannot be neglected. The microgels displayed a generic unusual slip behavior: the slip of microgel dispersion is suppressed in a parallel-plate geometry with rough surface and start to slop at the wall in a geometry with smooth surface. In addition, the shear stress-dependent slip phenomenon is due to a lubricating layer formed by deformed microgels[75, 76].

Atomic force microscopy (AFM) is a powerful technique that can be used to obtain both the vertical force and the lateral force between a sharp tip and the surface. The deformation behaviors of polystyrene microspheres was firstly investigated using AFM in 1998[77]. The quantitative computation of the elastic modulus of microgels/nanogels requires the measurement of indentation by converting AFM force-displacement curves into force-indentation curves. The external load applied through the

cantilever to the tip can be calculated using Hooke law, which helps to obtain the elastic modulus of single particle[78]. For typical applications of AFM in the measurement of elastic modulus of microgels/nanogels, the individual microgel/nanogel was placed on a silica/mica plate in the air/water environment. The elastic modulus of microgels/nanogels was calculated from the force-indentation curves using the Hertzian model[79-81]. In the case of microgels/nanogels, there are no uniform size-dependent behaviors of the mechanical properties. The ionic functional groups consisted in microgels/nanogels and/or the crystalline domains formed between polymer chains are affect the deformation of microgels/nanogels and thereby result in the change of corresponding elastic modulus[82].

To apply microgels/nanogels technologies subterranean, the thermal stability of microgels/nanogels should be investigated under reservoir conditions. Although thermogravimetric analysis (TGA) has been used to analyze the changes in physical and chemical properties of material as a function of temperature, the water-free testing environment cannot simulate the reservoir conditions. Microgels/nanogels dispersions are commonly aged in sealed glass ampoules and stand at reservoir temperature for a long period to simulate the influence of reservoir environment on the properties of microgels/nanogels. After a certain intervals of time, the ampoules are broken and the viscosity of aged microgel/nanogel dispersion was measured and compared with their original apparent viscosity[83]. The degradation of polymer chains consisted in microgels/nanogels and their polymeric structures can be illustrated using corresponding technologies, including TGA, FTIR, and SEM.

2.5. EOR APPLICATIONS

Numerous oil service companies and oil companies devoted their efforts to the development of microgels/nanogels applications. The mechanical and thermal stability of microgels/nanogels promise them can be applied in the harsh reservoir conditions (high temperature and high salinity)[84]. To displace crude oil in the unswept area during conventional water flooding, microgels are utilized to block the pore-throat in the high permeable zone and divert injected fluid. Chauveteau et al. found that the partially attractive microgels adsorbed at the rock surface in a multilayer state and induce drastic permeability barriers whereas fully repulsive microgels adsorbed as a monolayer and can propagate in porous medium[85]. The microgel is able to form a quasi-irreversibly adsorbing layer with a thickness equals to two times of the viscometric radius of gyration[86]. In addition, the thickness of adsorbing layer was not affected by salinity and shear rate while the adsorption tends to increase with salinity[87, 88]. The microgel is an ideal disproportionate permeability modifier that the relative permeability to oil was not affect by adsorbed microgel layer whereas the relative permeability to water decreased to 1/7[89]. Microgel maintains several plugging mechanisms than adsorbing at the rock surface. The microgels are able to plug the throats, which size is smaller than themselves, and accumulate to form effective plugging at the pore-throats[90]. The microgels with a matching factor from 0.21 to 0.29 showed a good plugging performance and in-depth migration while microgels with a matching factor less than 0.21 cannot form effective plugging and higher than 0.29 were hard to migrate[91]. Microgels/nanogels are generally regarding as in-depth permeability controlling agent because the small diameter and deforming ability render the microgels/nanogels to transport in porous medium in

directing and deformable passing states[92]. Compared with rigid gel particles, soft gel particles are more likely to transport into cores and form plugging[93]. Mixing microgels with different particle sizes resulted in a higher plugging efficiency than the microgels with a uniform size[94].

Nanogels can reduce the permeability of both high permeable and low permeable rock. However, the residual resistance factor in high permeable rock is much lower than that of low permeable rock[95]. Different with microgels, nanogels preferred to form multilayer adsorption at the rock surface. The thickness of adsorbing layer and the adsorbing rate were dominated by the electrostatic interactions between nanogels and rock surface[96]. Moreover, nanogels can reduce the interfacial tension and help to form o/w emulsions by adsorbing at the oil-water interfaces[97]. The crude oil-in-water emulsion stabilized by polyacrylamide (PAM) and poly((2-(acryloyloxy)ethyl)trimethylammonium chloride) (PAETAC) nanogels maintained a salt-independent stability[98]. Residual oil was found to be produced in o/w emulsion state during the nanogel flooding period in a sandstone core[96]. Although nanogels can improve the oil recovery from outcrop core, the salt-sensitivity of PAM-based nanogels turned to form aggregation at the inlet of core and plug the surface[99].

Microgels/nanogels have been applied to reduce the water cut and increase the oil/gas recovery in the gas storage well and oil producing well. Field application in Liuzan, China, 2008 showed that microgels with size from 10 to 30 μm of a concentration from 1500 to 2000 mg/L at an injection amount of 5-8 t/well can increase the injection pressure by 1-5 MPa and improve the water injection profile[100]. After the microgel treatment, the average oil producing increased from 0.5 to 3.7 t/d while water cut reduced

by 5.4 % for more than 6 months in a field application in JX oil field[90]. The microgels have also been placed in the high permeable streaks surrounding the wellbore to reduce the water and sand production[101]. However, the oil containing in the microgel emulsion induced the formation of a tight film on the rock surface and reduce the gas permeability. Although back flow could remove the tight film, using microgel dispersion rather than microgel emulsion during the treatment could eliminate the formation damage induced by multiphase.

The microgels can be successfully applied in the formations at temperature from 45 to 126 °C, salinity from 2,000 to 300,000 mg/L, permeability from 0.87 to 3000 mD with a permeability variation from 0.54 to 0.84 and a porosity from 9 to 35 % based on the data from 154 of microgel treatment from 2005 to 2016[102]. Generally, the microgels with large particle size are applied at a high concentration while the small microgels are applied with a large treat volume at a low concentration. The substantial water reduction mostly occurs at relatively early water cut stage (<80 %).

For the applications of microgels/nanogels for hydraulic fracturing, the microgels/nanogels dispersions have to support and carry the proppants to the opened fractures and flow back efficiently. A potential candidate for hydraulic fracturing is the stimuli sensitive microgels, which swell and shrink triggered by the surrounding environments. The dispersion of poly(N-isopropylacrylamide) (PNIPAM) and polyacrylamide (PAM)-based microgels showed a temperature/pH responsive rheology that the reservoir temperature and/or alkaline environment decrease the viscosity of the microgel dispersions and induce the dispersion to flow back[103]. In another concept, researchers think that the microgels could plug the surface of rock matrix and help the

pressure build up during the fracturing work. In such cases, the microgels have to stand a relatively high differential pressure that would deform microgels and force microgels transport in rock matrix.

PAPER

I. SURFACE CHARGE EFFECT OF NANOGEL ON EMULSIFICATION OF OIL IN WATER FOR FOSSIL ENERGY RECOVERY

Jiaming Geng, Jingyang Pu, Lizhu Wang*, and Baojun Bai*

Department of Geosciences and Geological and Petroleum Engineering, Missouri University of Science and Technology, Rolla, MO 65401, USA

* Corresponding Author:
Lizhu Wang and Baojun Bai
Department of Geosciences and Geological and Petroleum Engineering
Missouri University of Science and Technology
1400 N. Bishop
Rolla, MO 65409
E-mail: wangliz@mst.edu; baib@mst.edu

ABSTRACT

Crosslinked polymeric hydrogels in nano-size, termed as nanogels, have significant technological applications by stabilizing Pickering emulsion. Herein, we present our experimental observations and the results of the emulsion stability analysis on the effects of nanogel concentration, oil-to-water ratio, nanogel charge, and ambient temperature. The nanogel with neutral-charge showed extraordinarily high emulsifying ability, interfacial tension between decane and water was reduced from 51.98 $mN \cdot m^{-1}$ to less than 6.04 $mN \cdot m^{-1}$, compared to 47.5 $mN \cdot m^{-1}$ by nanosilica. When treated with neutral-charged nanogel, the oil-in-water emulsion exhibited long-term stabilization, 90 % emulsion remained after one month at room temperature, showing the highest stability among the reported literature of Pickering emulsions. However, inorganic silica

nanoparticles displayed emulsion stability in minutes. Of particular interest was that the emulsion volume remained 82 % after thermal treatment at 65 °C for 48 h. The resulting high emulsion stability was attributed to a combination of high hydrophilicity, sufficient steric repulsion, and high surface coverage of nanogel. These observations indicated that the resulting nanogel can be a promising candidate toward enhanced oil recovery.

Key words: Nanogel; Interfacial tension; Pickering emulsion; Enhanced oil recovery.

1. INTRODUCTION

In recent years, there have been increased research interests in using oil-in-water emulsion stabilized with inorganic nanoparticles, known as Pickering emulsion [1], for enhanced oil recovery (EOR), especially in harsh condition reservoirs. The reasons are that inorganic nanoparticles not only stabilize micron-sized oil drops by forming absorbed nanoparticle layers but also perform better resistance at harsh condition than surfactants do [2-4]. Nanosilica is the most used nano-material to form Pickering emulsions because it is commercially available and having hydrophilic property [5]. Pickering emulsion can be injected into high-permeability-zone for conformance control as it is much more viscous than displacing water and stable at high salt concentration condition [6, 7]. Nanosilica facilitates residual oil recovery by reducing interfacial tension between oil and water [8-10] and forming stable Pickering emulsion *in situ* [11-13]. Despite these advantages, nanosilica is not applied in petroleum industry [14, 15]. The main reason is that nanosilica cannot form stable Pickering emulsions in the absence of surface modification with grafted functional polymer chains. However, the modification is significantly time-consuming and dramatically increase production cost.

Therefore, more efforts have been devoted to improving the properties of inorganic nanomaterials.

Nanogel has been used for medical diagnostic test [16, 17], antibody purifications [18, 19], drug delivery systems [20, 21], etc. The application of crosslinked polymeric hydrogels to stabilize oil-in-water emulsion named Mickering emulsion was reported by Binks' and Ngai's group [22-24]. Binks et al. used poly(4-vinylpyridine)/silica nanocomposite microgel particles to stabilize methyl myristate in Milli-Q water and found that microgels were no longer absorbed at oil-water interfaces in their swollen form [24]. Emulsions stabilized by temperature and pH-responsive poly(N-isopropylacrylamide) microgels showed surprising robustness at high pH and phase separated at low pH or high temperature due to the low interface coverage of microgels [22]. The stabilization of emulsion was associated with physical properties of hydrogel particles, while surface charges are independent of emulsion stability. Recently, Pickering emulsions were reported, which stabilized solely by soft nanogels, like cyclodextrin [25], gelatin [26], chitosan [27] or ethyl cellulose [28]. However, to the best of our knowledge, there is no reported work regarding the effect of the surface charge of nanogel on the stability of Pickering emulsion in the application in EOR.

In this study, three nanogels with positive, neutral, and negative charge were synthesized using free-radical suspension polymerization as characterized by corresponding techniques. We demonstrated how the interfacial tensions between decane and nanogel water were reduced by absorbing nanogels at the interfaces. The presence of hydrophilic and pendant polymer chains enabled us to prepare stable oil-in-water emulsion at high temperatures. The emulsion stabilized by neutral-charged nanogels,

which had minimum electrostatic repulsion among nanogels at absorbed layer, was compared with emulsions stabilized by positive and negative charged nanogels. This demonstration showed the advantages of reducing interfacial tension and forming stable oil-in-water emulsions by adsorbing nanogels at the interfaces for enhanced oil recovery.

2. EXPERIMENTAL

2.1. MATERIALS

All chemicals and reagents were purchased from Sigma-Aldrich (St. Louis, MO) and used as received except further noted. Acryloyloxyethyltrimethyl ammonium chloride (AETAC) was purchased from Sigma-Aldrich and used as received. Acrylamide (AM) was purified by recrystallization from acetone and dried under vacuum at 25 °C for one day. To prepare Na-AMPS in the lab scale, solid NaOH was added to a stirring solution of 2-Acrylamido-2-methylpropane sulfonic acid (AMPS) in ethanol at room temperature. The reaction mixture was vigorously stirred for 1 h and the precipitate was filtered, washed with ethanol and dried under vacuum at 25 °C for one day [29]. Nanosilica (20-30 nm) was purchased from US Research Nanomaterials, Inc without further purification. 1 wt.% sodium chloride (NaCl) solution was used throughout experiments.

2.2. NANOGEL SYNTHESIS

All nanogels were prepared by suspension polymerization. A typical nanogel polymerization is as follows: a stirring solution of acryloyloxyethyltrimethyl ammonium chloride (AETAC) (9.684 g, 0.05 mol) and N,N’-methylene bis(acrylamide) (MBAA)

(0.077 g, 0.05 mmol) in water (10.24 mL) was added to n-decane (40 mL) containing Span® 80 (21 g) and Tween® 60 (9 g) in a 250 mL three-neck flask and bubbled with nitrogen while kept in a preheated water bath at 40 °C for 15 min. Then, ammonium persulfate (0.02 g, 0.088 mmol) in water (0.2 mL) was added to the flask under stirring. The emulsion mixture was stirred at 40 °C for 2 h, the resulted emulsion was precipitated into acetone and the precipitate was isolated by centrifugation. The precipitate was rinsed with acetone several times to remove surfactants and unreacted monomers. The final product was isolated as a white powder and dried under vacuum at 45 °C overnight for further characterization and evaluations.

2.3. MORPHOLOGY AND SIZE DISTRIBUTION STUDIES

Scanning electron microscopy (SEM) images were collected on a Hitachi S-4700 FESEM microscope (Tokyo, Japan) operated at 15.0 kV to elucidate the microstructures of the nanogels. All images were captured of nanogels coated with Au/Pd prior to imaging. The size distribution of nanogels was examined by Dynamic light scattering (DLS) (Malvern NanoSizer ZS90). The measurements were carried out at a scattering angle of 90° with the light source (He-Ne laser, 4.0 mW 633 nm) at 25 °C. Transmission electron microscopy (TEM) images were collected on Tecnai F20 by using holey carbon film copper grids.

2.4. INTERFACIAL TENSION MEASUREMENTS

The interfacial tension between n-decane and nanogel dispersion was determined by axisymmetric drop shape analysis using pendant drop method (Ramé-hart advanced

goniometer 500-F1). The interfacial tension values were obtained using Young-Laplace equation.

2.5. EMULSION PREPARATION AND CHARACTERIZATION

To make oil-in-water emulsions with nanogels, brine containing different nanogel concentrations (1000, 2000, 5000, and 10000 ppm) were prepared by dispersing nanogel powders in 1 wt.% NaCl. Certain volumes of n-decane and nanogel dispersion were placed in a glass vial. The mixture had a total volume of 10 mL and was emulsified using an ultrasonic homogenizer (VC-1500, Sonics&Materials Inc.) with a CV-294 probe under 640 W for 3 minutes. The emulsion stability was determined by monitoring the homogenized emulsion as a function of time. The average diameter and polydispersity index of emulsified oil droplets were observed and calculated using an Olympus optical microscope (CK X41).

3. RESULTS AND DISCUSSIONS

3.1. SYNTHESIS OF NANOGEL VIA SUSPENSION POLYMERIZATION

The suspension polymerization of nanogel with different charges based on AM, Na-AMPS, and AETAC was presented in Figure 1. Nonionic surfactants were used to stabilize suspended monomer phase to prevent bringing charges from surfactants to nanogels during polymerization. Nanogels were synthesized by a typical free radical polymerize of the monomer with different charges to evaluate charge effect on oil-in-water emulsions. AM, Na-AMPS, and AETAC were reacted with MBAA to produce crosslinked nanogel with neutral, negative, and positive charges respectively.

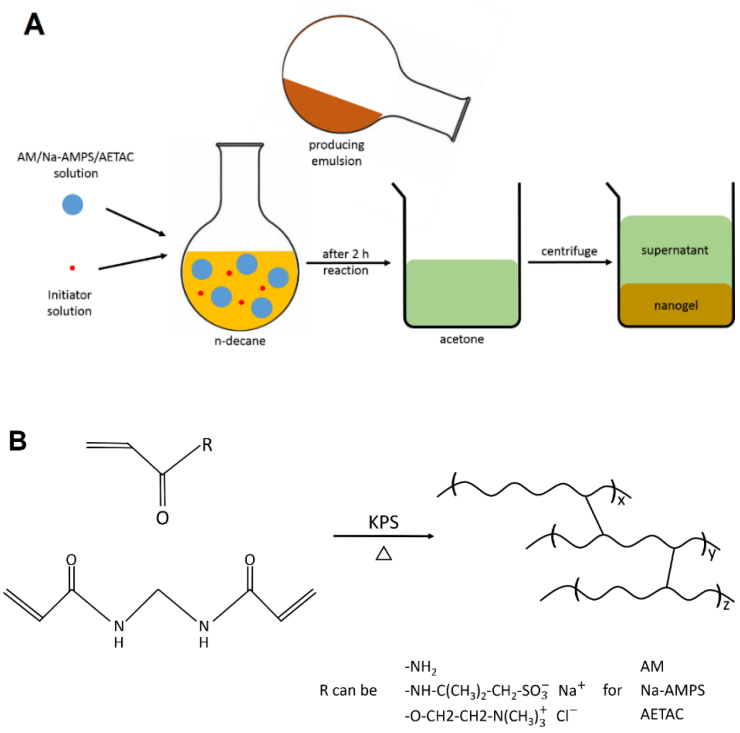

Figure 1. Schematic representation of (A) suspension polymerization and purification of nanogel and (B) the synthetic procedures for the preparation of crosslinked polymer nanogels, obtained via suspension polymerization.

The characterization of as-prepared nanogels, such as the surface zeta potentials, pH, and hydrodynamic diameters in 1 wt.% NaCl, are listed in Table 1. Neutral-charged nanogel had negative zeta potential presumably due to the hydrolysis of amide moieties to carboxylic groups.

The average diameter of the nanogels in SEM and TEM images is the diameter in the dry state (Figure 2). Compared with the hydrodynamic diameter in fully swelling form from DLS measurements, the diameter in the dry state is much smaller. The results from DLS, SEM and TEM demonstrated NN, AN, and CN were successfully synthesized by inverse suspension polymerization with narrow size distribution and spherical morphologies.

Table 1. Physical properties of synthesized nanogel and nanosilica.

Property	Neutral-charged nanogel (NN)	Anionic nanogel (AN)	Cationic nanogel (CN)	Nanosilica (SN)
Charge	Neutral	Negative	Positive	Negative
Charge density (mmol/g)	0	4.36	5.16	N/A
Zeta potential (mV)	-1.76	-35.90	34.75	-18.43
Diameter (nm)	220.14	241.62	151.14	1925.5
Polydispersity index (PDI)	0.236	0.268	0.482	0.197
Swelling ratio	51.92	20.61	12.10	N/A
pH (1000 ppm nanogel)	7.8	7.0	4.9	7.0

3.2. EMULSIFICATION PROPERTIES OF NANOGELS

Nanoparticles can markedly alter the interfacial properties of water-oil by adsorption, resulting from the huge surface due to the small size of nanoparticle [30, 31]. The interfacial tension between oil and water can be decreased by nano- and micro-sized particles through adsorption to stabilize oil-in-water or water-in-oil emulsion [5, 32].

Different from the small particles used in previous studies, nanogels in this work have the capacity to swelling several to hundreds of times as governed by crosslinker concentration upon contacting with external media. The kinetic interfacial tension between oil and nanogel dispersion measurements was performed to investigate the adsorption process in detail. N-decane, a pure substance, was used to study interfacial properties and emulsion behavior in our work to eliminate the influences of different compositions that crude oil consists.

Interfacial tension data were recorded (Figure 3) using three nanogel dispersions (NN, AN, and CN) at room temperature, at different concentrations ranging from1000 to 10000 ppm. All dynamic interfacial tension exhibited similar profile, at different nanogel

concentrations, suggesting nanogels functioned in a similar fashion of reducing interfacial tension.

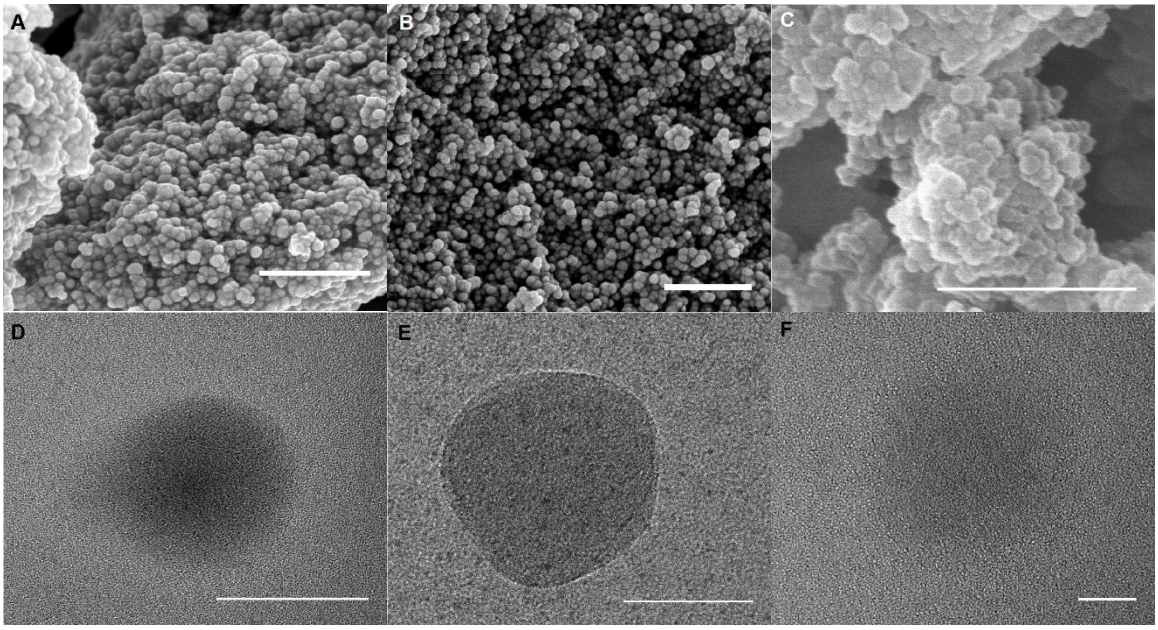

Figure 2. SEM images of NN (A), AN (B), and CN (C), scale bar is 500 nm; and TEM photos of NN (E), AN (F), and CN (G), scale bar is 50 nm.

The interfacial tension decreased rapidly at the early stage. Subsequently, the decrease in interfacial tension slowed, and finally, the change in interfacial tension decreased further and approached to an equilibrium value. The interfacial tension of 1000 ppm ANs decreased from 31.6 to 6.6 $mN \cdot m^{-1}$, while that of 10000 ppm ANs decreased to 6.33 $mN \cdot m^{-1}$, but at a much faster rate. The same trend was also observed in the measurements of NNs where the interfacial tension decreased from 41.16 to 8.83 $mN \cdot m^{-1}$for 1000 ppm and 6.04 $mN \cdot m^{-1}$ for 10000 ppm. However, the time to achieve the interfacial tension equilibrium of CNs was much longer than that of ANs and NNs. Furthermore, in the inserted Figure 3, these data are plotted on a logarithmic time scale

which points to the three stages of adsorption characterized by different slopes (only two stages were observed during CNs measurements).

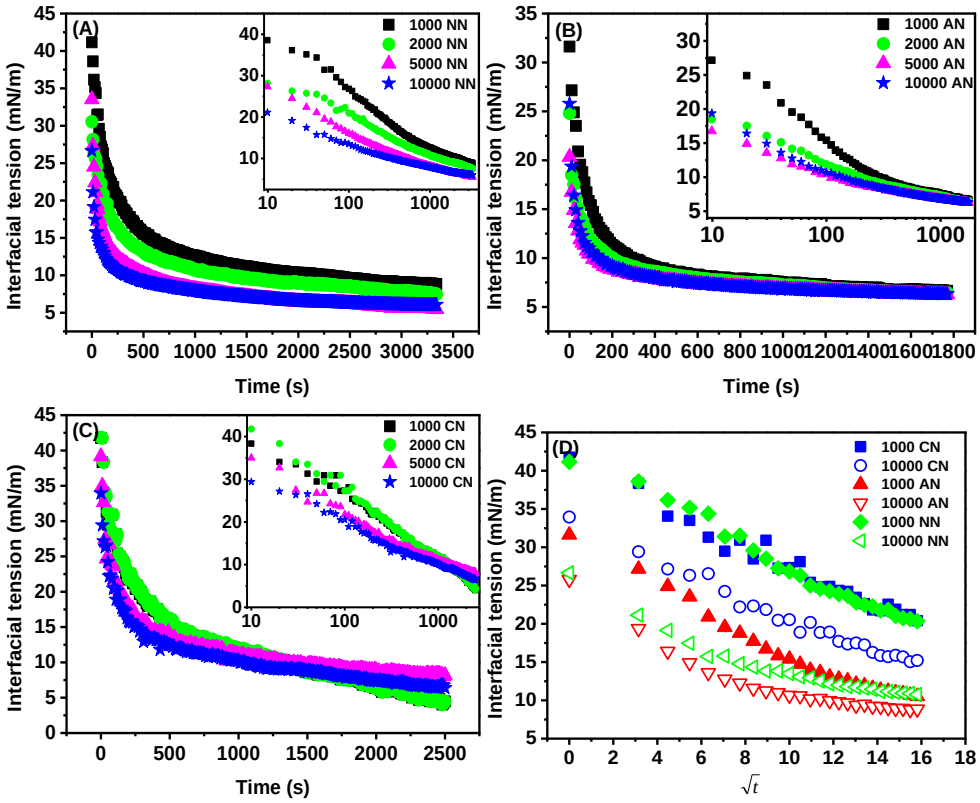

Figure 3. Dynamic interfacial tension between n-decane and (A) neutral; (B) anionic; and (C) cationic nanogel dispersion with 1000, 2000, 5000, and 10000 ppm concentrations. (D) Interfacial tension of nanogel samples at early stage as a function of $\sqrt{t}$.

The early stage of the adsorption was dominated by the diffusion of nanogels to the free oil-water interface. At this stage, the backward movement of nanogel from the sub-surface of the oil-water interface to the bulk may be neglectable so that the diffusion-controlled model derived by Ward and Tordai can be used to describe the early stage [33]. The dynamic interfacial tension of oil-water interface at the early stage can be written as:

$$\sigma_d = \sigma_0 - 2RTC_0\sqrt{\frac{Dt}{\pi}}$$

where σ_0 is the interfacial tension between oil and water, C_0 is the bulk concentration of nanogel, D is the diffusion coefficient, and T is the Kelvin temperature. The dynamic interfacial tension remained linear as a function of $\sqrt{t}$ until reaching the next stage, at which nanogels continued adsorbing, ordering and re-arrangement at the interface [34, 35].

As shown in Figure 3D, experimental data were well in agreement with the model function. However, even though the start point whose interfacial tension was equal to 51.98 $mN \cdot m^{-1}$ under 25 °C [36] was not recorded, from the rest data at the early stage, diffusion coefficient can be calculated. Linear fits were obtained for all nanogel samples at the early stage to analysis the diffusivity of three nanogels. The fitted parameters and calculated results are shown in Table 2.

Table 2. Measured, fitted and calculated adsorption parameters of nanogel samples.

Sample	Average diameter (nm)	Concentration (mol/L)	Temperature (K)	Slope	R^2	D (m^2/s)
NN 1000	59.01	$1.14*10^{-5}$	298	-1.110	0.971	122.12
NN 2000	59.01	$2.29*10^{-5}$	298	-0.839	0.970	17.44
NN 5000	59.01	$5.72*10^{-5}$	298	-1.994	0.999	15.76
NN 10000	59.01	$1.14*10^{-4}$	298	-1.704	0.999	2.88
AN 1000	88.13	$3.21*10^{-6}$	298	-1.697	0.979	3618.81
AN 2000	88.13	$6.42*10^{-6}$	298	-1.473	0.971	681.63
AN 5000	88.13	$1.61*10^{-5}$	298	-1.208	0.998	73.35
AN 10000	88.13	$3.21*10^{-5}$	298	-1.878	0.990	44.32
CN 1000	65.83	$9.84*10^{-6}$	298	-1.457	0.923	284.15
CN 2000	65.83	$1.97*10^{-5}$	298	-1.593	0.877	84.92
CN 5000	65.83	$4.92*10^{-5}$	298	-1.747	0.918	16.34
CN 10000	65.83	$9.84*10^{-5}$	298	-1.369	0.977	2.51

The diffusion coefficients D of three nanogels at different concentrations were calculated and the results were plotted in Figure 4. For each nanogels with the same charge, the diffusion coefficients decreased when the nanogel concentrations increased. These observations pointed to the fact that with increasing nanogel adsorption at the interface the adsorption switched from a diffusion-controlled to an interaction-controlled process [37]. Furthermore, the diffusion coefficient of AN was much larger than those of NN and CN, which might be due to nanogel affinity and charges. Introducing charges to nanogel made nanogel more hydrophilic and thus, dramatically increased the diffusion coefficient of nanogels in water. Although the crosslinking density of CN was equal to that of AN, the smaller hydrodynamic diameter made CN more rigid compared to AN. It has been reported that soft gel particles exhibited faster interfacial tension reduction than rigid gel particles did. As a consequence, the diffusion coefficient of CN calculated from kinetic interfacial tension was smaller than the diffusion coefficient of AN [38, 39].

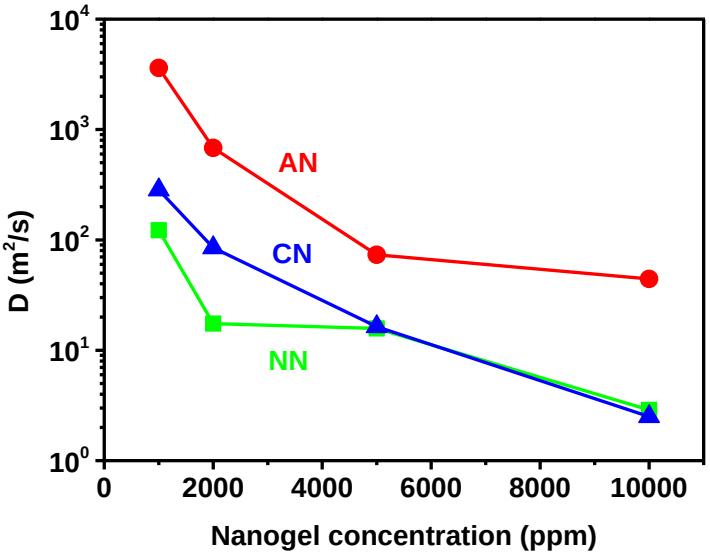

Figure 4. The calculated diffusion coefficient of nanogels of different concentrations.

For nanogel with 10000 ppm, the interfacial tension reached the equilibrium state, at which adsorption rate of nanogel onto oil/water interface was equal to desorption rate, in 200 s, while more than 400 s was needed to achieve equilibrium for a concentration of 1000 ppm (Figure 3). Since the interfacial tension was dominated by both diffusion and rearrangement of nanogels, the sample with charged nanogels could become stable because of the fast diffusion rate and the steric hindrance on nanogel rearrangement at oil/water interface.

Since the diffusion flux, which quantified the amount of nanogel that flowed through a unit area during a unit time interval, was proportional to nanogel concentration, the interfacial tension will be the positive correlation to nanogel concentration. When desorption and adsorption of nanogel reached equilibrium at the interface, the influence of concentration was neglectable. For instance, the influence of concentration can be neglected when nanogel concentration of NN was above 5000 ppm and CN was above 1000 ppm (Figure 3).

Nanogel decreased the interfacial tension by forming an irreversible adsorbing layer at the oil-water interface. The ability of nanogel dispersion for interfacial tension reduction was related to nanogel concentrations. Insufficient nanogels were adsorbed at the oil-water interface at equilibrium state in the dispersion at low nanogel concentration. The equilibrium interfacial tension was dominated by the coverage of nanogel at the oil-water interface. The equilibrium interfacial tension decreased rapidly from 36.22 to 2.70 mN/m due to the coverage of CN at the oil-water interface (Figure 5). As compared to emulsions stabilized by CN, AN, and NN stabilized emulsion showed more interfacial tension reduction when nanogel concentration was below 1000 ppm. The interfacial

tension turned to be constant when nanogel concentration was above 1000 ppm because of the steric hindrance prevent nanogel further adsorbing at the oil-water interface.

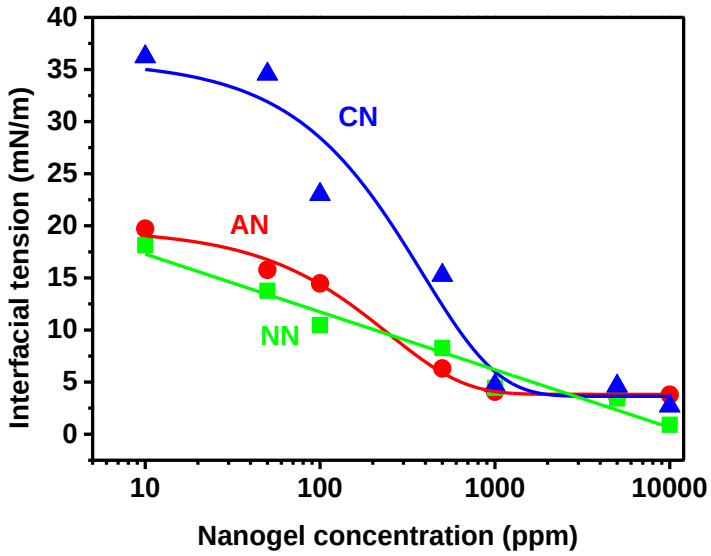

Figure 5. Equilibrium interfacial tension between decane and nanogel dispersion of different nanogel concentrations.

Emulsion stability is one of the key factors to evaluate the interfacial properties of oil-in-water emulsions. Figure 6A, B, and C displayed the emulsion volume as a function of time after ultrasonic homogenization of three nanogels at various water-to-oil ratios. The volume of the emulsion maintained long-term stability after approaching their corresponding steady states, where the emulsion volume was proportional to the friction volume of oil for all samples stabilized by nanogels. An obvious coalescence of emulsion droplets was found in emulsions stabilized by cationic nanogel after 7 days. This feature indicated that nanogels can stabilize emulsion within a short time (i.e. less than 2 days), and NN and AN were able to stabilize oil in water emulsion as long as 30 days at room

temperature. However, CN of 1000 ppm was unable to stabilize oil lower than 50% friction volume over 2 weeks.

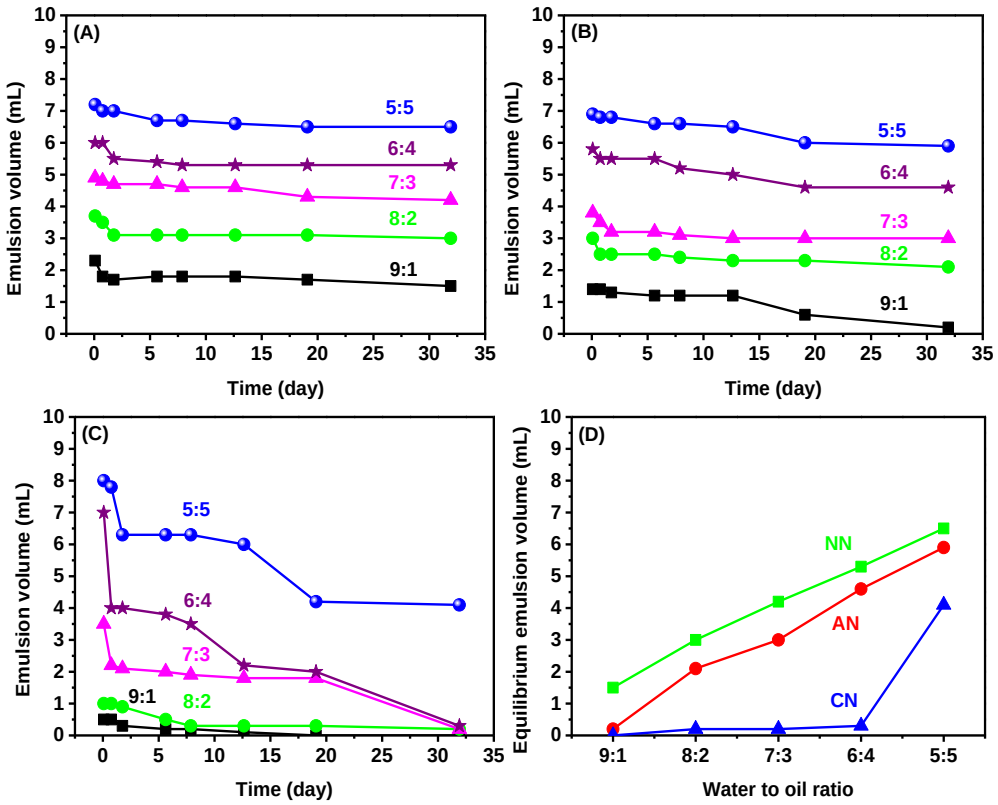

Figure 6. Emulsion volume of (A) neutral-charged nanogel, (B) anionic nanogel, (C) cationic nanogel samples with different water-to-oil ratios as a function of time; (D) equilibrium emulsion volume of NN, AN, and CN nanogel samples with 9:1, 8:2, 7:3, 6:4, and 5:5 water-to-oil ratios.

The equilibrium emulsion volume strongly depended on the surface charges of nanogels, particularly at the water-to-oil ratio of 9:1 to 6:4 (Figure 6D). The equilibrium emulsion volume of NN samples was larger than that of AN and CN.

Effect of charge of nanogel on the stability of nanogel stabilized o/w emulsion was investigated by measuring average diameter of emulsified oil droplets using an

optical microscope (Figure 7). It was observed that the emulsion stabilized by NN was stable with negligible change in average size in 48 hours. It was also observed that the average diameter of oil droplets increased dramatically after homogenization. The average diameter of oil droplets stabilized by neutral-charged nanogels was much smaller than that stabilized by cationic/ anionic nanogels.

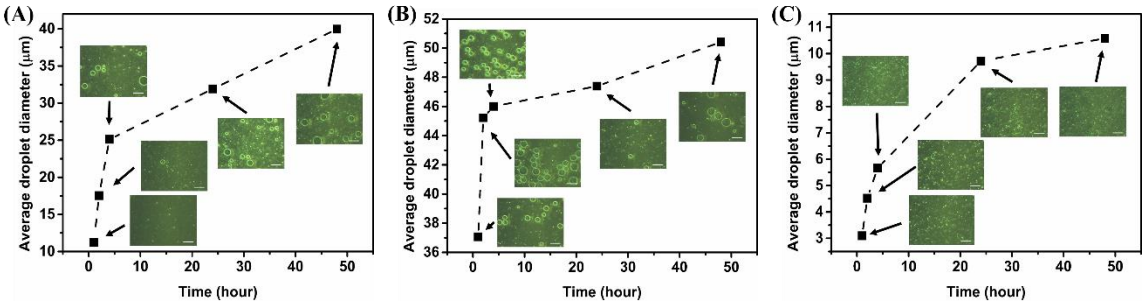

Figure 7. Effect of charge of nanogels on the stability of nanogel stabilized decane-in-water emulsion: average diameter of oil drops stabilized by (A) AN, (B) CN, and (C) NN.

This observation was in good agreement with the model in which the oil-in-water emulsion was stabilized with the nanogel by adsorbing at interfaces between oil and water. The desorption energy of nanogel was much greater compared with adsorption so that the nanogel forms a comparable stable layer at the interface and prevent droplets coalescing by steric hindering [32, 40]. When charges were introduced to the nanogels, the electrostatic repulsion makes nanogels repel each other (Figure 8). Accordingly, the emulsion stability was reduced due to the unstable adsorbing layer. The emulsion volumes of three nanogels at 1:9 oil-to-water ratio were shown in Figure 9A, B, and C as a function of time. Nanogels at concentrations ranging from 500 to10000 ppm were applied to stabilize oil-in-water emulsions and the emulsion volume kinetic was similar to all the samples. As for samples treated with nanogels, a fast decrease of emulsion volume

occurred in the first few hours to several days depending on the nanogel concentration. The fast decrease of emulsion volume was mostly due to the coalescence of the tiny oil droplets.

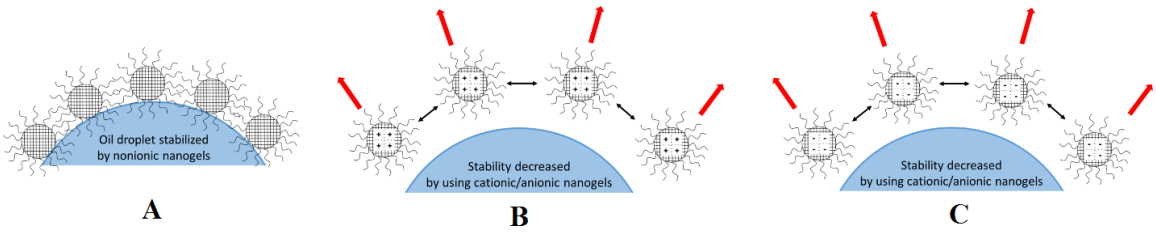

Figure 8. Schematic representation of emulsion stabilized by A) neutral-charged nanogels; B) cationic nanogels, and C) anionic nanogels.

This difference was related to the average sizes of emulsion droplets, which influenced directly by the nanogel concentration [41]. High nanogel concentration was essential to achieve high nanogel coverage of droplets and network of nanogels surrounding emulsion droplets, which increased the stability of the emulsion [42]. Different from the previous results, for emulsion stabilized by charged nanogels, the equilibrium emulsion volume was not proportional to the nanogel concentration (Figure 9D). When the concentration of charged nanogel was higher than 2000 ppm for AN, and 5000 ppm for CN, the increasing trend of equilibrium emulsion volume changed as a function of nanogel concentration. Compared to neutral-charged nanogel sample, the adsorbing layer of emulsion treated with charged nanogel was not stable. The inter droplets repulsion may be attributed to the stability of emulsions containing AN or CN. When nanogel adsorbed at the surface of emulsion droplets at a high water-to-oil ratio,

these droplets can be considered as microspheres with surface charges provided by the adsorbed nanogels.

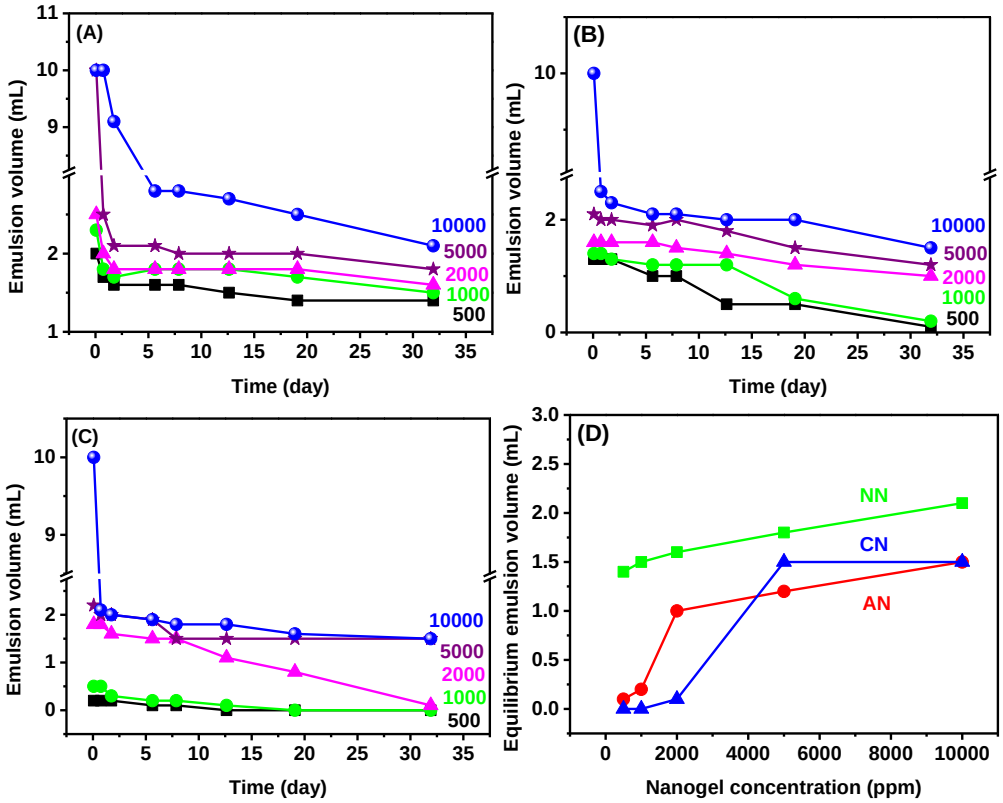

Figure 9. Emulsion volume of (A) neutral-charged nanogel, (B) anionic nanogel, (C) cationic nanogel samples with different concentrations as a function of time; (D) equilibrium emulsion volume of NN, AN, and CN nanogel samples with 500, 1000, 2000, 5000, and 10000 ppm.

Although charges containing in nanogels decreased the stability of the adsorbed layer, at the same time, they prevented the effective collision of emulsion droplets by electrostatic repulsion. At high nanogel ratio, electrostatic repulsion overwhelmed the decreased stability of absorbed layer. Thus, the emulsions of AN and CN samples were more stable at high nanogel concentrations. Nanogels can be used as emulsifier without

other stabilizers to produce stable o/w emulsions while nanosilica are mostly used as co-stabilizer together with surfactants and polymers [43, 44]. Compared to emulsions stabilized by microgels, the emulsions stabilized by nanogels has a less average diameter of emulsified oil droplets. Moreover, nanogel concentration (1000 ppm) is sufficient to produce stable o/w emulsion which is insufficient for microgels [45, 46].

3.3. TEMPERATURE EFFECT ON EMULSION STABILITY

To correlate the effect of temperature on the emulsion stability, the emulsion volume was determined at temperatures of 25, 40, and 65 °C. The mixture of oil (1 mL) and nanosilica or nanogel dispersion (9 mL) with concentration varies from 500 to 10000 ppm was homogenized for 2 minutes before aging at different temperatures. The results of emulsion volume were shown in Figure 10 as a function of nanoparticle/ nanogel concentration at different temperatures after 48 hours. Nanosilica showed less emulsion stability, which phase separated in 5 minutes, while the emulsions stabilized by nanogels were more stable at 25 than 65 °C. Although the increased kinetic energy of decane molecules at surface tend to overcome the net attractive force from bulk oil at a higher temperature, the adsorbed nanoparticle firm will separate from the emulsion. Oil droplets covered with fewer nanoparticles became unstable and turned to collision and coalescence, thus destabilizing oil-in-water emulsion. A phase separation occurred in emulsions treated with nanosilica within 5 minutes. For emulsions treated with nanogels, especially samples with high nanogel concentrations, emulsified oil droplets were suspended in water after homogenizing (Figure 11). At this time, the emulsion volume was equal to the total volume of the oil and nanogel dispersion. Afterwards, oil droplets

started to flow up and coalescent. For samples with 500 and 1000 ppm charged nanogels, the oil droplets were fully flowed up within 2 h at 40 °C and 65 °C. Though it took more than 5 days for all the oil droplets to flow up in emulsion treated with 10000 ppm charged nanogels, a distinguishable line can be observed in 6 hours.

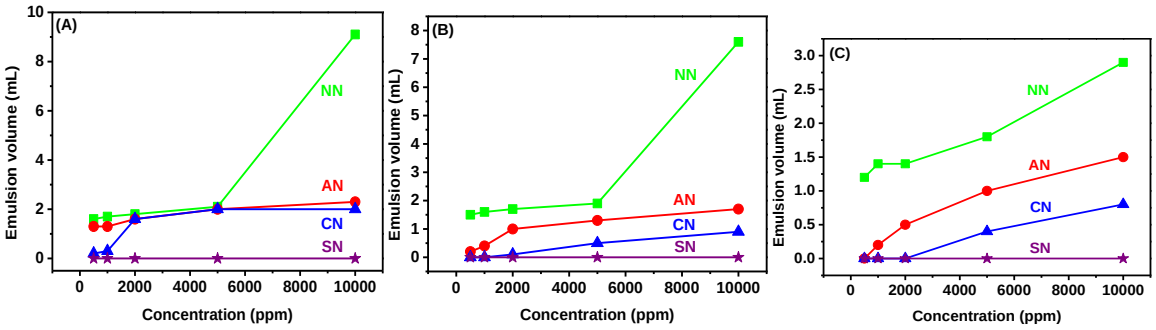

Figure 10. The volume of emulsion treated with nanosilica or nanogels at (A) 25, (B) 40, and (C) 65 °C after 48 h.

An increase in ambient temperature would increase both the flow-up rate and coalescence rate of emulsified oil droplets. The flow-up rate and coalescence rate of emulsified oil droplets were also decreased with increasing nanogel concentration. The change in emulsion stability with nanogel concentration showed to support steric stabilization mechanism. Similar with polymers, the crosslinked polymer chains on nanogel are solvated in 1 wt/% NaCl and turn to be collapsed in decane [47]. If the adsorbed nanogels fully covered the interface, there will be sufficient polymer chains to provide steric repulsion. Furthermore, nanogels in concentrated dispersion will prevent flowing up of emulsified oil droplets due to steric repulsion among adsorbed and dispersed nanogels.

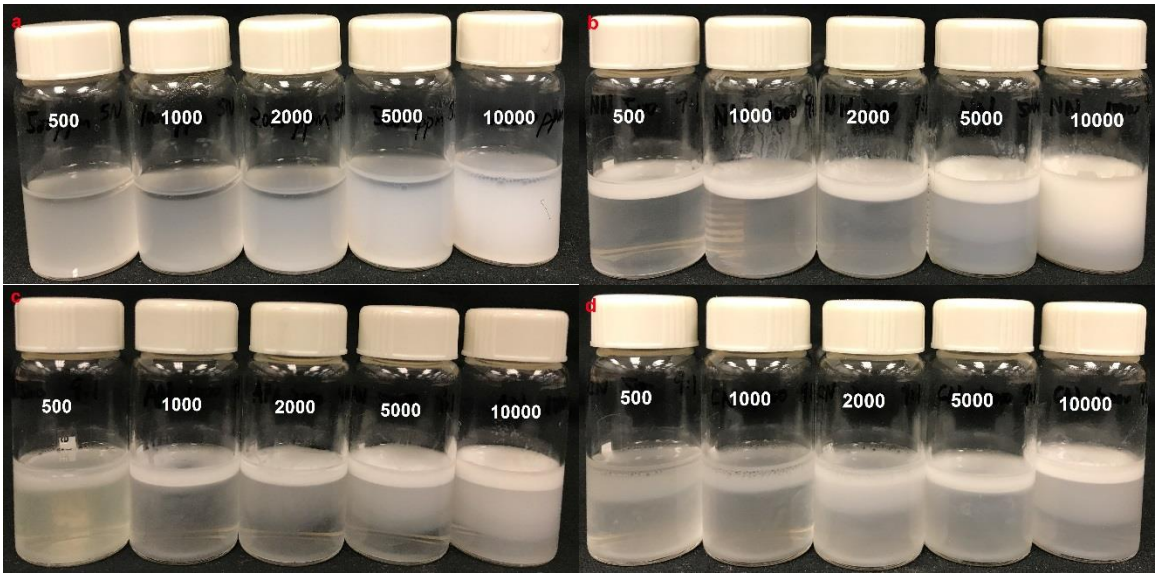

Figure 11. The mixture of decane (1 mL) and nanoparticle dispersion (9 mL) at 40 °C after 48 h.

4. CONCLUSIONS

In this study, three nanogels with positive, neutral, and negative charge via suspension polymerization were obtained. The charge of nanogels was elucidated with zeta-potential measurements, while DLS, SEM, and TEM were applied to characterize the morphology and the swelling ratio. When the nanosilica was dispersed in 1 wt.% NaCl, nanosilica was prone to be in the aggregation state in the presence of salt as evidenced by their apparent larger hydrodynamic diameter than the pristine sample. No participation occurred or polymeric nanogel dispersions for 6 months. Polymeric nanogels markedly decreased the interfacial tension between oil and water compared to nanosilica. Oil-in-water emulsion stabilized by neutral-charged nanogel remained more than 90 % of its original volume at 25 °C for 30 days while emulsion treated with nanosilica fully phase separated in 5 minutes after homogenization. Neutral-charged

nanogel was able to stabilize oil-in-water emulsion to remain 82 % of its original volume at 65 °C after 48 h.

ACKNOWLEDGEMENTS

The authors would like to express their grateful acknowledgement to the financial support from DOE under the contract of DE-FE0024558.

REFERENCES

[1] S.U. Pickering, Pickering: emulsions, J. Chem. Soc. Faraday Trans. 91(23) (1907) 2001-2021.

[2] T. Zhang, M. Roberts, S.L. Bryant, C. Huh, Foams and emulsions stabilized with nanoparticles for potential conformance control applications, SPE International Symposium on Oilfield Chemistry, Society of Petroleum Engineers, 2009.

[3] R.D. Kaminsky, R.C. Wattenbarger, J. Lederhos, S.A. Leonardi, Viscous oil recovery using solids-stabilized emulsions, SPE Annual Technical Conference and Exhibition, Society of Petroleum Engineers, 2010.

[4] T. Zhang, D. Davidson, S.L. Bryant, C. Huh, Nanoparticle-stabilized emulsions for applications in enhanced oil recovery, SPE improved oil recovery symposium, Society of Petroleum Engineers, 2010.

[5] R. Aveyard, B.P. Binks, J.H. Clint, Emulsions stabilised solely by colloidal particles, Adv. Colloid Interface Sci. 100 (2003) 503-546.

[6] I. Kim, A.J. Worthen, M. Lotfollahi, K.P. Johnston, D.A. DiCarlo, C. Huh, Nanoparticle-stabilized emulsions for improved mobility control for adverse-mobility waterflooding, IOR 2017-19th European Symposium on Improved Oil Recovery, Society of Petroleum Engineers, 2017.

[7] N. Griffith, Y. Ahmad, H. Daigle, C. Huh, Nanoparticle-stabilized natural gas liquid-in-water emulsions for residual oil recovery, SPE Improved Oil Recovery Conference, Society of Petroleum Engineers, 2016.

[8] B.l.m. Brunier, N. Sheibat-Othman, M. Chniguir, Y. Chevalier, E. Bourgeat-Lami, Investigation of Four Different Laponite Clays as Stabilizers in Pickering Emulsion Polymerization, Langmuir 32(24) (2016) 6046-6057.

[9] E. Guzmán, D. Orsi, L. Cristofolini, L. Liggieri, F. Ravera, Two-dimensional DPPC based emulsion-like structures stabilized by silica nanoparticles, Langmuir 30(39) (2014) 11504-11512.

[10] A. Vílchez, C. Rodríguez-Abreu, J. Esquena, A. Menner, A. Bismarck, Macroporous polymers obtained in highly concentrated emulsions stabilized solely with magnetic nanoparticles, Langmuir 27(21) (2011) 13342-13352.

[11] Y. He, F. Wu, X. Sun, R. Li, Y. Guo, C. Li, L. Zhang, F. Xing, W. Wang, J. Gao, Factors that affect pickering emulsions stabilized by graphene oxide, ACS Appl. Mater. Interfaces 5(11) (2013) 4843-4855.

[12] P. Joyce, C.P. Whitby, C.A. Prestidge, Bioactive hybrid particles from poly (d, l-lactide-co-glycolide) nanoparticle stabilized lipid droplets, ACS Appl. Mater. Interfaces 7(31) (2015) 17460-17470.

[13] J.W. Salari, J. van Heck, B. Klumperman, Steric stabilization of Pickering emulsions for the efficient synthesis of polymeric microcapsules, Langmuir 26(18) (2010) 14929-14936.

[14] S. Chen, Q. Yang, H. Xiao, H. Shi, Y. Ma, Local pH monitoring of small cluster of cells using a fiber-optic dual-core micro-probe, Sens Actuators B Chem 241 (2017) 398-405.

[15] Y.-H. Park, J.N. Kim, S.H. Jeong, J.E. Choi, S.-H. Lee, B.H. Choi, J.P. Lee, K.H. Sohn, K.L. Park, M.-K. Kim, Assessment of dermal toxicity of nanosilica using cultured keratinocytes, a human skin equivalent model and an invivo model, Toxicology 267(1) (2010) 178-181.

[16] U. Hasegawa, M.N. Shin-ichiro, S.C. Kaul, T. Hirano, K. Akiyoshi, Nanogel-quantum dot hybrid nanoparticles for live cell imaging, Biochem. Biophys. Res. Commun. 331(4) (2005) 917-921.

[17] M. Oishi, Y. Nagasaki, Stimuli-responsive smart nanogels for cancer diagnostics and therapy, Nanomedicine 5(3) (2010) 451-468.

[18] Y. Hoshino, W.W. Haberaecker III, T. Kodama, Z. Zeng, Y. Okahata, K.J. Shea, Affinity purification of multifunctional polymer nanoparticles, J. Am. Chem. Soc 132(39) (2010) 13648-13650.

[19] Y. Hoshino, Y. Arata, Y. Yonamine, S.-H. Lee, A. Yamasaki, R. Tsuhara, K. Yano, K.J. Shea, Y. Miura, Preparation of nanogel-immobilized porous gel beads for affinity separation of proteins: fusion of nano and micro gel materials, Polym. J. 47(2) (2015) 220-225.

[20] K. Raemdonck, J. Demeester, S. De Smedt, Advanced nanogel engineering for drug delivery, Soft matter 5(4) (2009) 707-715.

[21] H. Zhang, Y. Zhai, J. Wang, G. Zhai, New progress and prospects: The application of nanogel in drug delivery, Mater. Sci. Eng. C 60 (2016) 560-568.

[22] T. Ngai, H. Auweter, S.H. Behrens, Environmental responsiveness of microgel particles and particle-stabilized emulsions, Macromolecules 39(23) (2006) 8171-8177.

[23] S. Schmidt, T. Liu, S. Rütten, K.-H. Phan, M. Möller, W. Richtering, Influence of Microgel Architecture and Oil Polarity on Stabilization of Emulsions by Stimuli-Sensitive Core–Shell Poly (N-isopropylacrylamide-co-methacrylic acid) Microgels: Mickering versus Pickering Behavior?, Langmuir 27(16) (2011) 9801-9806.

[24] B.P. Binks, R. Murakami, S.P. Armes, S. Fujii, Effects of pH and salt concentration on oil-in-water emulsions stabilized solely by nanocomposite microgel particles, Langmuir 22(5) (2006) 2050-2057.

[25] S. Kawano, T. Kida, M. Akashi, H. Sato, M. Shizuma, D. Ono, Preparation of Pickering emulsions through interfacial adsorption by soft cyclodextrin nanogels, Beilstein J. Org. Chem. 11 (2015) 2355.

[26] H. Tan, G. Sun, W. Lin, C. Mu, T. Ngai, Gelatin particle-stabilized high internal phase emulsions as nutraceutical containers, ACS Appl. Mater. Interfaces 6(16) (2014) 13977-13984.

[27] X.-Y. Wang, M.-C. Heuzey, Chitosan-based conventional and pickering emulsions with long-term stability, Langmuir 32(4) (2016) 929-936.

[28] N. Bizmark, M.A. Ioannidis, Ethyl Cellulose Nanoparticles at the Alkane–Water Interface and the Making of Pickering Emulsions, Langmuir 33(40) (2017) 10568-10576.

[29] L. Wang, Y. Long, H. Ding, J. Geng, B. Bai, Mechanically robust re-crosslinkable polymeric hydrogels for water management of void space conduits containing reservoirs, Chem. Eng. J. 317 (2017) 952-960.

[30] H. Fan, A. Striolo, Nanoparticle effects on the water-oil interfacial tension, Phys. Rev. E 86(5) (2012) 051610.

[31] K. Du, E. Glogowski, T. Emrick, T.P. Russell, A.D. Dinsmore, Adsorption energy of nano-and microparticles at liquid− liquid interfaces, Langmuir 26(15) (2010) 12518-12522.

[32] V.J. Cunningham, E.C. Giakoumatos, P.M. Ireland, C.J. Mable, S.P. Armes, E.J. Wanless, Giant Pickering droplets: effect of nanoparticle size and morphology on stability, Langmuir 33(31) (2017) 7669-7679.

[33] A. Ward, L. Tordai, Time‐dependence of boundary tensions of solutions I. The role of diffusion in time‐effects, J. Chem. Phys. 14(7) (1946) 453-461.

[34] V.R. Dugyala, J.S. Muthukuru, E. Mani, M.G. Basavaraj, Role of electrostatic interactions in the adsorption kinetics of nanoparticles at fluid–fluid interfaces, Phys. Chem. Chem. Phys. 18(7) (2016) 5499-5508.

[35] N. Bizmark, M.A. Ioannidis, D.E. Henneke, Irreversible adsorption-driven assembly of nanoparticles at fluid interfaces revealed by a dynamic surface tension probe, Langmuir 30(3) (2014) 710-717.

[36] S. Zeppieri, J. Rodríguez, A. López de Ramos, Interfacial tension of alkane+ water systems, J. Chem. Eng. Data 46(5) (2001) 1086-1088.

[37] S. Kutuzov, J. He, R. Tangirala, T. Emrick, T. Russell, A. Böker, On the kinetics of nanoparticle self-assembly at liquid/liquid interfaces, Phys. Chem. Chem. Phys. 9(48) (2007) 6351-6358.

[38] G. González, C. José, J.M. Asua, Flocculation efficiency of blends of short and long chain polyelectrolytes, Colloids Surf. Physicochem. Eng. Aspects 385(1-3) (2011) 166-170.

[39] Y. Wu, S. Wiese, A. Balaceanu, W. Richtering, A. Pich, Behavior of temperature-responsive copolymer microgels at the oil/water interface, Langmuir 30(26) (2014) 7660-7669.

[40] Y. Chevalier, M.-A. Bolzinger, Emulsions stabilized with solid nanoparticles: Pickering emulsions, Colloids Surf. Physicochem. Eng. Aspects 439 (2013) 23-34.

[41] B.P. Binks, T.S. Horozov, Colloidal particles at liquid interfaces, Cambridge University Press2006.

[42] J. Thieme, S. Abend, G. Lagaly, Aggregation in Pickering emulsions, Colloid. Polym. Sci. 277(2-3) (1999) 257-260.

[43] T. Sharma, G.S. Kumar, B.H. Chon, J.S. Sangwai, Thermal stability of oil-in-water Pickering emulsion in the presence of nanoparticle, surfactant, and polymer, Journal of Industrial and Engineering Chemistry 22 (2015) 324-334.

[44] Y. Li, C. Dai, H. Zhou, X. Wang, W. Lv, M. Zhao, Investigation of spontaneous imbibition by using a surfactant-free active silica water-based nanofluid for enhanced oil recovery, Energy & Fuels (2017).

[45] A.J. Morse, D. Dupin, K.L. Thompson, S. Armes, K. Ouzineb, P. Mills, R. Swart, Novel Pickering emulsifiers based on pH-responsive poly (tert-butylaminoethyl methacrylate) latexes, Langmuir 28(32) (2012) 11733-11744.

[46] J. Tang, M.F.X. Lee, W. Zhang, B. Zhao, R.M. Berry, K.C. Tam, Dual responsive pickering emulsion stabilized by poly [2-(dimethylamino) ethyl methacrylate] grafted cellulose nanocrystals, Biomacromolecules 15(8) (2014) 3052-3060.

[47] M. O'neill, M. Yates, K. Harrison, K. Johnston, D. Canelas, D. Betts, J.M. Desimone, S. Wilkinson, Emulsion stabilization and flocculation in CO2. 1. Turbidimetry and tensiometry, Macromolecules 30(17) (1997) 5050-5059.

II. TRANSPORTATION AND POTENTIAL ENHANCED OIL RECOVERY MECHANISMS OF NANOGELS IN SANDSTONE

Jiaming Geng, Haifeng Ding, Pu Han, Yizhou Wu, and Baojun Bai*

Department of Geosciences and Geological and Petroleum Engineering, Missouri University of Science and Technology, Rolla, MO 65401, USA

* Corresponding Author
Baojun Bai
Department of Geosciences and Geological and Petroleum Engineering
Missouri University of Science and Technology
1400 N. Bishop
Rolla, MO 65409
E-mail: baib@mst.edu

ABSTRACT

The transportation and potential enhanced oil recovery mechanisms of nano-sized crosslinked polymeric particles (nanogels) with different charges are described herein. Three nanogels with different types of charges have been synthesized by suspension polymerization using acrylamide, 2-acrylamido-2-methylpropanesulfonic acid, and [2-(acryloyloxy)ethyl] trimethylammonium chloride (AETAC) monomers. The charged nanogels showed spherical morphology, porous structures, and narrow size distribution. The charged nanogels were able to adsorb onto the rock surface and modify the wettability, a critical parameter of the nanogel to recover residual oil. In addition, the static and dynamic adsorption of charged nanogels in sandstone has been demonstrated. Furthermore, the charged nanogels could reduce the permeability of water much more than the permeability of oil and emulsify residual oil as demonstrated by core flooding

experiments. The nanogels with appropriate charges could offer the candidate through disproportionate permeability reduction and in-situ emulsification for enhanced oil recovery.

Key words: Nanogel; Adsorption; Wettability; Enhanced oil recovery.

1. INTRODUCTION

Nano-sized crosslinked polymeric particles (nanogels) are considered as attractive agents for in-depth treatment in the heterogeneous reservoirs, especially in the low permeable reservoirs[1, 2]. The nanogels can easily transport to the in-depth of formation due to the small size of nanogels, which is much smaller than the diameter of pores and throats in the oil reservoirs[3]. The nanogels are able to settle down and divert water or gas flow through high permeability zones to the unswept zones and enhance oil recovery when the pressure gradient decreases in the in-depth of formation[4-6]. Compared with the conventional in-depth plugging agents like in-situ gels, the nanogels have several advantages such as low viscosity[7, 8], temperature and salt resistance[9]. In addition, the nanogels are able to reduce relative permeability of water more than that of oil, because the hydrophilic polymeric networks in nanogels contribute to the differential permeability reduction[10]. Furthermore, the nanogels can adsorb at the oil-water interfaces to reduce the interfacial tension and stabilize oil-in-water emulsions[11, 12], which helps to improve the recovery of the residual oil trapped in oil reservoirs.

Lab-scaled experiments have stated that nanogels can adsorb and form the mechanical blockage in porous media, which greatly reduce the relative permeability of water[3, 6]. In Lenchenkov's experiments, the adsorption of nanogels was found to be

dependence on the flow rate in high permeable porous media, which indicated a multilayer adsorption of nanogels[6]. The adsorption of polyacrylamide-based nanogels on the rock surface is driven by Van der Waals' force and hydrogen bond during the nanogels transport in porous media[13]. In addition, the nanogel concentration in the effluent was found to be smaller than the concentration injected, even after the injection of several pore volumes, which suggested the mechanical entrapment of the nanogels in porous media. The pore throats might be blocked by the nanogel agglomeration due to the dramatically increased size. However, the polyacrylamide-based nanogels were not stable in formation water due to the insufficient electrostatic repulsion, and in consequence, the nanogels accumulated in the inlet section and not penetrated into the depth of sandstone.

The surface charges of nanogels can prevent the nanogels aggregate in formation water so that it can enhance the stability of nanogels during the transportation in porous media[14]. The surface charges profoundly affect the adsorption and rearrangement of nanogels at the solid surface as well[15]. Positively charged nanogels are attracted to negatively charged surfaces, while negatively charged nanogels are attracted to positively charged surfaces. Considered the surface charge of most sandstone reservoir is negative[16], which plays an important role in the nanogel adsorption and transportation, it is essential to clarify the interaction between charged nanogels and rock surface to systematically understand the transportation and permeability reduction mechanisms of nanogels. However, to the best of our knowledge, no studies have reported the adsorption mechanisms of nanogels in porous media, especially using nanogels with different charges.

In this study, we synthesized the nanogels with narrative size distribution using free-radical suspension polymerization and characterized their properties using corresponding technologies. We investigated the rheology of nanogels with different charges under shearing from 40 to 100 s^{-1} and the surface modification properties of charged nanogels on sandstone cores. In addition, the static and dynamic adsorption processes of nanogels onto sandstone surface were dominated by the electrostatic interactions. Furthermore, it has been demonstrated that the nanogels were able to reduce water permeability much more than oil permeability and emulsify residual oil through core flooding experiments. The transportation and adsorption mechanism of charged nanogels through the porous media was discussed based on the parallel capillary tube model.

2. EXPERIMENTAL

2.1. MATERIALS

The All chemicals and reagents were purchased from Sigma-Aldrich (St. Louis, MO) and used as received except further noted. Acrylamide was recrystallized to remove the inhibitor and 2-acrylamido-2-methylpropanesulfonic acid (AMPS) was neutralized to generate the corresponding sodium salt (AMPS-Na). The synthesis of nanogels is free-radical suspension polymerization at 1000:1 mol/mol monomer to crosslinker ratio. Nanogels were washed three times with acetone, dried *in vacuo* at room temperature to afford a white solid powder.

2.2. MORPHOLOGY AND SIZE DISTRIBUTION STUDIES

The solid powder of nanogels and the dispersion of nanogels after lyophilized were placed onto the electrically conductive film and coated with Au-Pd to imaging. A Hitachi S-4700 FESEM microscope (Tokyo, Japan) was used to collect scanning electron microscope (SEM) images at 15.0 kV. Dynamic light scattering (DLS) measurements on swollen nanogels were performed by a Malvern ZS90 Nanosizer (Malvern Instruments, Ltd., U.K.) at a scattering angle of 90° with an incident beam of a wavelength at 633 nm at 25 °C. The measurements were based on three repeated results of each sample. The intensity size distribution was obtained from analysis of the correlation functions by the multiple narrow mode algorithms in the instrument software.

2.3. RHEOLOGICAL PARAMETERS MEASUREMENTS

The rheological parameters of the nanogel dispersions were measured with a Brookfield DV3T rheometer at 25 °C.

2.4. CONTACT ANGLE MEASUREMENTS

Equilibrium contact angle was measured between n-decane (drop) and the nanogel dispersion (surrounding solution) on sandstone cores, which had immersed in the nanogel dispersion for 10 days. The measurements were performed at 25 °C by placing a drop of n-decane at the surface of sandstone. Contact angles were determined by fitting the Young-Laplace equation to the drop profile.

2.5. STATIC AND DYNAMIC ADSORPTION MEASUREMENTS

For static adsorption measurements, the Berea sandstone cores saturated with 1 wt.% NaCl (Table 1) were immersed in 1000 ppm nanogel dispersions at 25 °C for 10 days. The concentration of nanogel in dispersions was measured using Shimadzu UVmini-1240 UV-Vis spectrophotometer as a function of time with the appropriate mixture of 1 wt.% NaCl as a reference.

Table 1. Physical properties of sandstone cores for static adsorption measurements.

Sample	Core length (cm)	Core diameter (cm)	Surface area (cm^2)
PAM	1.350	2.498	20.40
PAMPS-Na	1.354	2.498	20.43
PAETAC	1.351	2.498	20.40

Nanogel dispersion (300 μL) was diluted by 1 wt.% NaCl to a concentration that fell in the linear range following Lambert-Beer Law and concentration of nanogel was quantified by the Lambert-Beer equation:

$$A = \varepsilon cL$$

where A is the absorbance, ε is the absorptivity, c is the concentration of the sample, and L is the path length of light through the sample.

For the dynamic adsorption measurements, the nanogel dispersions were injected through the sandstone cores (Table 2) saturated with 1 wt.% NaCl (Figure 1). The nanogel concentration in the effluent was measured in the same way in the static adsorption measurements as a function of injection volume.

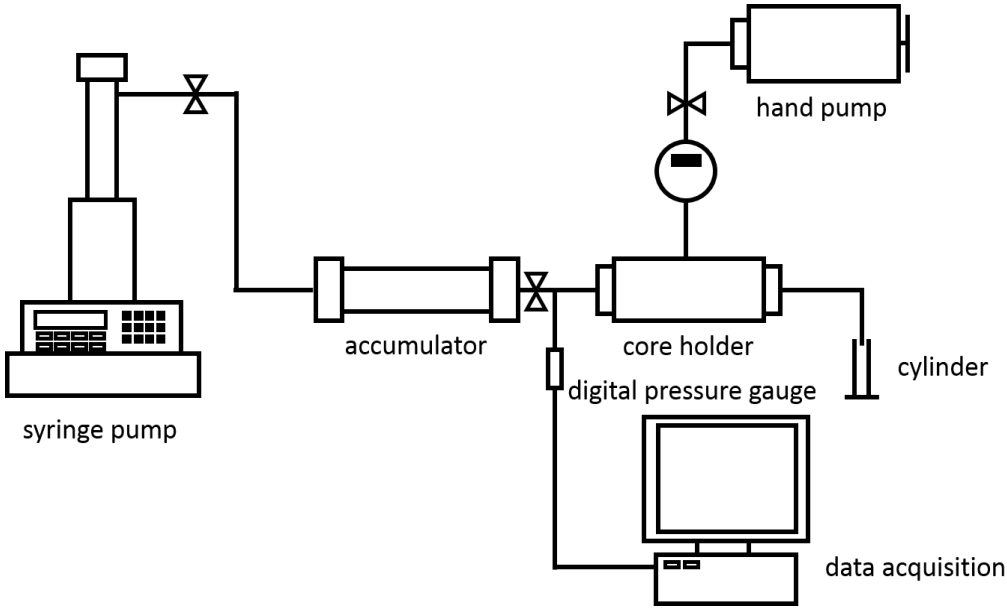

Figure 1. Schematic diagram of single core equipment for dynamic adsorption and core flooding experiments.

Table 2. Physical properties of sandstone cores for dynamic adsorption and core flooding.

Sandstone Core	Length (cm)	Diameter (cm)	Pore volume (mL)	Permeability (mD)
PAM adsorption	5.25	2.54	5.45	196.33
PAMPS-Na adsorption	5.40	2.54	5.66	306.31
PAETAC adsorption	5.25	2.54	5.45	297.93
PAM flooding	5.03	2.52	4.72	85.19
PAMPS-Na flooding	5.40	2.52	5.18	94.72
PAETAC flooding	5.60	2.52	5.32	81.71

2.6. CORE FLOODING EXPERIMENTS

The plugging efficiency and enhanced oil recovery ability of the nanogels were simulated and evaluated by the core flooding experiment. The sandstone cores (Table 2) were dried in 130 °C oven and vacuumed before saturated with 1 wt.% NaCl. The brine permeability of each sandstone cores was measured and then, several pore volumes (PV) of decane were injected following the equipment shown in Figure 1. Brine was injected

to reach the residual oil saturation at a constant flow rate of 0.25 mL/min. Afterward, the nanogel dispersions were injected through the cores until the injection pressure became constant. A post-brine flooding was conducted to elucidate the water diversion after the nanogel treatment.

3. RESULTS AND DISCUSSIONS

3.1. MORPHOLOGY AND SIZE DISTRIBUTION OF NANOGELS

The physicochemical properties of the synthesized nanogels are listed in Table 3, including surface ζ-potentials, polydispersity index in 1 wt.% NaCl, and pH. The negative ζ-potential of PAM nanogel presumably was caused by the hydrolysis of amide moieties to carboxylic groups.

Table 3. Physicochemical properties of PAM, PAMPS-Na, and PAETAC nanogels.

Property	PAM	PAMPS-Na	PAETAC
Charge	Neutral	Negative	Positive
Surface ζ -potential (mV)	-1.76	-35.90	34.75
Polydispersity index (PDI)	0.236	0.268	0.482
pH (1000 ppm nanogel)	7.8	7.0	4.9

The monodisperse charged nanogels with uniformed geometry were synthesized via suspension polymerization following our previous work[17]. As shown in Figure 2, the average hydrodynamic diameter of PAMPS-Na, PAM, and PAETAC nanogels in 1 wt.% NaCl solution was 241.62, 220.14, and 151.14 nm, respectively. The narrow size distributions suggest the good stability of the synthesized nanogels in 1 wt.% NaCl solution. The hydrodynamic diameter of AMPS-Na nanogels measured by DLS was

approximately larger compared to the size as visualized by SEM, as illustrated in Figure 3B, where swelled nanogels were observed. The difference in the diameter results from SEM and DLS was due to the dangling polymer chains on the surface of nanogels.

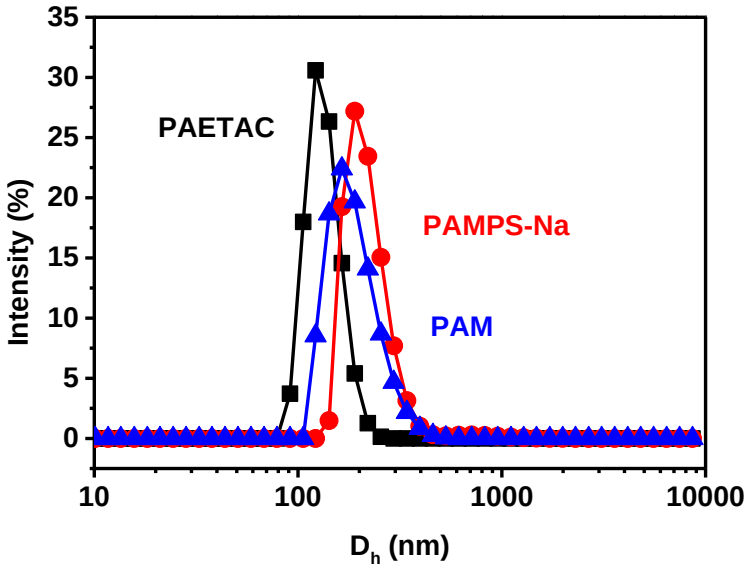

Figure 2. Hydrodynamic diameter distribution of PAM, PAMPS-Na, and PAETAC nanogels in 1 wt.% NaCl measured at C ~ 100 mg/L, and T = 25 °C.

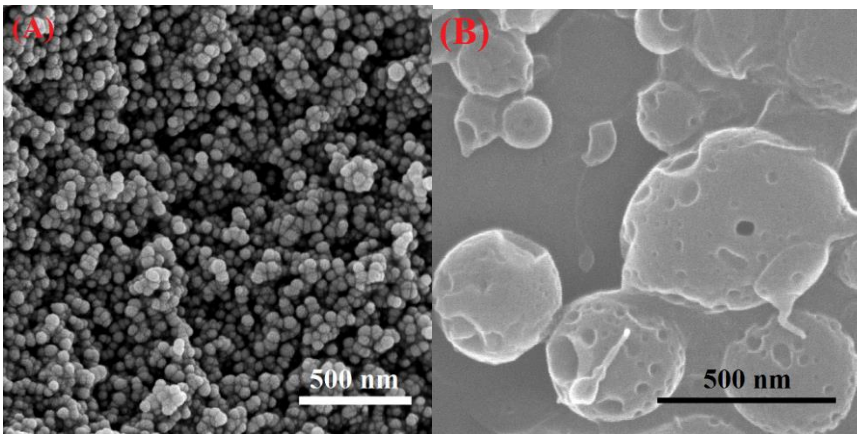

Figure 3. SEM micrographs of PAMPS-Na nanogel before (A) and after (B) swelling in 1 wt.% NaCl.

Furthermore, the diameter of PAMPS-Na nanogels increased ~5 times after swelled in 1 wt.% NaCl solution. The morphological features of the PAMPS-Na nanogels elucidated by SEM showed a porous structure with an irregular pore distribution, which accounted for high water content, deformable features of the nanogels.

3.2. RHEOLOGICAL PROPERTIES OF NANOGEL DISPERSIONS

The viscosity of nanogel dispersions was obviously affected by the concentrations of nanogel as shown in Figure 4A, B and C. At low shear rates, the viscosity of dispersed PAM and PAETAC nanogels decreased as the shear rate increased, which demonstrated the breakage of preformed interparticle structures. The viscosity of PAETAC and PAMPS-Na nanogel dispersions kept constant and showed to be a Newtonian fluid when the shear rate is higher than 40 s^{-1}. However, for PAM nanogel dispersion showed the properties of a dilatant fluid at the shear rate above 100 s^{-1}. Before applied shear, the Van der Waals' attraction drove the formation of interparticle structure among the dispersed nanogels.

At low shear rates, the dispersions of PAM and PAETAC nanogels displayed the shear thinning behavior due to the breakage of the interparticle structure. However, the viscosity of PAMPS-Na nanogel dispersion showed to be a Newtonian fluid because of the electrostatic repulsion hindered the formation of interparticle structure. When the shear rate is above 100 s^{-1}, the shear-induced the deformation of the nanogels and increased the attraction among dispersed nanogels, which resulted in the dilatant behavior of the dispersions of PAM nanogels[18, 19]. Nevertheless, the electrostatic repulsion among charged nanogels overcame the attraction caused by nanogel deformation and the

viscosity of the dispersion of charged nanogels kept constant at high shear rates from 100 to 150 s^{-1}.

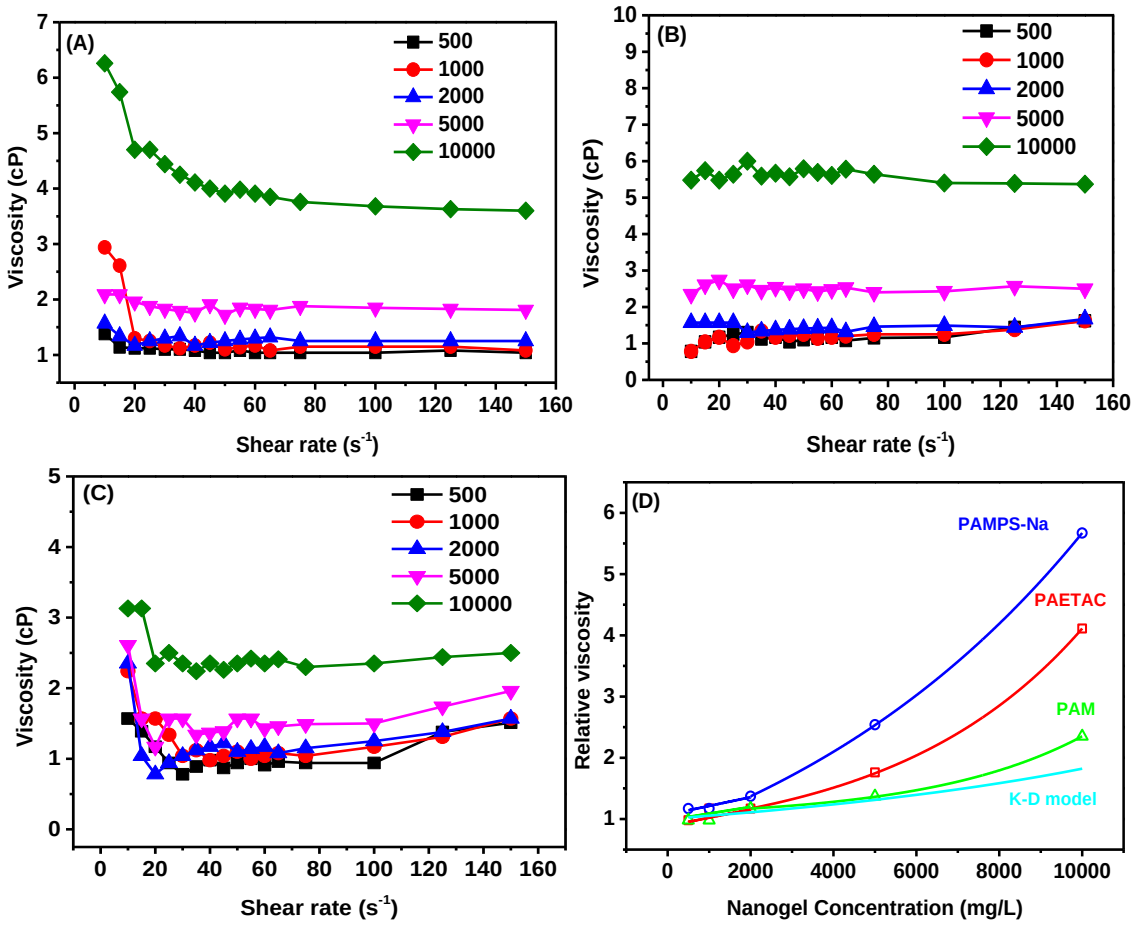

Figure 4. Viscosity of nanogel dispersion at different shear rates.

The relative viscosities of nanogel dispersions at a constant shear rate (40 s^{-1}) at different nanogel concentrations are shown in Figure 4D. By fitting of the data, the relative viscosity (η_r) is found to be an exponential function of concentration in PAMPS-Na and PAETAC nanogel dispersions while a linear function of concentration in PAM nanogel dispersion. This concentration-dependent slope change indicates a change in polymer interaction[20] in PAMPS-Na and PAETAC samples. Below 2000 mg/L, the

nanogel is well dispersed and nanogel-solvent interactions dominate the flow behavior of nanogel dispersion. When the nanogel concentration is greater than 5000 mg/L, the average inter-particle spacing is reduced and the particle-particle reaction is no longer negligible. When compared relative viscosities of nanogels with Krieger-Dougherty model[8], which was applied to fit the relative viscosity of dispersed hard spherical particles, a much higher viscosity profile was found for PAMPS-Na and PAETAC nanogels. The abruptly exponentially scale of nanogel viscosity was caused by the long-range interactions among nanogels. When the concentration of nanogel was higher than 5000 mg/L, the nanogels turned to form percolation[21, 22] that resulted in the exponentially increased nanogel viscosity.

3.3. NANOGEL EFFECT ON WETTABILITY ALTERATION

A To investigate the effect of nanogels on the wettability of sandstone surface, the static sessile drop experiments were performed on nanogel adsorbed sandstone cores. The contact angles were measured between the nanogel dispersions and decane on the sandstone surface, which were immersed in the nanogel dispersions for 10 days. As displayed in Figure 5, the contact angle of sandstone cores adsorbed PAM and PAMPS-Na nanogels decreased from 23.63° to 18.69° and 15.53°, respectively whereas the contact angle of sandstone core adsorbed PAETAC nanogels increased to 26.66°. The change of wettability reflected by the contact angle was caused by the adsorbed nanogel layer on the sandstone surface. The polymer chains on nanogel attracted water to spread on the surface of the adsorbed layer by dipole-dipole attraction, which was dominated by the affinity of polymer chains to water. The PAM and PAMPS-Na nanogels, which were

more hydrophilic than the surface of sandstone, provided a smaller contact angle. Vice versa, the PAETAC nanogels that were more hydrophobic than the sandstone surface increased the contact angle and turned rock surface to less water-wet.

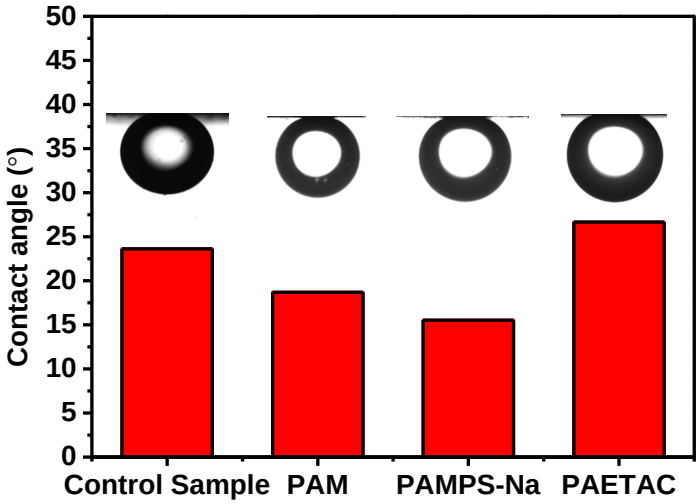

Figure 5. Contact angle of sandstone cores and after adsorbed PAM, PAETAC, and PAMPS-Na nanogels.

3.4. STATIC ADSORPTION OF NANOGELS ON SANDSTONE

Urine In order to investigate the mechanism of controlling process of nanogel adsorption, the pseudo-first and second order kinetic models[23] were used to fit the static adsorption experiments data

Pseudo-first order model:

$$q_t = q_e[1 - \exp(-k_1 t)]$$

Pseudo-second order model:

$$q_t = \frac{q_e^2 k_2 t}{[q_e k_2 t + 1]}$$

where q_t is the amount of nanogel adsorbed at t, q_e is the amount of nanogel adsorbed at equilibrium, k_1 and k_2 are the rate constant for pseudo-first and second order model, respectively.

The fitting curves of pseudo-first and second order models of charged nanogels adsorption onto sandstone surface are shown in Figure 6. It was clear that the adsorption process can be divided into two processes: a relative fast uptake of nanogels during the initial stage, and followed by a slow adsorption period until reached an equilibrium adsorption. The value of equilibrium adsorption and corresponding parameters were obtained through the application of the pseudo-first order model for PAETAC nanogel and pseudo-second order model for PAMPS-Na and PAM nanogel samples (Table 4). The rate constant k_1 of PAMPS-Na is considerably higher than the rate of PAM nanogels, which is in agreement with our previous results of the diffusion coefficients of charged nanogels[17]. The non-linear fitting curve of adsorption data suggested that two or more factors controlled the nanogel adsorption process[24]. As shown in Figure 6, the adsorption kinetics of PAETAC nanogel was fitted better by pseudo-first order model and the equilibrium adsorption concentration of PAETAC is much higher than PAM and PAMPS-Na nanogels. Generally, the pseudo-second order model is applied to estimate adsorption behavior based on the whole range while in the pseudo-first order model, the adsorption is dominated by one factor. Because of the negative charge of sandstone surface, the adsorption of PAETAC nanogels was driven by both electrostatic attraction and Van der Waals' force whereas the adsorption of PAM and PAMPS-Na nanogels was controlled by electrostatic repulsion and Van der Waals' attraction. The good following in the pseudo-first order model of PAETAC nanogel adsorption indicated the electrostatic

interaction between nanogel and rock surface had overwhelmed the effect of other forces on the adsorption process.

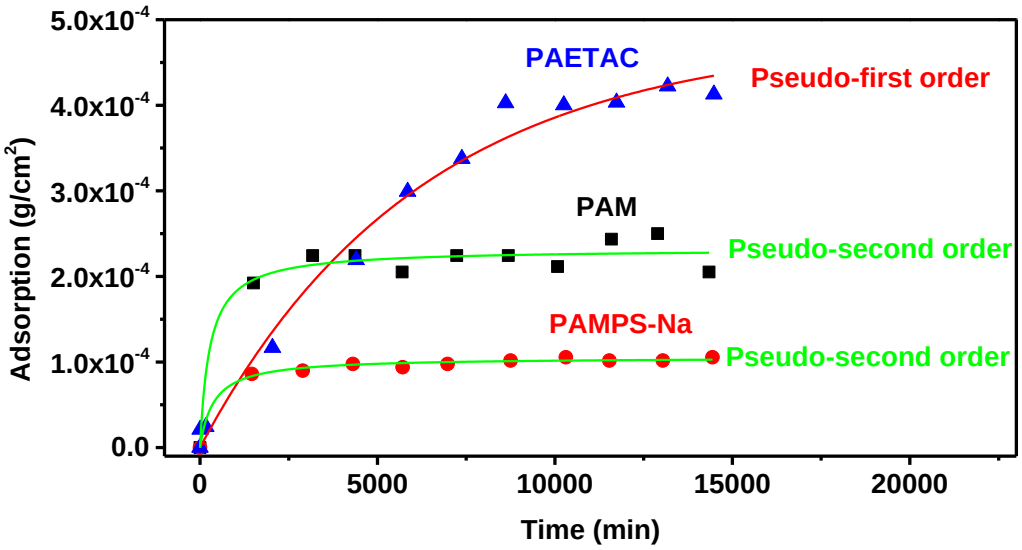

Figure 6. Static adsorption curve for 1000 mg/L PAM, PAETAC, and PAMPS-Na nanogels uptake on sandstone cores at 25 °C.

Table 4. Kinetic parameters for PAM, PAMPS-Na, and PAETAC adsorption on sandstone cores.

Nanogel	Fitting Model	k_1 (h^{-1})	k_2 ($g \cdot cm^{-2}h^{-1}$)	Q_e ($g \cdot cm^{-2}$)	R_{adj}^2
PAM	Pseudo-second order	N/A	936.0744	$2.32071*10^{-4}$	0.95383
PAMPS-Na	Pseudo-second order	N/A	1480.2384	$1.05432*10^{-4}$	0.99133
PAETAC	Pseudo-first order	$9.7413*10^{-3}$	N/A	$4.80362*10^{-4}$	0.98654

The equilibrium adsorption concentration of single layer adsorption of mono-dispersed nanogels is:

$$Q = \frac{m}{A} = \frac{\frac{4}{3}\pi r^3 \rho}{4\sqrt{3}r^2} = \frac{\pi r \rho}{3\sqrt{3}}$$

where r and ρ are the radius and density of nanogel, respectively. Because of the high-water content of swelled nanogels, the density of nanogel is assumed to equal to the density of 1 wt.% NaCl solution. If there is no deformation of nanogels during the static adsorption process, the equilibrium adsorption concentration of PAM, PAMPS-Na, and PAETAC nanogels are $6.7*10^{-6}$, $7.3*10^{-6}$, and $4.6*10^{-6}$ g/cm^2, respectively. However, the adsorption concentration of PAETAC nanogel at the surface of sandstone, which is ~$4.8*10^{-4}$ g/cm^2 calculated from the pseudo-first order model, is around two times of the adsorption concentration of PAM nanogel and four times of PAMPS-Na nanogel. The experimental results indicated a multilayer adsorption of nanogel onto the sandstone surface that is dominated by the electrostatic interactions.

3.5. DYNAMIC ADSORPTION AND DESORPTION OF NANOGELS ON SANDSTONE

In general, the kinetics of dynamic adsorption is different with that of static adsorption[25]. As transportation of nanogel in porous media under a dynamic adsorption, the volumetric flow will cause the multilayer adsorption on pore surface. Moreover, the complexed porous structure may cause log-jam phenomenon at the entrance of the pore throat. In dynamic adsorption measurements, nanogel dispersions with a concentration of 1000 mg/L were injected through sandstone cores until no more nanogel adsorbed on the pore surface. Then, 1 wt.% NaCl solution was injected into sandstone cores to desorb nanogel from the rock surface. The differential pressure was recorded to determine the adsorbing and blocking behavior of nanogels.

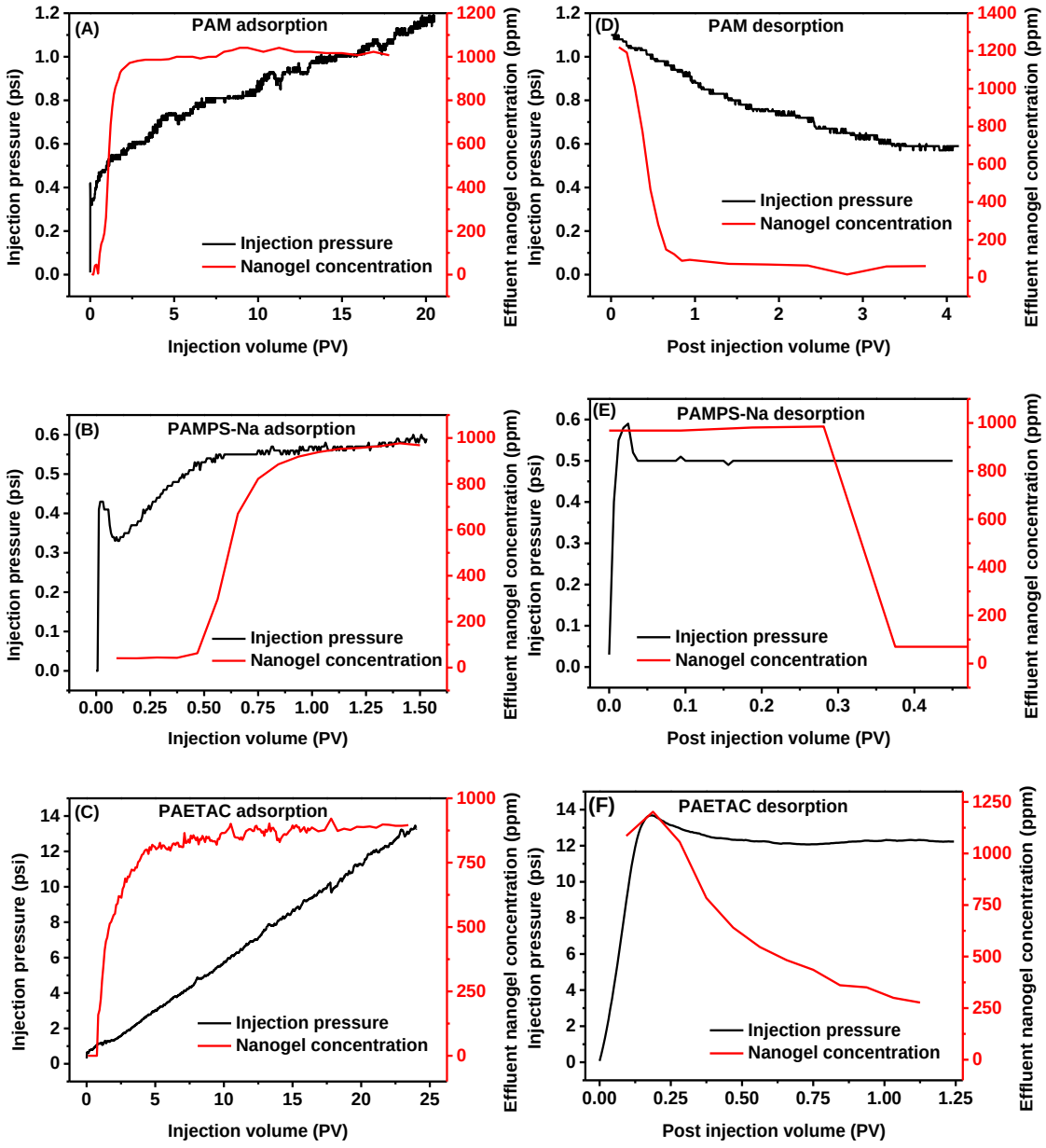

Figure 7. Differential pressure and concentration of nanogel in effluent versus injection volume curve of dynamic adsorption measurements of A) PAM, B) PAMPS-Na, and C) PAETAC nanogel and dynamic desorption measurements of D) PAM, E) PAMPS-Na, and F) PAETAC nanogel.

The differential pressure suddenly increased to 0.4 psi, then increased at a rate of 0.04 psi per PV during the injection of PAM nanogel dispersion (Figure 7A). No PAM nanogel was detected in the effluent until 0.75 PV of PAM nanogel injection. The

concentration of nanogel increased dramatically and reached the concentration of injected dispersion at 2.35 PV, which indicated a piston-like displacement of nanogel inside the core. For PAMPS-Na nanogel, an obvious bump in differential pressure appeared at the start point of injection, which is presumably due to the threshold injection pressure (Figure 7B). The differential pressure increased at a constant rate of 0.55 psi per PV during the injection of PAETAC nanogel dispersion (Figure 7C). After injected 0.84 PV, PAETAC nanogel started to be detected in the effluent. The concentration of nanogel increased from 0 to 827 mg/L at a rate of 183.8 mg/L per PV, and then, turned to a much slower increasing rate of 3.8 mg/L per PV.

The increased differential pressure can be caused by the narrowed flow path by nanogel adsorbing on the rock surface and/or reduced flow path amount by bridging and aggregating to block pore throats. It is simply assumed that the sandstone core was the assembly of many paralleled capillary tubes with same diameter and length. The length of these capillary tubes is assumed to equal to the length of the sandstone core, which means that tortuosity is not considered in this assumption. Based on the relationship between effluent nanogel concentration and injection volume, accumulative residual nanogel was calculated by the integration. The radius of capillary tubes was calculated by applying the following equations[26]:

$$r = \sqrt{\frac{8K}{\Phi}}$$

where K is the permeability, and Φ is the porosity of core. If the deformation of residual nanogels is neglectable, the total pore volume before nanogel flooding is equal to the summary of pore volume after nanogel flooding and volume of residual nanogels:

$$n\pi r_b^2 L = \phi V_{bulk}$$

$$n\pi r_a^2 L + V_{nanogel} = n\pi r_b^2 L$$

Injection pressure can be calculated using Poiseuille's Law because of the flow of nanogel is quite slow and can be considered as a laminar flow in the porous medium:

$$P = \frac{8Q\mu L}{\pi n r^4}$$

All the calculated parameters are listed in Table 5. The differences between calculated and measured differential pressure are significant, as the value of measured injection pressure is several to tens of times of calculated one. This difference indicated that the arrangement of nanogels in the porous medium is in not only multilayer adsorption state on rock surface but also blockage of nanogel agglomeration, which dominated the differential pressure in the porous medium. Furthermore, in sandstone cores, PAETAC nanogel with positive charges provide more and/or stronger adsorption than PAM and PAMPS-Na nanogel.

Table 5. Calculated capillary radius before and after nanogel adsorption, capillary number, and differential pressures.

Sample	r_b (m)	r_a (m)	n	P_{meas} (psi)	P_{calc} (psi)
PAM	$2.77*10^{-6}$	$2.62*10^{-6}$	$4.31*10^{6}$	1.18	0.39
PAMPS-Na	$3.44*10^{-6}$	$3.40*10^{-6}$	$2.82*10^{6}$	0.59	0.22
PAETAC	$3.41*10^{-6}$	$3.14*10^{-6}$	$2.84*10^{6}$	13.46	0.29

The dynamic desorption behaviors of nanogel systems were studied at room temperature. The differential pressure of PAM nanogel sample decreased from 1.1 to 0.6 psi and then became constant in the dynamic desorption measurement (Figure 7D), indicated the unblocking and transportation of nanogel aggregations. The concentration

of nanogel in effluent drops to 100 mg/L in 0.7 PV, which is due to the displacement of nanogel dispersion remained in pores. In comparison with the decrease in differential pressure of PAM sample, the PAMPS-Na and PAETAC samples showed a slight decrease, which is less than their P_{calc}, during brine injection. Although the differential pressure curve appeared a similar trend in PAMPS-Na and PAETAC nanogel desorption measurements, the relationship between nanogel concentration and brine injected volume is different (Figure 7E, F). For instance, the concentration of PAMPS-Na nanogel decreased from 1000 to 70 mg/L after 0.375 PV of injection while for PAETAC nanogel, the concentration decreased in a power law relationship with injection volume. The trend of differential pressure and nanogel concentration could be ascribed to desorption of nanogel from pore surface.

Furthermore, the different responding rates of injection pressure and effluent nanogel concentration were observed in both the dynamic adsorption and desorption measurements. The heterogeneous pore size distribution in the sandstone core resulted in the detection of nanogels in the effluent in less than 1 PV during the dynamic adsorption measurements. In addition, the effluent nanogel concentration reached their equilibrium concentration after more than 1 PV of nanogel injection. The electrostatic interactions between sandstone and nanogels contributed to the different effluent nanogel concentration profile that the electro-repulsion accelerated the dynamic adsorption process to reach equilibrium state whereas electro-attraction prolonged it. In the desorption measurements, the nanogel dispersions resisted in the pores and throats were flushed out quickly by the displacing water that resulted in the dramatically drop of

effluent nanogel concentration. After that, the slowly desorption of nanogel from the rock surface lead to the decrement of injection pressure.

3.6. PROFILE CONTROL AND OIL DISPLACEMENT EFFECTS OF NANOGELS

In the core flooding experiment, the plugging efficiency and cumulative oil recovery were evaluated by the differential pressure and oil recovery as displayed in Figure 8. The oil recovery was increased during the nanogel injection and the 2nd water flooding. For instance, PAM nanogel increased differential pressure from 7.5 to 17 psi and helped to recover 9.62 % oil during the nanogel injection (Figure 8A). There was 4.24% oil produced from the sandstone core in 2nd water flooding due to water diversion. Similar differential pressure profiles were observed in PAMPS-Na and PAETAC samples (Figure 8B, C) and the cumulative oil recovery was increased during both the nanogel injection and 2nd water flooding. The core flooding experiments demonstrated that the water flow can be diverted to the unflushed zone after nanogel injection. An interesting observation is that the oil produced during the nanogel injection is in oil-in-water emulsion state while the oil produced during the 2nd water flooding is in the bulk oil phase (Figure 8D, E). The emulsified oil droplets in effluent implied that the nanogels can spontaneously emulsify and wash out the residual oil in porous media. The adsorbed nanogel layers at the oil-water interfaces helped reduce the oil-water interfacial tension and stabilize oil-in-water emulsions[17]. Furthermore, additional oil was produced from the porous media during the 2nd water flooding because the nanogel adsorbed on sandstone surface and blocked the pore throats significantly increased the differential pressure and divert displacing fluid to the unflushed zone.

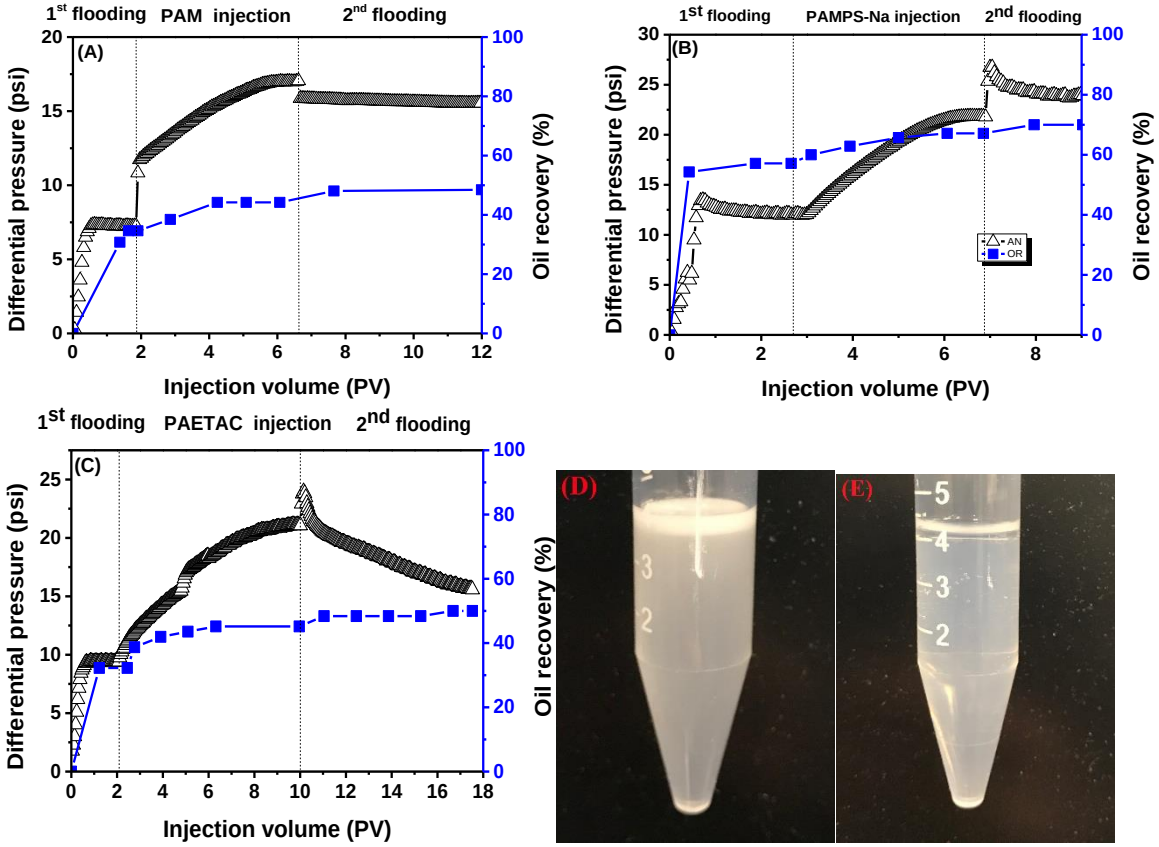

Figure 8. Injection pressure and oil recovery of oil saturated sandstone flooded using A) PAM nanogel; B) PAMPS-Na nanogel; C) PAETAC nanogel. Photo of D) effluent during nanogel injection; E) effluent during 2nd flooding.

In the dynamic adsorption experiments of the nanogels, the differential pressure is dramatically influenced by the charge of nanogels. However, the differential pressure of the core flooding experiment is independent of the charge of nanogels. A possible hypothesis for the underlying cause of this behavior is that the presence of oil hindered the adsorption of nanogel on the rock surface and the mechanical entrapment of nanogels dominated the differential pressure.

4. CONCLUSION

In summary, the nanogels used in chemical enhanced oil recovery has been described. Crosslinking of AETAC, AM, and AMPS-Na monomers by suspension polymerization generated nanogels with positive, neutral, and negative charges, respectively. The morphology and size distribution of nanogels were demonstrated by SEM and DLS. Compared to dispersed nanoparticle system, the viscosity of nanogels presented an exponential relationship with concentration, which indicated percolation among nanogels. Rheological studies demonstrated the nanogels' ability to be easily injected into the matrix in reservoirs. The contact angle of sandstone showed slightly decrease upon the hydrophilicity of adsorbed nanogels, and the sandstone had a larger contact angle after adsorbed PAETAC nanogels. The kinetic of nanogel adsorption was controlled by the surface charge of sandstone and nanogel as demonstrated by static and dynamic adsorption measurements. The nanogels showed good plugging efficiency in 1 wt.% NaCl solution. In addition, it has been demonstrated that the nanogels had the ability to emulsify residual oil and enhance displacing efficiency. The second brine injection, which simulated post water flooding, demonstrated that nanogels could efficiently divert brine flow to enhance sweep efficiency.

ACKNOWLEDGEMENTS

The authors would like to express their grateful acknowledgement to the financial support from DOE under the contract of DE-FE0024558.

REFERENCES

(1) Hua, Z.; Lin, M.; Dong, Z.; Li, M.; Zhang, G.; Yang, J., Study of deep profile control and oil displacement technologies with nanoscale polymer microspheres. *J. Colloid Interface Sci.* **2014,** 424, 67-74.

(2) Irvine, R.; Davidson, J.; Baker, M.; Devlin, R.; Park, H. In Nano Spherical Polymer Pilot in a Mature 18° API Sandstone Reservoir Water Flood *in Alberta, Canada*, *SPE Asia Pacific Enhanced Oil Recovery Conference*, **2015**; Society of Petroleum Engineers: 2015.

(3) Almohsin, A. M.; Bai, B.; Imqam, A. H.; Wei, M.; Kang, W.; Delshad, M.; Sepehrnoori, K. In Transport of nanogel through porous media and its resistance to water flow, *SPE Improved Oil Recovery Symposium*, **2014**; Society of Petroleum Engineers: 2014.

(4) Wang, L.; Zhang, G.; Li, G.; Zhang, J.; Ding, B. In Preparation of microgel nanospheres and their application in EOR, *International Oil and Gas Conference and Exhibition in China*, **2010**; Society of Petroleum Engineers: 2010.

(5) Tian, Q. Y.; Wang, L.; Tang, Y.; Liu, C.; Ma, C.; Wang, T. In Research and application of nano polymer microspheres diversion technique of deep fluid, SPE *International Oilfield Nanotechnology Conference and Exhibition*, **2012**; Society of Petroleum Engineers: 2012.

(6) Lenchenkov, N. S.; Slob, M.; van Dalen, E.; Glasbergen, G.; van Kruijsdijk, C. In Oil Recovery from Outcrop Cores with Polymeric Nano-Spheres, *SPE Improved Oil Recovery Conference*, **2016**; Society of Petroleum Engineers: 2016.

(7) Moraes, R. R.; Garcia, J. W.; Barros, M. D.; Lewis, S. H.; Pfeifer, C. S.; Liu, J.; Stansbury, J. W., Control of polymerization shrinkage and stress in nanogel-modified monomer and composite materials. *Dent. Mater.* **2011,** 27, (6), 509-519.

(8) Liu, J.; Rad, I. Y.; Sun, F.; Stansbury, J. W., Photo-reactive nanogels as a means to tune properties during polymer network formation. *Polym. chem.* **2014,** 5, (1), 227-233.

(9) Bai, B.; Wei, M.; Liu, Y. In Field and lab experience with a successful preformed particle gel conformance control technology, SPE Production and Operations Symposium, **2013**; Society of Petroleum Engineers: 2013.

(10) Sydansk, R.; Xiong, Y.; Al-Dhafeeri, A.; Schrader, R.; Seright, R. In Characterization of partially formed polymer gels for application to fractured production wells for water-shutoff purposes, *SPE/DOE Symposium on Improved Oil Recovery*, **2004**; Society of Petroleum Engineers: 2004.

(11) Finnegan, M. P.; Zhang, H.; Banfield, J. F., Phase stability and transformation in titania nanoparticles in aqueous solutions dominated by surface energy. *J. Phys. Chem. C* **2007,** 111, (5), 1962-1968.

(12) Binder, W. H., Supramolecular assembly of nanoparticles at liquid–liquid interfaces. *Angew. Chem., Int. Ed.* **2005,** 44, (33), 5172-5175.

(13) Sorbie, K. S., Polymer-improved oil recovery. *Springer Science & Business Media*: **2013**.

(14) áO'Brien, R. W., Electroacoustic studies of moderately concentrated colloidal suspensions. *Faraday Discuss. Chem. Soc.* **1990,** 90, 301-312.

(15) Johnson, C. A.; Lenhoff, A. M., Adsorption of charged latex particles on mica studied by atomic force microscopy. *J. Colloid Interface Sci.* **1996,** 179, (2), 587-599.

(16) Nasralla, R. A.; Bataweel, M. A.; Nasr-El-Din, H. A., Investigation of wettability alteration and oil-recovery improvement by low-salinity water in sandstone rock. *J. Can. Pet. Technol.* **2013,** 52, (02), 144-154.

(17) Geng, J.; Pu, J.; Wang, L.; Bai, B., Surface charge effect of nanogel on emulsification of oil in water for fossil energy recovery. *Fuel* **2018,** 223, 140-148.

(18) Shao, Z.; Negi, A. S.; Osuji, C. O., Role of interparticle attraction in the yielding response of microgel suspensions. *Soft Matter* **2013,** 9, (22), 5492-5500.

(19) Zhou, Z.; Hollingsworth, J. V.; Hong, S.; Wei, G.; Shi, Y.; Lu, X.; Cheng, H.; Han, C. C., Effects of particle softness on shear thickening of microgel suspensions. *Soft Matter* **2014,** 10, (33), 6286-6293.

(20) Gupta, P.; Elkins, C.; Long, T. E.; Wilkes, G. L., Electrospinning of linear homopolymers of poly (methyl methacrylate): exploring relationships between fiber formation, viscosity, molecular weight and concentration in a good solvent. *Polymer* **2005,** 46, (13), 4799-4810.

(21) Dailing, E. A.; Setterberg, W. K.; Shah, P. K.; Stansbury, J. W., Photopolymerizable nanogels as macromolecular precursors to covalently crosslinked water-based networks. *Soft Matter* **2015,** 11, (28), 5647-5655.

(22) Ketz, R.; Prud'homme, R.; Graessley, W., Rheology of concentrated microgel solutions. *Rheol. Acta* **1988,** 27, (5), 531-539.

(23) Machado, F. M.; Bergmann, C. P.; Lima, E. C.; Royer, B.; de Souza, F. E.; Jauris, I. M.; Calvete, T.; Fagan, S. B., Adsorption of Reactive Blue 4 dye from water solutions by carbon nanotubes: experiment and theory. *Phys. Chem. Chem. Phys.* **2012,** 14, (31), 11139-11153.

(24) Wan, J.; Tao, T.; Zhang, Y.; Liang, X.; Zhou, A.; Zhu, C., Phosphate adsorption on novel hydrogel beads with interpenetrating network (IPN) structure in aqueous solutions: kinetics, isotherms and regeneration. *RSC Adv.* **2016,** 6, (28), 23233-23241.

(25) Nakamura, K.; Matsumoto, K., Protein adsorption properties on a microfiltration membrane: a comparison between static and dynamic adsorption methods. *J. Membr. Sci.* **2006,** 285, (1-2), 126-136.

(26) Zaitoun, A.; Kohler, N. In Two-phase flow through porous media: effect of an adsorbed polymer layer, *SPE Annual Technical Conference and Exhibition*, **1988**; Society of Petroleum Engineers: 1988.

III. EXPERIMENTAL STUDY ON CHARGED NANOGELS FOR INTERFACIAL TENSION REDUCTION AND EMULSION STABILIZATION AT VARIOUS SALINITIES AND OIL TYPES

Jiaming Geng, Pu Han, and Baojun Bai*

Department of Geosciences and Geological and Petroleum Engineering, Missouri University of Science and Technology, Rolla, MO 65401, USA

* Corresponding Author
Baojun Bai
Department of Geosciences and Geological and Petroleum Engineering
Missouri University of Science and Technology
1400 N. Bishop
Rolla, MO 65409
E-mail: baib@mst.edu

ABSTRACT

Nanoparticles have been systematically investigated for their EOR mechanisms, such as rock wettability alternation, oil displacement by disjoining pressure, and the stabilization of emulsion and foam. Nanogels are nano-sized crosslinked polymeric particles that have the properties of both nanoparticles and hydrogels. The goal of this study is to investigate the oil-water interfacial behavior in the presence of nanogels, especially the dynamic interfacial tension and the stability of oil-in-water (o/w) emulsions. The nanogels synthesized in this study are able to reduce the oil-water interfacial tension and stabilize the o/w emulsions. The diameter and zeta-potential of the charged nanogels are dramatically influenced by the brine salinity whereas the neutral charged nanogels are barely affected by salt. The synthesized nanogels are stable in

distilled water and brines at room temperature for more than 60 days. The dynamic interfacial tension results show that the nanogels are able to reduce the oil-water interfacial tension to as much as 1/30 of the original value. In addition, the interfacial tension reduction is more significant at high salinity (ranging from 10,000 to 50,000 ppm NaCl concentration). Emulsion stability results demonstrated that the stability of emulsified oil drops was controlled by both the strength of the adsorbed nanogel layers and the interactions among oil drops. The salt dependent interfacial tension and emulsion stability indicated that the appropriate charged nanogel can be a promising candidate for enhanced oil recovery.

1. INTRODUCTION

Nearly 2,000 billion barrels of conventional oil and 5,000 billion barrels of heavy oil will remain in reservoirs worldwide after conventional recovery methods have been exhausted (Thomas 2008). One reason is that much residual oil is left in porous media after water flushing due to unfavorable wetting conditions. For example, residual oil is trapped at the center of pores and throats in water-wetted reservoirs and on the rock surface in oil-wetted reservoirs (Wagner and Leach 1959). Thus, the efficiency with which water will displace oil from a porous medium is related to the nature of the capillary force present. By reducing the oil-water interfacial tension, the capillary forces can be reduced or eliminated, which helps to recover the residual oil (Fanchi 2005, Tiab and Donaldson 2015).

Emulsion system, formed by lowering interfacial tension between oil and water, has been widely investigated and applied for enhanced oil recovery for their potential to

significantly improve the oil recovery in reservoirs (Weideman 1996, Opawale and Burgess 1998). The EOR mechanisms of emulsifiers can be attributed to either reducing residual oil saturation by forming micro-emulsions (Pei et al. 2015) or improving sweep efficiency by reducing mobility ratio (Fu et al. 2012). Traditionally, surfactants have been studied to form and stabilize the emulsion. However, unsatisfactory stability of corresponding emulsions (Hirasaki 1981, Sheng 2010) and very large adsorption to rock surfaces limits their applications in oil fields. Recently, nanoparticles such as nanosilica, nano-metallic oxide, nano-clay, and nano-graphene oxide have been investigated to reduce oil-water interfacial tension, stabilize oil-in-water (o/w) emulsion and alter rock surface wettability to enhance oil recovery (Cheraghian and Hendraningrat 2016, Ahmadi and Shadizadeh 2012, Yousefvand and Jafari 2015, Cheraghian 2016, El-Diasty and Aly 2015). It is well known that the nanoparticles with suitable size and surface chemistry strongly adsorb at liquid-liquid and/or liquid/air interfaces because the adsorption lowers the total system energy. The emulsion stability is significantly increased after adsorbing nanoparticles at the interfaces because they can provide steric hindrance to prevent droplets from coalescing. Although a high desorption energy from oil-water interfaces suggests promise for a long-term stability of emulsions stabilized by nanoparticles (i.e., a Pickering emulsion), salt sensitivity limits applications of these nanoparticles to stabilize emulsions (Zhang et al. 2014). Researchers have modified the surface of these nanoparticles by grafting small molecules, oligomers, or polymers on the surface of the nanoparticles to increase their stability in brines (Bagwe et al. 2006). However, surface modification is usually costly, and an energy and time consuming process because the

synthesized/natural nanoparticles need to be re-dispersed into solvent vehicle and modified, often needing high temperature.

Recent work has shown that nano-sized crosslinked polymeric hydrogels (nanogels) have similar abilities of interfacial tension reduction and emulsion stabilization because their huge surface energy provides an irreversible adsorption of nanogels at oil-water interfaces and steric hindrance (Bizmark et al. 2014). Dangling polymer chains on the surface of nanogels can prevent the coalescence of emulsified oil drops. The hydrophilic moieties in polymer chains promise good dispensability and stability of nanogels in aqueous solutions, even in brines. The wettability of particles at the oil-water interface plays an important role in the formation and stabilization of emulsions. When the particles are more hydrophilic (contact angle < 90°), they prefer to immerse in water phase and help to form o/w emulsions, and the reverse behavior is also true (Aveyard et al. 2003). When nanogels adsorb at oil-water interface, they deform in unusual manner: the nanogels adsorbed with a flattened morphology at oil-water and prevent drops from coalescing (Pinaud et al. 2014). The nanogels were stretched out when the surface coverage is low because of the free energy gain of covering larger interfacial area was greater as compared to the energy cost of the elastic deformation of nanogels (Deshmukh et al. 2015). Hydrophilic moieties in polymer chains and the hydrophobic nature of polymer backbones provide amphoteric properties of nanogels at oil-water interfaces, which are then similar with Janus nanoparticles. Besides the particle wettability, swelling caused by osmotic pressure decrease and charge distribution of nanogels also influences the stability of produced Mickering emulsions which are emulsions stabilized by soft particles (Pickering 1907, Ramsden 1904). Pascal

demonstrated that charges are not required to ensure the stability of Mickering emulsion and that the number of charges or their spatial distribution inside the gel particles or at their periphery do not affect the way gel particles adsorb at oil-water interface. Moreover, the flow properties of corresponding Mickering emulsions was not impacted by the charge of gel particles (Massé et al. 2014). Conversely, based on Brugger's results, oil droplets stabilized by charged gel particles were better dispersed rather than forming aggregates, which resulted in a significant viscosity increase of emulsion system (Brugger et al. 2008). Some researchers believe that the stabilization of droplets is not due to electrostatic repulsion, insisting that viscoelastic properties of the interface seem to play a dominant role in determining the stability of droplets (Brugger et al. 2010). While electrostatic repulsion within nanogels definitely affect the stability of Mickering emulsions, it was neglected by these researchers due to the large size and low crosslinking density (low charge density) of their gel particles. The addition of salt leads to an increase in the degree of ionization of a pyridyl group in gel particles, increasing the hydrophilic character of the particles and hence inducing coalescence of oil drops in water, which means the salinity of brine is crucial to the stability of emulsion (Wang and Alvarado 2008). Currently, researchers are interested in the stimuli-responsive behavior of Mickering emulsions, especially in applications where surfactants are unwelcome (Brugger et al. 2009). However, in oil reservoirs, the multi-components in crude oil and the high salinity of formation fluids each would play important roles in the properties of corresponding Mickering emulsions. Unfortunately, few researchers have investigated the oil type and the salt concentration effects on the properties of corresponding Mickering emulsions.

In this paper, three nanogels with different charges were synthesized through inverse suspension polymerization as evaluated in several brines by corresponding techniques. We demonstrated how the decane/water and crude oil/water interfacial tension were reduced by adsorbing nanogels at different NaCl concentrations. The o/w emulsions stabilized by the synthesized nanogels were prepared through ultrasonic homogenization and evaluated at different NaCl concentrations at room temperature. The equilibrium emulsion volume and the creaming time were used to elucidate the mechanisms of nanogels in emulsion stabilization. The experimental procedures, results, and analysis were described next.

2. METHODOLOGY

2.1. MATERIALS

The nanogels were synthesized through a suspension polymerization using three different monomers (acrylamide, sodium salt of 2-acrylamido-2-methylpropane sulfonic acid, and [2-(acryloyloxy)ethyl]trimethylammonium chloride) and N,N'-methylenebis(acrylamide) (Geng, Ding, et al. 2018). The produced nanogels were precipitated in acetone, washed by acetone for three times, and isolated through ultracentrifuge. The white precipitation was collected and in vacuo dried at room temperature.

The synthesized nanogels (1,000 ppm) with positive, negative, and neutral charges were dispersed in sodium chloride (NaCl) solutions with the concentrations from 1,000 to 50,000 ppm.

Two oils were used in this study: n-decane (0.92 cP at room temperature) from Fisher science and a York crude oil (API 36°, 0.845g/cc, 9.25 cP) from TMD Energy, Inc.

2.2. DIAMETER AND ZETA-POTENTIAL OF NANOGELS

The diameter and zeta-potential of the synthesized nanogels were measured at different brine concentrations at room temperature using a Malvern Nanosizer ZS90.

2.3. DYNAMIC INTERFACIAL TENSION MEASUREMENTS

The interfacial tension between oil and nanogel dispersions was determined by the axisymmetric drop shape analysis using pendant drop method (Ramé-hart advanced goniometer 500-F1). The oil drop (decane and crude oil) was immersed in the nanogel dispersions from a precise syringe. The interfacial tension between oil and water was measured as soon as the oil droplet was formed. The interfacial tension values were obtained using the Young-Laplace equation.

2.4. O/W EMULSION STABILITY MEASUREMENTS

To prepare the oil-in-water (o/w) nanogel emulsions, nanogel dispersions at different NaCl concentrations (1000, 2000, 5000, 10000, and 50000 ppm) were prepared by dispersing nanogel powders in NaCl solutions. Then, the nanogel dispersion was mixed with decane/ crude oil at a volume ratio of 9:1. The mixture had a total volume of 10 mL and was emulsified using an ultrasonic homogenizer (VC-1500, Sonics & Materials Inc.) with a CV-294 probe at 160 W for 60 seconds. The emulsion stability was

determined by monitoring the volume of emulsion phase as a function of time. The creaming time of emulsions was considered as an important parameter to characterize the repulsions among the emulsified oil drops.

3. RESULTS AND DISCUSSIONS

3.1. HYDRODYNAMIC DIAMETER AND ZETA-POTENTIAL OF NANOGELS

The dried powder of nanogels was dispersed in several brines. After that, the nanogel dispersions were aged at 60 °C for 24 hours so that the nanogels can reach their fully swelling state. The hydrodynamic diameter of the positive and negative charged nanogels were more sensitive to the salt concentration compared with the neutral charged nanogels (Figure 1). The diameter of anionic and cationic nanogels gradually decreased from 273.2 to 248.6 nm and from 207.1 to 170.2 nm, respectively, as the NaCl concentration increased from 1,000 to 10,000 ppm. Above the concentration of 10,000 ppm, the hydrodynamic diameter of charged nanogels was merely influenced by NaCl. The ionic moieties of the nanogels, the sulfonic groups of anionic nanogels and the quaternary amine of cationic nanogels provided the electrostatic repulsion among the polymer chains that leaded to the swelling of nanogels. However, the sodium and chloride ions in the brines reduced the electrostatic repulsions among the polymer chains, which induced the shrinkage of the polymeric networks of nanogels. As a result, the hydrodynamic diameter of charged nanogels was smaller at higher NaCl concentration. Moreover, with the NaCl concentration further increasing, the hydrodynamic diameter of the charged nanogels was more dependent on the affinity between water and the polymeric networks. Thus, the hydrodynamic diameter of charged nanogels became

constant at the NaCl above 10,000 ppm. For the neutral charged nanogels, the hydrodynamic diameter was slightly affected by the NaCl presumably due to the hydrolysis of amide moieties to carboxylic groups.

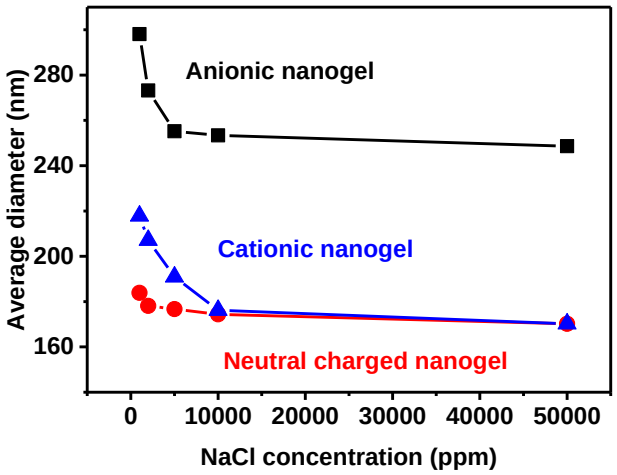

Figure 1. Average hydrodynamic diameter of cationic, anionic, and neutral charged nanogels at various NaCl concentrations.

Furthermore, the zeta-potential of nanogels, a parameter reflects the stability of their dispersions, was related to the NaCl concentration. As shown in Figure 2, the zeta-potential of anionic nanogels increased by the NaCl from -53.25 to -26.25 mV whereas the zeta-potential of cationic nanogels decreased from 47 to 13.75 mV. However, for the neutral charged nanogels, the zeta-potential was barely affected by the NaCl and kept ~ -2 mV as the NaCl concentration increased from 1,000 to 50,000 ppm.

For the nanogel dispersions, a high zeta-potential confers the stability of nanogels that the electrostatic repulsions can exceed the attractive force and resist aggregation and /or flocculation. The increased ionic strength (NaCl concentration) reduced the zeta-

potential of charged nanogels by screening effect. However, compared with rigid nanoparticles, such as nanosilica and nano-Fe_2O_3 (Metin et al. 2011), the hydrophilic polymer chains of the nanogels enhanced the stability of dispersed nanogels.

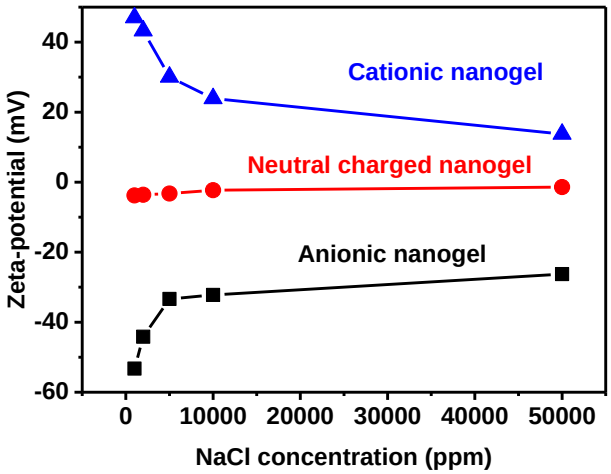

Figure 2. Zeta-potential of cationic, anionic, and neutral charged nanogels at various NaCl concentrations.

3.2. SALINITY EFFECT ON THE OIL-WATER INTERFACIAL TENSION REDUCTION

The interfacial tension between crude oil and brines as well as between decane and brines was measured by pendant drop method at room temperature. As shown in Figure 3, the interfacial tension between crude oil and water decreased from 37.03 to 28.32 mN/m as the NaCl concentration increased from 0 to 50,000 ppm. However, for decane and water, the interfacial tension was not influenced by NaCl as much as crude oil and water. The salinity related interfacial tension of crude oil was caused by the dissolved charged composites. When the salinity of surrounding solution increased, the attraction was increased of the water molecules to the crude oil molecules at the oil-water

interfaces. Compared with crude oil, the non-polar property of decane molecules hindered the screening effect from NaCl and resulted in the salt-independent interfacial tension.

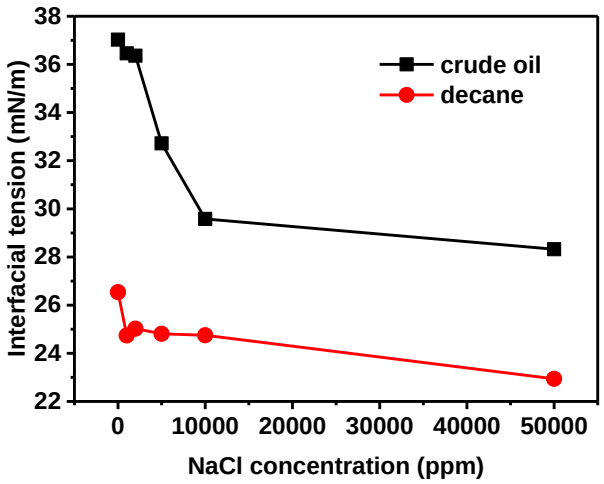

Figure 3. The equilibrium crude oil/water and decane/water interface tension at various NaCl concentrations.

Nanogels can markedly alter the oil-water interfacial properties by adsorption, resulting from huge surface due to the small size of nanogels (Fan and Striolo 2012, Du et al. 2010). The interfacial tension between oil and water can be decreased by microgels and nanogels through adsorption (Geng, Pu, et al. 2018, Aveyard et al. 2003). The nanogels are able to deform at the oil-water interfaces driven by the polymer-solvent affinity. Herein, the dynamic interfacial tension measurements between decane/ crude oil and nanogel dispersions were performed and discussed in detail. A typical interfacial tension kinetic between decane and cationic nanogels at 1,000 ppm NaCl was displayed in Figure 4. The dynamic interfacial tension can be divided into three stages: the early

stage that both the interfacial tension and the surface area decreased rapidly; the second stage that the interfacial tension and surface area decreased at a slower rate; the third stage that the surface area of oil drop keep constant while the interfacial tension kept decreasing; and the last stage that the interfacial tension reach the equilibrium value. Compared with the nanoparticles reported by Bizmark (Bizmark et al. 2014), the decrease of the oil-water interfaces in the presence of nanogels was much quicker due to the higher diffusivity of the nanogels. After the early stage, which was dominated by the diffuse process of nanogels from the nanogel dispersion to the oil-water interface, the ordering and rearrangement of nanogels at the interface started to control the interfacial tension kinetic (Dugyala et al. 2016). At the second stage, the coverage of nanogels at the oil-water interface continuously increased leaded to a further decreasing in both interfacial tension and surface area. When the nanogels had a high coverage at the oil-water interface, the adsorbed nanogels hindered the continuous adsorption of nanogels from the dispersion and the deformation of nanogels contributed to the reduction of interfacial tension. At the last stage, the kinetic reached an equilibrium state with no more change in the interfacial tension. The surface area slowly increased presumably due to the buoyance of the pendent oil drop.

Interfacial tension kinetics were recorded using three nanogel dispersions (cationic, anionic, and neutral charged nanogels) at different NaCl concentrations and two oils (decane and crude oil) at room temperature (Figure 5). All the dynamic interfacial tension exhibited similar profile that suggesting the nanogels functioned in a similar fashion of reducing interfacial tension, even at different NaCl concentrations. The

decane/water interfacial tension was reduced from ~26 to ~11, 4, and 8 mN/m by cationic, anionic, and neutral charged nanogels, respectively.

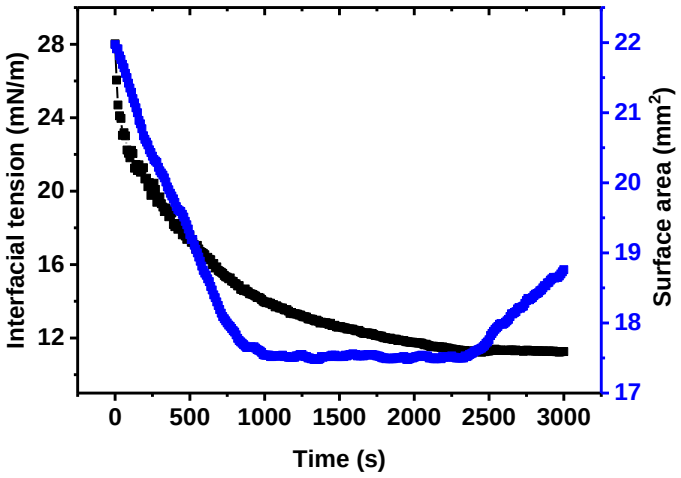

Figure 4. Dynamic interfacial tension and surface area of pendant oil drop of decane immersed in cationic nanogel dispersion at 1000 ppm NaCl.

The time to achieve the equilibrium state of neutral charged nanogels was the shortest among that of anionic and cationic nanogels. Moreover, the equilibrium interfacial tension of nanogels was influenced by the NaCl concentration of the nanogel dispersions that both low and high salinity helped to further reduce the decane/water interfacial tension.

The dynamic interfacial tension profiles between crude oil and water were similar with that between decane and water. However, the brine concentration effects on the equilibrium interfacial tension were different. As shown in the Figure 6, the equilibrium interfacial tension between crude oil and water was inverse proportion to the NaCl concentration by adsorbing cationic nanogels. The anionic and neutral charged nanogels

also showed a similar behavior that at 50,000 ppm NaCl concentration, the equilibrium interfacial tension achieved its minimum value.

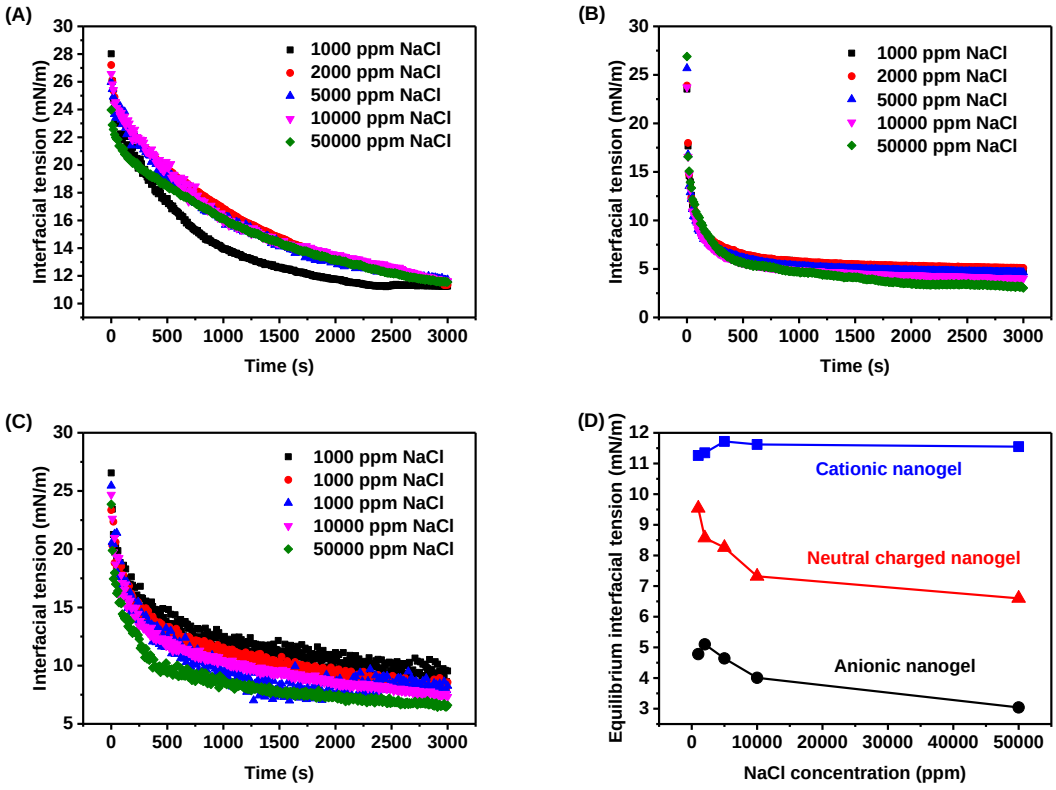

Figure 5. Dynamic interfacial tension between decane and water in the presence of (A) cationic nanogels, (B) anionic nanogels, and (C) neutral charged nanogels at NaCl concentrations varies from 1000 to 50000 ppm. (D) Equilibrium interfacial tension between decane and water at various NaCl concentrations with nanogels.

Nanogels decreased the interfacial tension through forming irreversible adsorbing layer at the oil-water interface. The ability of nanogels for interfacial tension reduction was related to not only the diameter but also the mechanical strength of the nanogels (Thieme et al. 1999). At low salinity (e.g. 1,000 ppm NaCl), the larger size of nanogels hindered the continuous adsorption and limited the amount of nanogels adsorbed at the oil-water interface. Meanwhile, the weak mechanical strength of nanogels at low salinity

rendered the nanogels efficiently deformation, which resulted in a high coverage of nanogels at the oil-water interfaces. Vice versa, nanogels became smaller and more rigid at higher salinity and influenced the interfacial tension by their coverage at the oil-water interface. Furthermore, the sodium and chloride ions in brines would reduce the electrostatic repulsion among the charged nanogels at the oil-water interface, which markedly increased the stability of adsorbed nanogel layers. Thus, high salinity enhanced the ability of nanogels for oil-water interfacial tension reduction.

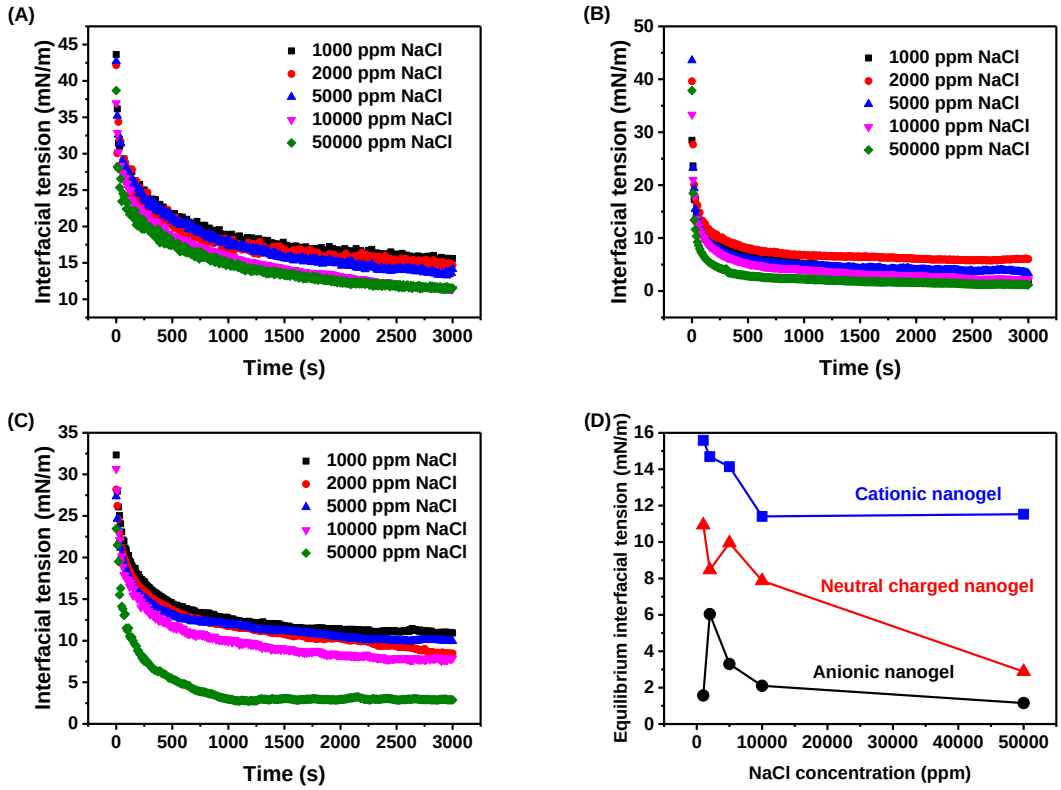

Figure 6. Dynamic interfacial tension between crude oil and water in the presence of (A) cationic nanogels, (B) anionic nanogels, and (C) neutral charged nanogels at NaCl concentration varies from 1000 to 50000 ppm. (D) Equilibrium interfacial tension between crude oil and water at various NaCl concentrations with nanogels.

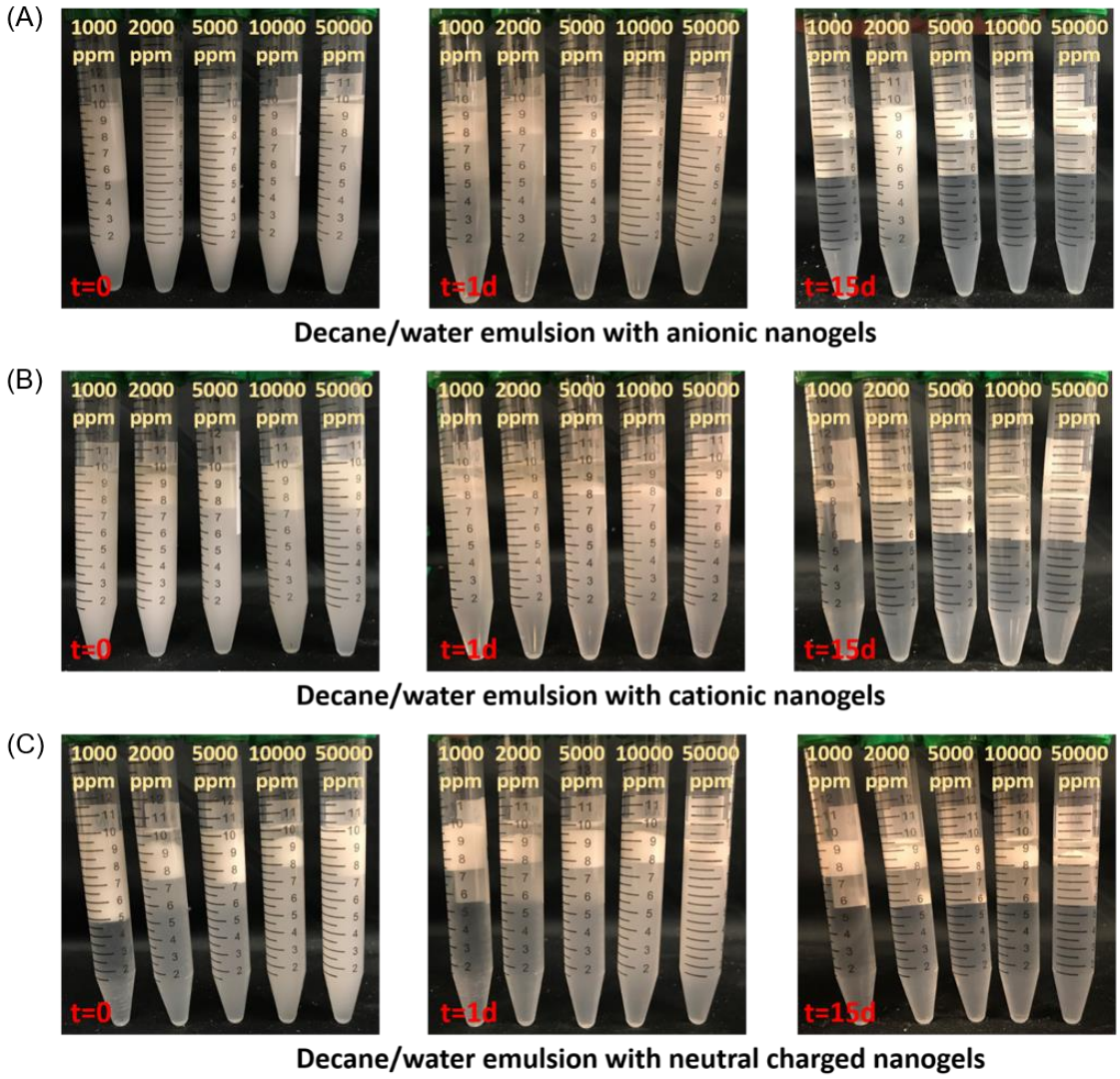

Figure 7. Photos of decane-in-water emulsions stabilized by (A) cationic nanogels, (B) anionic nanogels, and (C) neutral charged nanogels at various NaCl concentrations immediately, 1 day, and 15 days after the ultrasonic homogenization.

In our experiments, the emulsion stability was elucidated by the creaming and the emulsion volume kinetics. Figure 7 and Figure 8 show the photos of o/w emulsions stabilized by the nanogels immediately, 1 day, and 15 days after the ultrasonic homogenization. The emulsified oil droplets spontaneously float up due to the differential density between oil and water. An obvious creaming was found in the o/w emulsions

stabilized by neutral charged nanogels. Moreover, the creaming tuned to become more markedly at a higher NaCl concentration. These features indicated that the creaming of emulsion was controlled by both the buoyance of emulsified oil droplets and the interparticle forces.

The charges from nanogels introduced electrostatic repulsions among the adsorbed nanogel layers at the oil-water interfaces of each emulsified oil droplets. Meanwhile, by increasing the NaCl concentration, the electrostatic repulsion among emulsified oil drops was reduced significantly that resulted in the salt-related creaming.

The crude oi/water emulsions displayed a similar profile with the decane/water emulsions. However, the creaming of emulsions stabilized by cationic nanogels was much faster than that of anionic nanogels. The negative charge of crude oil enhanced the dispersity of emulsified oil drops by increasing the electrostatic repulsion among oil drops and nanogels. Nevertheless, the similar charges of crude oil and anionic nanogels hindered the adsorption of nanogels at the oil-water interface that resulted in an unstable o/w emulsion.

From the emulsion volume kinetics (Figure 9), the equilibrium emulsion volume indicated that, for decane/water emulsions, the emulsion stability was greatly influenced by the NaCl concentration whereas for crude oil/water emulsions, the emulsions stabilized by cationic nanogels showed some salt resistant properties. In all, the decane/water emulsions had their best stability at NaCl concentrations of 2,000 ppm for cationic nanogels and 5,000 ppm for anionic and neutral charged nanogels while the best stability of crude oil/water emulsions occurred at 1,000 ppm NaCl concentration. The emulsion stability was controlled by the strength of the adsorbed nanogel layers and the

interactions among emulsified oil drops (Cunningham et al. 2017, Chevalier and Bolzinger 2013). At high NaCl concentration, the nanogels were smaller and more rigid at the oil/water interfaces. As the strength of nanogel layers was relayed on the coverage of nanogels at the oil/water interfaces, the softer and smaller nanogels were more presumably to form a stronger adsorbed layer.

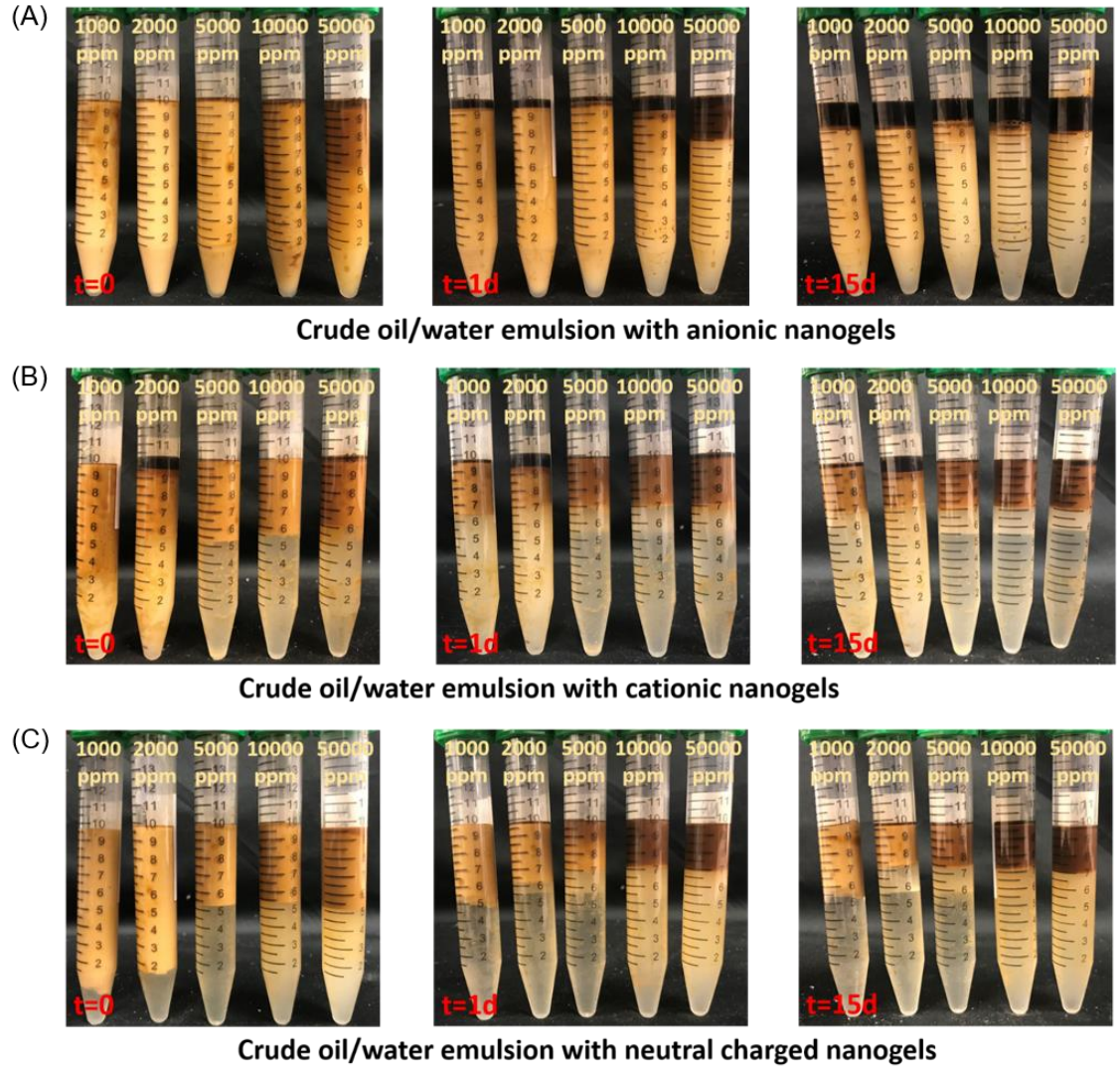

Figure 8. Photos of crude oil-in-water emulsions stabilized by (A) cationic nanogels, (B) anionic nanogels, and (C) neutral charged nanogels at various NaCl concentrations immediately, 1 day, and 15 days after the ultrasonic homogenization.

In addition, the electrostatic repulsion among adsorbed nanogel layers shielded the oil drops to prevent coalescence. Although the crude oil/water emulsions stabilized by anionic nanogels were very stable at low NaCl concentrations (<2,000 ppm), the salinity influenced the emulsions more obvious than emulsions stabilized by cationic and neutral charged nanogels due to screening effect from additional salt. In our previous study, we found that the oil-to-water ratio has a positive effect on equilibrium emulsion volume whereas the stability of emulsion shows similar trend and with the ratio varying from 1:9 to 5:5. (Geng, Pu, et al. 2018) Therefore, brine salinity and charge of nanogels have more significant impacts on emulsion stability than oil-to-water ratio. Our results suggested that nanogel sustains reliable stability of oil-in-water emulsion, especially at high salinity conditions (ranging from 10,000 to 50,000 ppm NaCl concentration).

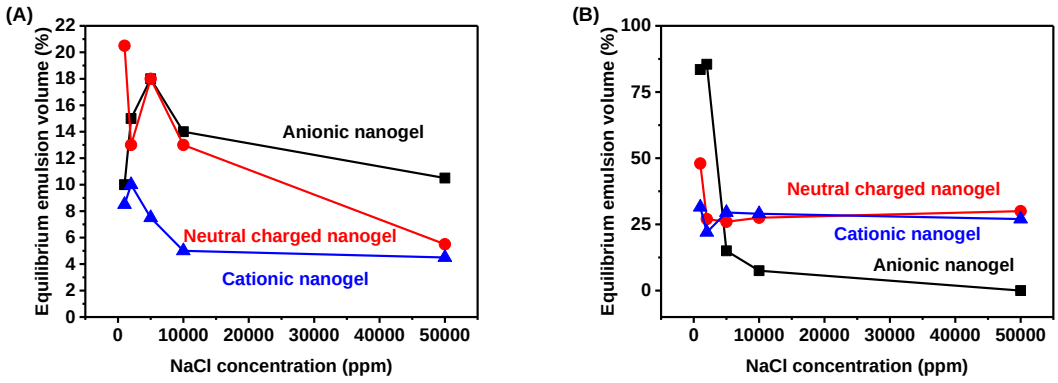

Figure 9. Equilibrium emulsion volume of (A) decane/water emulsions and (B) crude oil/water emulsions stabilized by nanogels at various NaCl concentrations.

4. CONCLUSION

The nanogels with different charges synthesized in this study can adsorb at the oil/water interfaces and reduce the oil/water interfacial tension. The o/w emulsions

stabilized by the synthesized nanogels are able to be stable at various NaCl concentrations. The following conclusions can be drawn from this study:

- The swelling ratio of anionic and cationic nanogels is related to NaCl concentrations whereas the swelling of neutral charged nanogels is independent to NaCl concentrations.
- The zeta-potential of charged nanogels is dominated by the NaCl concentration that at the higher NaCl concentration, the lower zeta-potential (absolute value) of nanogels.
- The nanogels are able to reduce the oil/water interfacial tension by adsorbing at the oil/water interfaces. Among three nanogels, anionic nanogels have the best performance in interfacial tension reduction.
- The equilibrium oil/water interfacial tension decreases with an increased NaCl concentration.
- The creaming of nanogel-stabilized o/w emulsions is dominated by the electrostatic repulsions among the emulsified oil drops and dispersed nanogels. The emulsions stabilized by charged nanogels have a longer creaming time than ones stabilized by neutral charged nanogels.
- The emulsion stability is dominated by the charge of nanogels and the salinity. For crude oil/water emulsions stabilized by cationic and neutral charged nanogels, the emulsion stability is independent of the NaCl concentration as high as 50,000 ppm.
- The interfacial tension kinetic and emulsion stability are influenced by the oil types. The interfacial tension of negative-charged crude oil reduced faster and reached a

lower equilibrium value than that of decane. Furthermore, the crude oil-in-water emulsion is more stable than the decane-in-water emulsion.

REFERENCES

Ahmadi, Mohammad Ali and Shadizadeh, Seyed Reza. 2012. Adsorption of novel nonionic surfactant and particles mixture in carbonates: enhanced oil recovery implication. *Energy & Fuels* **26** (8): 4655-4663.

Aveyard, Robert, Binks, Bernard P, and Clint, John H. 2003. Emulsions stabilised solely by colloidal particles. *Advances in Colloid and Interface Science* **100**: 503-546.

Bagwe, Rahul P, Hilliard, Lisa R, and Tan, Weihong. 2006. Surface modification of silica nanoparticles to reduce aggregation and nonspecific binding. *Langmuir* **22** (9): 4357-4362.

Bizmark, Navid, Ioannidis, Marios A, and Henneke, Dale E. 2014. Irreversible adsorption-driven assembly of nanoparticles at fluid interfaces revealed by a dynamic surface tension probe. *Langmuir* **30** (3): 710-717.

Brugger, Bastian, Rütten, Stephan, Phan, Kim‐Ho et al. 2009. The colloidal suprastructure of smart microgels at oil–water interfaces. *Angewandte Chemie* **121** (22): 4038-4041.

Brugger, Bastian, Rosen, Brian A, and Richtering, Walter. 2008. Microgels as stimuli-responsive stabilizers for emulsions. *Langmuir* **24** (21): 12202-12208.

Brugger, Bastian, Vermant, Jan, and Richtering, Walter. 2010. Interfacial layers of stimuli-responsive poly-(N-isopropylacrylamide-co-methacrylicacid)(PNIPAM-co-MAA) microgels characterized by interfacial rheology and compression isotherms. *Physical Chemistry Chemical Physics* **12** (43): 14573-14578.

Cheraghian, Goshtasp. 2016. Application of nano-fumed silica in heavy oil recovery. *Petroleum Science and Technology* **34** (1): 12-18.

Cheraghian, Goshtasp and Hendraningrat, Luky. 2016. A review on applications of nanotechnology in the enhanced oil recovery part B: effects of nanoparticles on flooding. *International Nano Letters* **6** (1): 1-10.

Chevalier, Yves and Bolzinger, Marie-Alexandrine. 2013. Emulsions stabilized with solid nanoparticles: Pickering emulsions. *Colloids and Surfaces A: Physicochemical and Engineering Aspects* **439**: 23-34.

Cunningham, Victoria J, Giakoumatos, Emma C, Ireland, Peter M et al. 2017. Giant Pickering droplets: effect of nanoparticle size and morphology on stability. *Langmuir* **33** (31): 7669-7679.

Deshmukh, Omkar S, van den Ende, Dirk, Stuart, Martien Cohen et al. 2015. Hard and soft colloids at fluid interfaces: Adsorption, interactions, assembly & rheology. *Advances in colloid and interface science* **222**: 215-227.

Du, Kan, Glogowski, Elizabeth, Emrick, Todd et al. 2010. Adsorption energy of nano- and microparticles at liquid− liquid interfaces. *Langmuir* **26** (15): 12518-12522.

Dugyala, Venkateshwar Rao, Muthukuru, Jyothi Sri, Mani, Ethayaraja et al. 2016. Role of electrostatic interactions in the adsorption kinetics of nanoparticles at fluid–fluid interfaces. *Physical Chemistry Chemical Physics* **18** (7): 5499-5508.

El-Diasty, Abdelrahman Ibrahim and Aly, Ahmed M. 2015. Understanding the mechanism of nanoparticles applications in enhanced oil recovery. *Proc.*, SPE North Africa Technical Conference and Exhibition.

Fan, Heng and Striolo, Alberto. 2012. Nanoparticle effects on the water-oil interfacial tension. *Physical Review E* **86** (5): 051610.

Fanchi, John R. 2005. Principles of applied reservoir simulation: Elsevier.

Fu, Xuebing, Lane, Robert H, and Mamora, Daulat Debataraja. 2012. Water-in-Oil emulsions: flow in porous media and EOR potential. *Proc.*, SPE Canadian Unconventional Resources Conference.

Geng, Jiaming, Ding, Haifeng, Han, Pu et al. 2018. The transportation and potential enhanced oil recovery mechanisms of nanogels in sandstone. *Energy & Fuels*.

Geng, Jiaming, Pu, Jingyang, Wang, Lizhu et al. 2018. Surface charge effect of nanogel on emulsification of oil in water for fossil energy recovery. *Fuel* **223**: 140-148.

Hirasaki, George J. 1981. Application of the theory of multicomponent, multiphase displacement to three-component, two-phase surfactant flooding. *Society of Petroleum Engineers Journal* **21** (02): 191-204.

Massé, Pascal, Sellier, Elisabeth, Schmitt, Véronique et al. 2014. Impact of Electrostatics on the Adsorption of Microgels at the Interface of Pickering Emulsions. *Langmuir* **30** (49): 14745-14756.

Metin, Cigdem O, Lake, Larry W, Miranda, Caetano R et al. 2011. Stability of aqueous silica nanoparticle dispersions. *Journal of Nanoparticle Research* **13** (2): 839-850.

Opawale, Foyeke O and Burgess, Diane J. 1998. Influence of interfacial properties of lipophilic surfactants on water-in-oil emulsion stability. *Journal of colloid and interface science* **197** (1): 142-150.

Pei, HH, Zhang, GC, Ge, JJ et al. 2015. Investigation of nanoparticle and surfactant stabilized emulsion to enhance oil recovery in waterflooded heavy oil reservoirs. *Proc.,* SPE Canada Heavy Oil Technical Conference.

Pickering, Spencer Umfreville. 1907. Cxcvi.—emulsions. *Journal of the Chemical Society, Transactions* **91**: 2001-2021.

Pinaud, Florent, Geisel, Karen, Massé, Pascal et al. 2014. Adsorption of microgels at an oil–water interface: correlation between packing and 2D elasticity. *Soft Matter* **10** (36): 6963-6974.

Ramsden, W. 1904. Separation of solids in the surface-layers of solutions and ‘suspensions’(observations on surface-membranes, bubbles, emulsions, and mechanical coagulation).—Preliminary account. *Proceedings of the royal Society of London* **72** (477-486): 156-164.

Sheng, JJ. 2010. Optimum phase type and optimum salinity profile in surfactant flooding. *Journal of Petroleum Science and Engineering* **75** (1-2): 143-153.

Thieme, J, Abend, S, and Lagaly, G. 1999. Aggregation in Pickering emulsions. *Colloid and Polymer Science* **277** (2-3): 257-260.

Thomas, S. 2008. Enhanced oil recovery-an overview. *Oil & Gas Science and Technology-Revue de l'IFP* **63** (1): 9-19.

Tiab, Djebbar and Donaldson, Erle C. 2015. Petrophysics: theory and practice of measuring reservoir rock and fluid transport properties: Gulf professional publishing.

Wagner, OR and Leach, RO. 1959. Improving oil displacement efficiency by wettability adjustment. *Transactions of the AIME* **216** (01): 65-72.

Wang, Xiuyu and Alvarado, Vladimir. 2008. Effect of salinity and pH on pickering emulsion stability. *Proc.*, SPE Annual Technical Conference and Exhibition.

Weideman, A. 1996. Regulation of Produced Water by the US Environmental Protection Agency in Produced Water 2: Environmental Issues and Mitigation Technologies, International Produced Water Symposium, M. Reed and S. Johnsen, eds, Plenum Press, New York (Reprint).

Yousefvand, H and Jafari, A. 2015. Enhanced oil recovery using polymer/nanosilica. *Procedia Materials Science* **11**: 565-570.

Zhang, Hua, Nikolov, Alex, and Wasan, Darsh. 2014. Enhanced oil recovery (EOR) using nanoparticle dispersions: underlying mechanism and imbibition experiments. *Energy & Fuels* **28** (5): 3002-3009.

IV. PH-RESPONSIVE PICKERING EMULSION STABILIZED BY POLYACRYLAMIDE NANOGELS FOR CRUDE OIL RECOVERY

Jiaming Geng†, *Jingyang Pu*†, *Yang Zhao*†, *Baihua Lin*†, *Baojun Bai**†, *and Schuman P. Thomas**‡

†Department of Geosciences and Geological and Petroleum Engineering, Missouri University of Science and Technology, Rolla, MO 65401, USA

‡Department of Chemistry, Missouri University of Science and Technology, Rolla, MO 65401, USA

*Corresponding Author:
Baojun Bai and Schuman Thosmas
Department of Geosciences and Geological and Petroleum Engineering
Missouri University of Science and Technology
1400 N. Bishop
Rolla, MO 65409
E-mail: baib@mst.edu; tschuman@mst.edu

ABSTRACT

Oil-in-water (o/w) Pickering emulsions stabilized by polyacrylamide (PAM) and poly(acrylamide-co-acrylic acid) nano-sized crosslinked polymeric particles (nanogels) under varies conditions are described herein. Nanogels with different crosslinking and charge degree were synthesized through suspension polymerization and characterized at various salinities and pH using dynamic light scattering (DLS) and scanning electron microscopy (SEM). The PAM nanogel-stabilized o/w Pickering emulsions were quickly demulsified in alkaline solutions whereas showed markedly stability in brines and under acidic conditions. Small amount of nanogels were sufficient for the formation of

Pickering emulsions as the average diameter of oil droplets was no longer decreased above the critical nanogel concentration of 1000 mg/L. In addition, the average diameter of oil drops showed to be independent of sonication period in the range of 15 to 240 s. Interestingly, the string-like structures of nanogels were found in the aromatic hydrocarbons/water Pickering emulsions, which significantly enhanced the emulsion stability. Compared to the crude oil, the corresponding Pickering emulsions showed excellent flow ability at various shear rates. The crude oil/water Pickering emulsions could be efficiently break triggered by alkaline, which suggest the potential utility for the recovery of crude oil.

Key words: Pickering emulsion; Nanogel; Enhanced oil recovery.

1. INTRODUCTION

Pickering emulsions[1], first recognized by Ramsden[2], consist in a class of emulsions stabilized by solid colloids. Compared with the Pickering emulsions stabilized by rigid colloids, the Pickering emulsions stabilized by soft gel particles have attracted much research attention because their stimuli-responsive properties open an avenue to prepare and break the emulsions on demand[3]. The temperature- and pH-responsive properties render Pickering emulsions the practical applications in food[4, 5], cosmetic[6], pharmacy[7-9], enzyme catalysis[10-12], and petroleum industry[13, 14], where controllable emulsion stability is essential.

The soft gel particles are able to spontaneously assemble at the oil-water interface and reduce the interfacial tension[15, 16]. In addition, the adsorbed gel particle layer at the oil-water interface can prevent the coalescence of oil drops by steric hindrance[17].

The anisotropic deformation of gel particles at the interface, which is caused by the different hydrophilicity of polymer backbones and the moieties consisted in the gel particles, helps to further improve the stability of Pickering emulsions[18, 19]. Furthermore, by stimulating the adsorbed gel particles, the Pickering emulsions are able to break in a short term. Currently, the temperature-responsive microgels, poly(N-isopropylamide) (PNIPAM)[20] and poly(N-isopropylamide-co-methacrylic acid) (PNIPAM-co-MAA)[18, 21], were applied to prepare the Pickering emulsions that were susceptible to temperature induced destabilization. The PNIPAM microgels are likely shrinking above their volume phase transition temperature (VPTT), which results in the breakage of corresponding Pickering emulsions. Ngai *et al.* proposed that the PNIPAM-co-MAA microgels at the interface likely to move deeper into the oil phase at high temperature due to the shrinkage of PNIPAM-co-MAA microgels[2]. The resulted reduction in the interface coverage decreased the stability of oil droplets and eventually broke the Mickering emulsions. However, the reservoir temperature is generally higher than the VPTT of temperature-responsive microgels, which is unable to form stable Pickering emulsions subsurface. Thus, the need for generation of stable Pickering emulsions at reservoir conditions that can be quickly broken at surface boost the development of stimuli-responsive Pickering emulsions.

A verity of pH-responsive microgels have been executed to generate Pickering emulsions that are easily break at acid or basic condition. For example, the tertiary and secondary amine group consisted in the poly(2-(diethylamino)ethyl methacrylate)[22, 23] and poly (2-(tert-butylamino)ethyl methacrylate)[24] microgels protonate at acid condition. The positive charges from protonated amine groups generate electrostatic

repulsions among the microgels adsorbed at the oil-water interfaces, which results in the breakage of the Pickering emulsions. However, the negative charges of crude oil might influence the breaking process of Pickering emulsions stabilized by acid-responsive microgels[25]. We envision that the Pickering emulsions stabilized by alkali-responsive microgels could provide an approach to break crude oil-in-water Pickering emulsions.

Inspired by the pH-responsive properties of gel particles, we sought to prepare stable Pickering emulsions that can be easily break at basic condition. Herein, we synthesized poly(acrylamide-co-acrylic acid) nanogels of different crosslinking and charge degrees through the free-radical suspension polymerization. We demonstrated the polyacrylamide-based nanogels are neutral charged at pH below 7 and negative charged at pH above 9. The size distribution analysis and emulsion state studies confirmed the nanogels can help to generate stable Pickering emulsions. Interestingly, the stability of the Pickering emulsions showed to be independent with the ultrasound time. Furthermore, it has been demonstrated that the Pickering emulsions stabilized by polyacrylamide-based nanogels were able to easily break at basic condition. The pH-responsive nanogels with the ability to stabilize oil-in-water Pickering emulsions offered the method up to date to produce crude oil from underground and separate at surface cost-effectively.

2. EXPERIMENTAL

2.1. MATERIALS

Acrylamide (AM), acrylic acid (AA), sodium hydroxide, n-decane, and sorbitane monooleate (Span® 80) were purchased from Alfa Aesar. Sodium chloride, hydrochloric

acid, N, N'-bismethylacrylamide (MBAA), ammonium persulfate, benzene, acetone, and polyethylene glycol sorbitan monostearate (Tween® 60) were purchased from Sigma-Aldrich. Hexane, cyclohexane, toluene, xylenes, octane, and n-dodecane were purchased from Oakwood Chemical. Nile red was from Molecular Probes. The light oil (API 19°, 0.94 g/mL) and the heavy oil (API 17.2°, 0.952 g/mL) from Alaska were used as received.

2.2. SYNTHESIS OF POLYACRYLAMIDE (PAM) NANOGEL

A solution of AM and MBAA in water with a total weight of 30 g (**Table 1**) was added to the mixture of Span 80 (21 g), Tween 60 (9 g), and decane (40 g). The mixture was degassed with nitrogen for 15 min at 40 ℃ before ammonium persulfate (20 mg, 0.088 mmol) added to initiate the polymerization. The mixture was stirred at 40 ℃ for 2 h with nitrogen purging before precipitated in acetone (500 mL) The PAM nanogel was further purified by acetone washing and dried *in vacuo* at 60 ℃ to give as a white solid.

2.3. SYNTHESIS OF POLY(ACRYLAMIDE-CO-ACRYLIC ACID) (PAM-CO-AA) NANOGEL

The PAM-co-AA nanogel was prepared in a similar fashion as the synthesis of PAM nanogel. A solution of AM, AA, and MBAA in water was suspended in the mixture of Span80, Tween 60, and decane, and then, polymerized at 40 ℃ for 2 h with nitrogen purging (Table 1). The synthesize nanogels were precipitated using acetone and dried in 60 ℃ oven after acetone for three times. The produced white powder was collected for the following characterization and evaluation.

Table 1. Synthetic parameters and physicochemical properties of the PAM and PAM-co-AA nanogels.

Nanogel	AM (g)	AA (g)	MBA (g)	Hydrodynamic diameter (nm)	Zeta potential (mV)	PH
$PAM_{100}MBA_{1}$	10.6619	0	0.2315	206	-9.186	7.0
$PAM_{100}MBA_{0.5}$	10.6634	0	0.1171	113	-8.23	7.2
$PAM_{100}MBA_{0.2}$	10.6635	0	0.0463	191	-4.746	7.2
$PAM_{100}MBA_{0.1}$	10.6624	0	0.0231	225	-1.913	7.1
$PAM_{100}MBA_{0.05}$	10.6623	0	0.0123	165	-2.272	7.2
$PAM_{90}AA_{10}$	9.5958	1.0801	0.0231	364	-28.65	5.0
$PAM_{80}AA_{20}$	8.5299	2.1627	0.0230	468	-33.57	4.6
$PAM_{70}AA_{30}$	7.4633	3.2425	0.0235	532	-36.62	4.4
$PAM_{60}AA_{40}$	6.3969	4.3236	0.0233	638	-38.12	4.4

2.4. PREPARATION OF PICKERING EMULSIONS STABILIZED BY NANOGELS

NaCl solutions with salt concentrations from 0 to 2 wt.% were subjected to prepare the nanogel dispersions. The nanogel dispersions were aged at 60 ℃ for 12 h to let nanogels fully swell and then, mixed with the oil at a water to oil ratio of 9:1 and sonicated to form the Pickering emulsions.

2.5. NANOGELS AND PICKERING EMULSIONS CHARACTERIZATION

Size distribution and zeta potential of the nanogels at different pH and salt concentrations were measured using a Malvern Nanosizer ZS90 at 25 ℃. The size

distribution of the Pickering emulsions were elucidated using an Olympus microscope 48 h after the emulsion preparation while the digital photos of the Pickering emulsions were taken 24 h after preparation. The average diameter and size distributions of the emulsified oil droplets were calculated from the images of the emulsions. The microstructures of the lyophilized emulsion droplets were elucidated using a Hitachi S4700 FESEM microscope at 15.0 kV accelerating voltage. The samples were freeze-dried and sputter coated with Au/Pd prior to imaging.

3. RESULTS AND DISCUSSIONS

3.1. PHYSICOCHEMICAL PROPERTIES OF NANOGEL

The Nanogels are crosslinked polymeric particles with dried particle size in the range from 1 to 100 nm that are able to swell tens to several hundred times in water. Herein, PAM and PAM-co-AA nanogels, which can swell from 30-50 to several hundred nm in water, were prepared using the free radical suspension polymerization (Table 1). Microstructures of nanogels under hydrated state govern their behavior at the oil-water interface in reservoir environments. The microstructure of fully swelled nanogels were elucidated using SEM from the freeze-dried samples. PAM nanogels showed porous network with pore size of ~10 to 100 nm while maintained a spherical configuration. The porous microstructures may contribute to the anisotropic deformation of nanogels at the oil-water interface and enhance the responding rate of nanogels to the surrounding environment[26].

The stimuli-responsive behaviors of nanogels to the surrounding environment are important parameters for the Pickering emulsions breaking on demand. The

hydrodynamic diameter and zeta potential were applied to illustrate the stimuli-responsive behaviors of nanogels under various environmental conditions. As indicated in Figure 1A, the hydrodynamic diameter and zeta potential of PAM nanogels were almost independent to the increased NaCl concentration. The salinity insensitive properties of the PAM nanogels was due to the neutral charged acrylamide moieties in the polymeric networks. Apparently as shown in Figure 1B, the hydrodynamic diameter and zeta potential of PAM nanogels were almost constant in the acidic solutions (pH in the range from 1.0 to 7.0). However, at alkaline environments, the size of the PAM nanogels increased as pH increase. For example, the nanogel had the hydrodynamic diameter of ~200 nm at pH 7.0 while the nanogel at pH 13.0 showed 2.5 times in diameter. Meanwhile, the zeta potential of the PAM nanogels reduced from ~-2 to ~-25 mV when pH spanned from 7.0 to 13.0. Therefore, the PAM nanogels had good resistance against salinity and acidic conditions as well as the responsive behaviors to the alkaline environments.

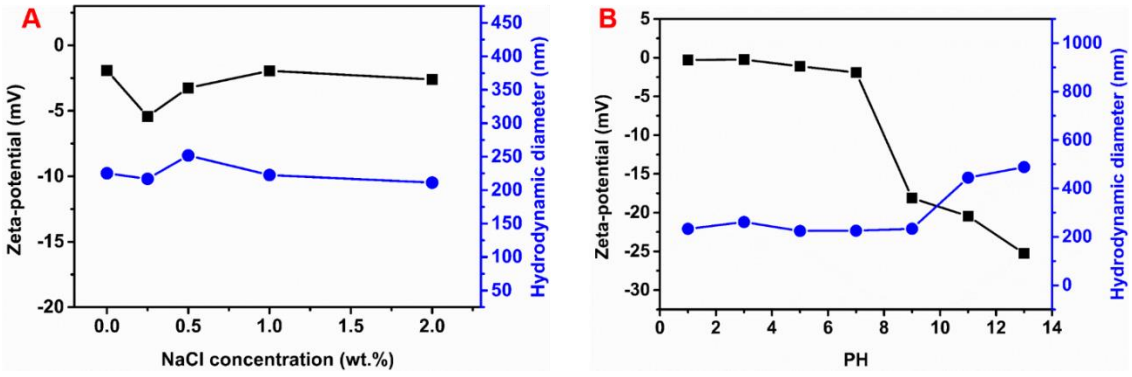

Figure 1. The average hydrodynamic diameter and zeta-potential of the nanogels at different (A) NaCl concentrations and (B) pH.

Under basic conditions, the acrylamide moieties in the PAM nanogels would be hydrolyzed in the presence of the hydroxide (OH^-) ions to the dissociated carboxylate (COO^-) moieties, which would increase the hydrodynamic diameter of the PAM nanogels due to the stronger electrostatic repulsion in the polymeric network.

3.2. EFFECT OF SALT CONCENTRATION ON PICKERING EMULSION

Salinity of the reservoir is a key factor that influence the properties of nanogels and consequently, the stability of corresponding Pickering emulsions. Salt effect on the Pickering emulsion 24 h after preparation was examined at different salt concentrations. We found the creaming process of the Pickering emulsions was almost independent of salt concentration in the range of 0-2 wt.% as indicated by the constant volume of emulsion phase (Figure 2). However, the salinity influence the average diameter of emulsified oil droplets. Higher frequency of emulsified oil drops with large diameter were observed in 2 wt.% NaCl solution than in distilled water (Figure 3). Based on our observation, the average diameter of emulsified oil drops increased from 5 to 21 μm at the NaCl concentration from 0 to 2 wt.%. The marked increment of drop diameter could due to screening effect of the electrostatic interactions of nanogels adsorbed at the oil drop surface[27]. The presence of high concentration sodium salt weakened the electrostatic repulsion among emulsified oil drops and induced the coalescence of the oil drops.

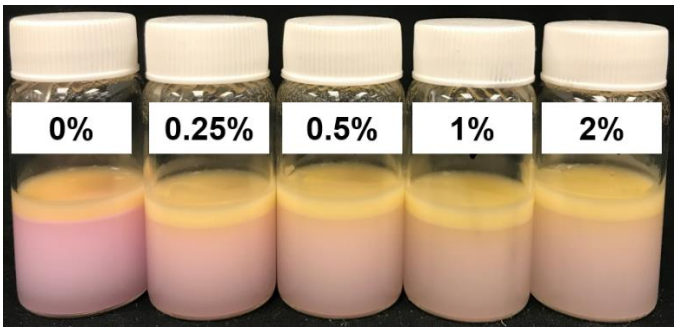

Figure 2. Decane/water emulsions stabilized by the $PAM_{100}MBAA_{0.1}$ nanogels at various NaCl concentrations.

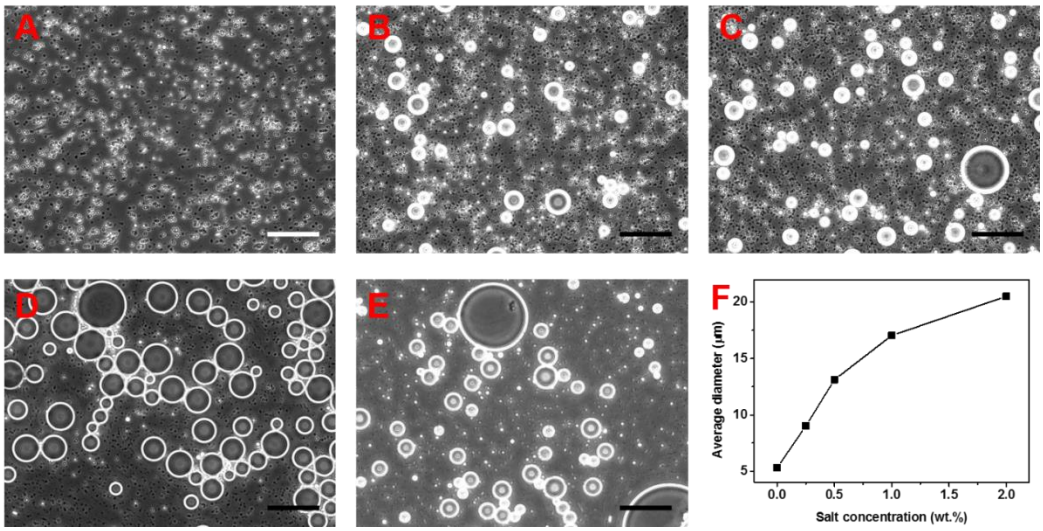

Figure 3. Decane/water Pickering emulsions stabilized by the $PAM_{100}MBAA_{0.1}$ nanogels at (A) 0, (B) 0.25, (C) 0.5, (D) 1, and (E) 2 wt.% NaCl concentrations (scale bar=50μm). (F) The average diameter of emulsified oil drops at different NaCl concentrations.

3.3. EFFECT OF PH ON PICKERING EMULSION

To The behavior of the Pickering emulsions was examined under different pH. The pH of the Pickering emulsions in the experiment was adjusted by addition of minimal concentrated HCl or NaOH to NaCl solution, ranging from 1.0 to 13.0. We found the emulsion stability significantly reduced under pH 13.0 while the creaming

process of the emulsion phase dramatically delayed in basic conditions than the samples in acidic conditions (Figure 4). Under strong basic condition (pH=13.0), the emulsified oil drops tended to agglomerate and coalescence, which markedly reduced the stability of the Pickering emulsions (Figure 5). Under such conditions, the associated acrylamide ($CONH_2$) groups consisting in the nanogels would be hydrolyzed to the form of dissociated carboxylate (COO^-) moieties, which would introduce negative charges into the nanogels adsorbed at the oil-water interfaces and, in consequence, reduced the mechanical strength of the adsorbed nanogel layer and delayed the creaming process. However, at acidic environment the proton (H^+) in the aqueous solution could reduce the repulsion among polymer chains in the nanogels by screening effect, thus leading to the shrinkage of the nanogels. The smaller nanogels rendered the oil-water interface with a higher nanogel coverage and enhanced the stability of Pickering emulsions[18, 28].

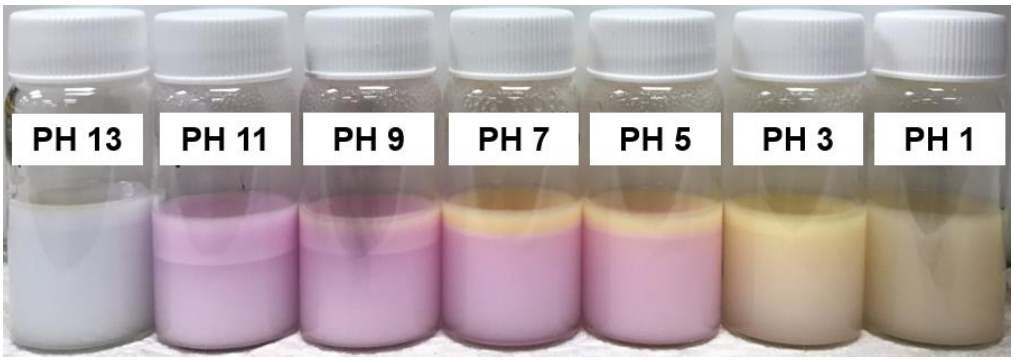

Figure 4. Decane/water emulsions stabilized by the $PAM_{100}MBAA_{0.1}$ nanogels at pH from 1 to 13.

3.4. EFFECT OF NANOGEL CONCENTRATION ON PICKERING EMULSION

In this work, the PAM nanogel concentration ranged from 100 to 2000 mg/L in distilled water at the oil-water ratio of 1:9. We found that the separated oil phase was no

longer observed when the nanogel concentration was above 500 mg/L (Figure 6). Meanwhile, as the nanogel concentration spanned from 100 to 2000 mg/L, the average diameter of emulsified oil drops decreased from 12 to 5 μm as shown in Figure 7. The smaller diameter of oil drops at nanogel concentration of 1000 mg/L was presumably due to the increased total surface area induced by continuous absorbing of nanogels.

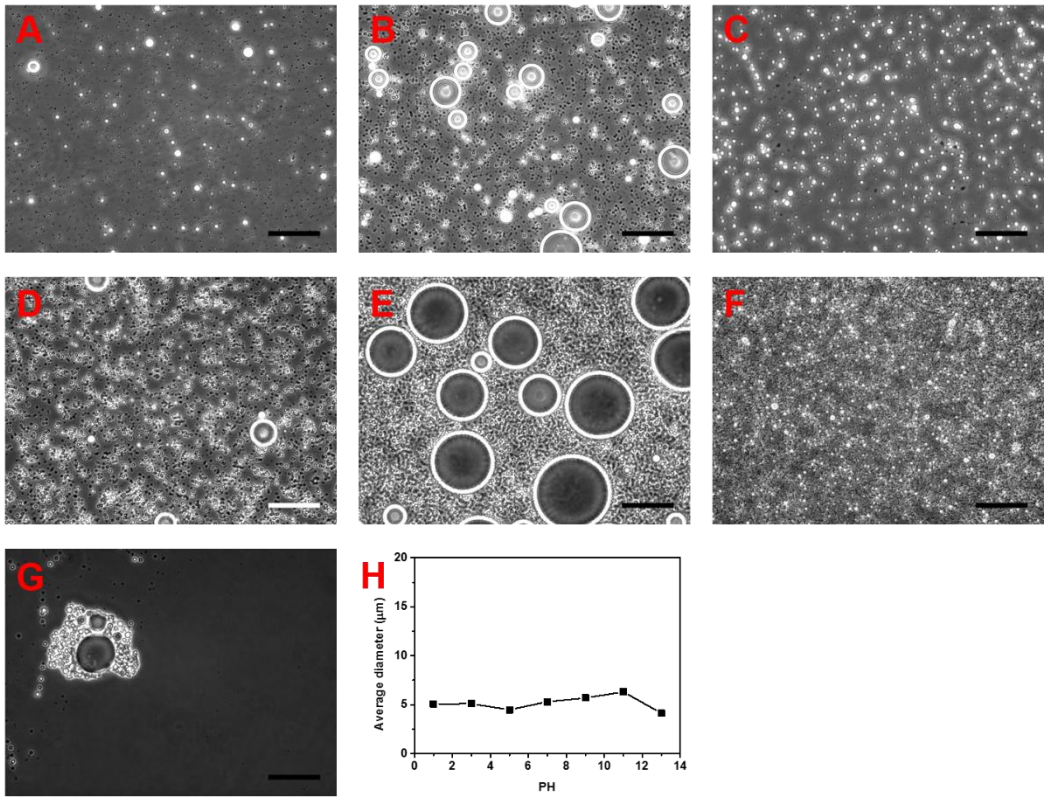

Figure 5. Decane/water Pickering emulsions stabilized by the $PAM_{100}MBAA_{0.1}$ nanogels at pH from (A~G) 1 to 13 (scale bar=50μm), and (H) the average diameter of emulsified oil drops.

The average diameter of emulsified oil drops turned to be constant when the nanogel concentration was above the critical concentration of 1000 mg/L. However, the shape of oil drops became aspheric at nanogel concentration of 2000 mg/L, which is

consistent with previous report that the dispersed nanogels in the continuous phase would enhance the emulsion stability by forming inter dispersed phase structures[29]. This result indicated that the synthesized PAM nanogels would help to form stable Pickering emulsions at a relatively low concentration.

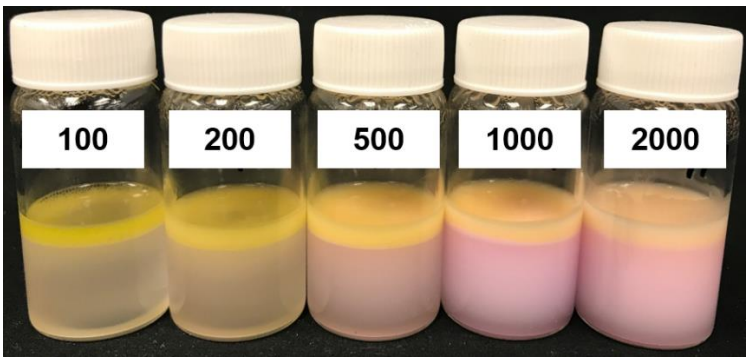

Figure 6. Decane/water emulsions stabilized by the $PAM_{100}MBAA_{0.1}$ nanogels at nanogel concentrations from 100 to 2000 mg/L.

3.5. EFFECT OF ULTRASOUND ON PICKERING EMULSION

For the *in situ* emulsification, shear between the formation fluid and the rock surface induced the fragmentation of oil drops[30]. In this experiment, the effect of fragmentation energy on the behavior of Pickering emulsions was illustrated using ultrasound with different durations in the range of 15 to 240 s. The volume of emulsion phase exhibited an interesting dependence on the sonication time as shown in Figure 8 and Figure 9. The increased in sonication time barely affect the resulted volume of the emulsion phase and average diameter of the emulsified oil drops, which indicated small amount of energy was sufficient to form the nanogel-stabilized o/w Pickering emulsions. Based on our previous research, the PAM nanogels are able to reduce the oil-water interfacial tension by ~10 times that helped minimize the energy required for the

emulsification[13, 31]. Furthermore, the anisotropic deformation of nanogels at the oil-water interface increases the interfacial viscosity and prevents the small oil drops coalescence into big ones.

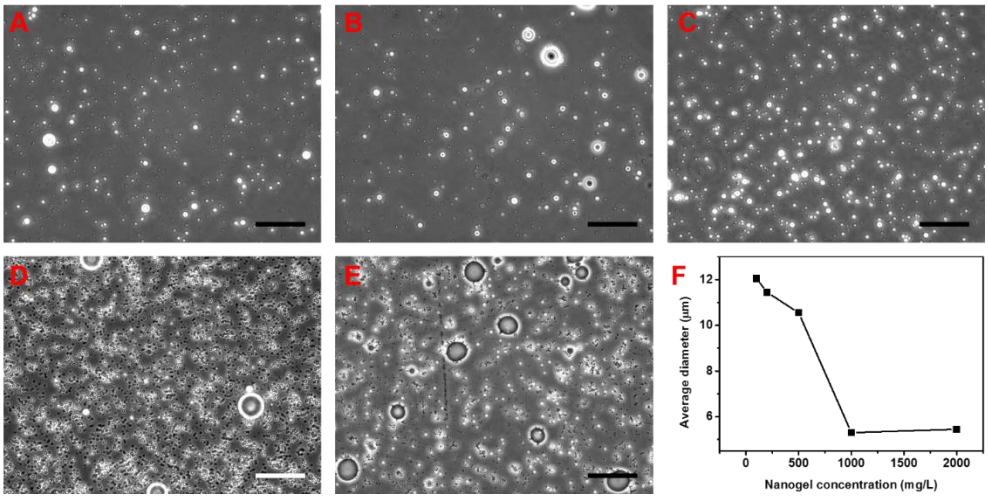

Figure 7. Decane/water Pickering emulsions stabilized by the $PAM_{100}MBAA_{0.1}$ at nanogel concentrations from (A~E) 100 to 2000 mg/L (scale bar=50μm), and (F) the average diameter of emulsified oil drops.

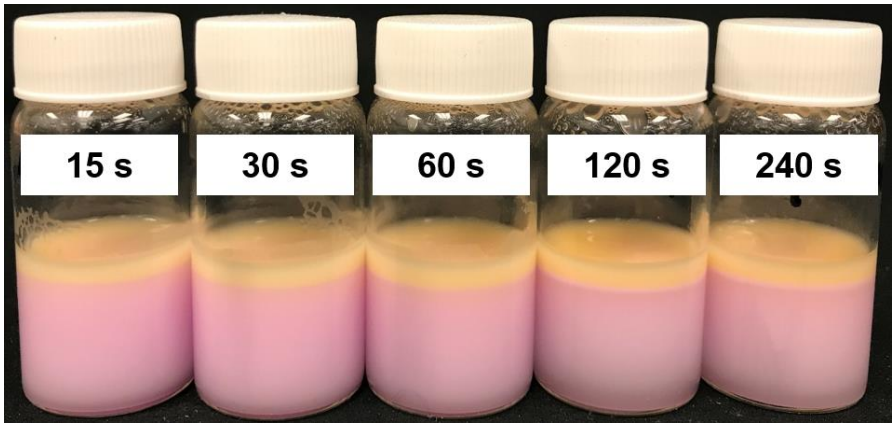

Figure 8. Pickering emulsions stabilized by the $PAM_{100}MBAA_{0.1}$ nanogels under different sonication periods.

3.6. EFFECT OF OIL TYPE ON PICKERING EMULSION

Considered the complex composition of crude oil, several alkanes and aromatic hydrocarbons were applied to illustrate the effect of oil type on the behavior of Pickering emulsions. In our cases, all the formed Pickering emulsions were o/w emulsions and the volume of emulsion phase increased with the molecular weight of oil.

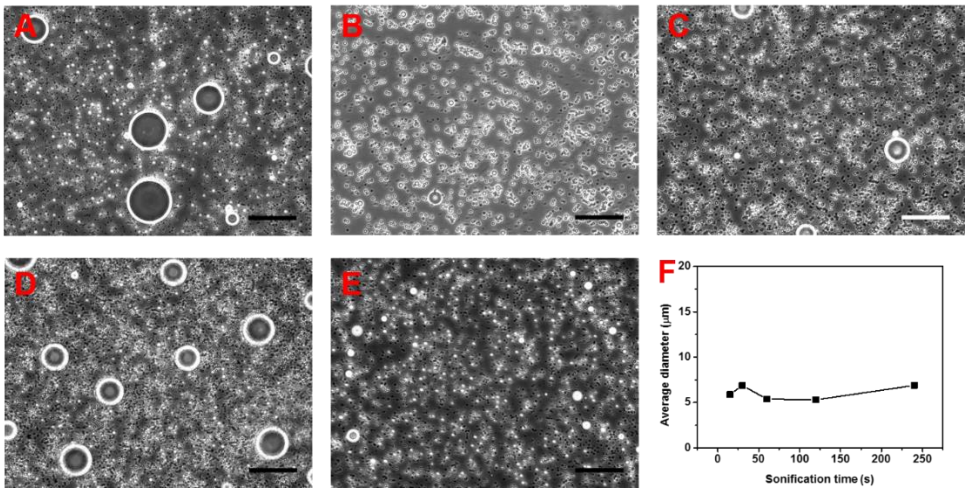

Figure 9. Pickering emulsions under sonication period in the range of (A~E) 15 to 240 s (scale bar=50μm), and (F) the average diameter of emulsified oil drops.

For instance, a marked separated oil phase was observed in the hexane/water emulsion while no creaming was formed in the dodecane/water emulsion 24 h after sonication. In addition, although the viscosity of cyclohexane and benzene is similar at room temperature, the benzene/water Pickering emulsion had a longer creaming period compared with cyclohexane/water Pickering emulsion. In general, the emulsified oil drops are stabilized through steric hindrance and/or charge hindrance. A more viscous oil phase was less likely to coalescence with each other that results in the improved stability of the corresponding Pickering emulsions. To identify the cause of the different behaviors

of cyclohexane/water and benzene/water Pickering emulsions, optical microscopy and SEM were applied on the emulsions and freeze-dried samples, respectively. As displayed in Figure 10, the average diameter of emulsified cyclohexane drops was ~ 80 μm, which was more than 8 times to the average diameter of benzene drops. Furthermore, for the cyclohexane/water emulsion, the nanogels maintained their spherical morphology at the oil-water interfaces whereas the nanogels stayed in an interestingly string-like structures in the benzene/water emulsion (Figure 11).

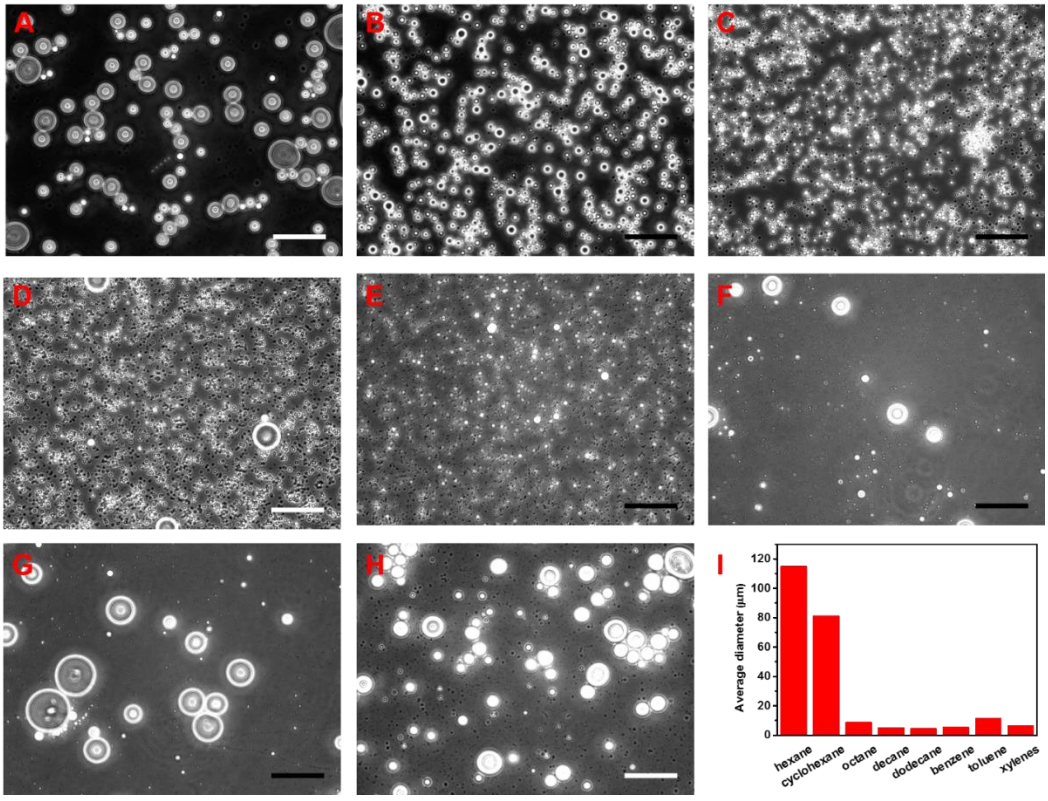

Figure 10. Pickering emulsions stabilized by the $PAM_{100}MBAA_{0.1}$ nanogels using (A) hexane, (B) cyclohexane, (C) octant, (D) decane, (E) dodecane, (F) benzene, (G) toluene, and (H) xylenes as oil phase (scale bar=50μm), and (I) the average diameter of emulsified oil drops.

Therefore, the PAM nanogel-stabilized benzene/water Pickering emulsion had good stability in comparison with cyclohexane/water Pickering emulsion. Different with the alkanes, the delocalized π bond rendered polarity to the aromatic hydrocarbons that enhanced the affinity between the PAM nanogels and the aromatic hydrocarbons. The PAM nanogels adsorbed at the aromatic hydrocarbon-water interfaces were softened and aggregated with each other, and in consequence, turned into string-like structures filled with oil drops. Compared with the isolated oil drops covered by nanogels, the oil drops filled in the string-like structures were less likely to aggregate and coalescence.

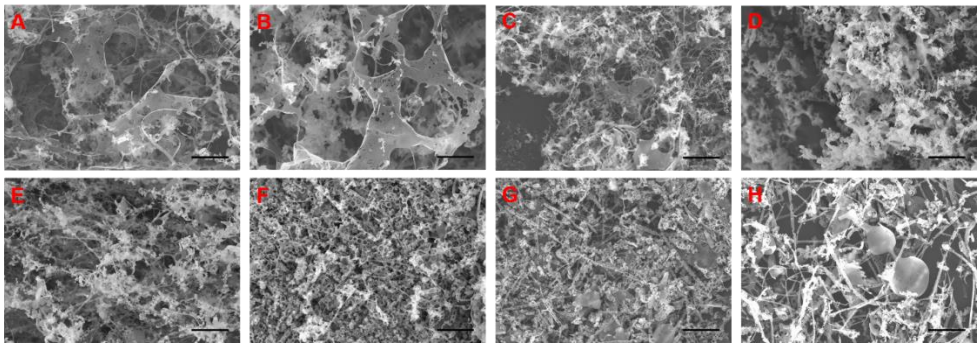

Figure 11. Microstructures of nanogel-stabilized Pickering emulsions using (A) hexane, (B) cyclohexane, (C) octant, (D) decane, (E) dodecane, (F) benzene, (G) toluene, and (H) xylenes as oil phase (scale bar=20μm).

3.7. RHEOLOGY OF CRUDE OIL/WATER PICKERING EMULSION

During the nanogel treatment, the nanogel dispersions were injected to the formation to allow the shear-induced emulsification in the porous media. Under such conditions, the crude oil stayed in the pores would be fragmented into small oil drops and transported through the rock matrix before producing out. The viscosity of the o/w Pickering emulsion is crucial to nanogel flooding, particularly for the heavy oil

reservoirs. In our studies, the viscosities of crude oil samples and corresponding Pickering emulsions with an oil to water ratio of 1:3 were measured at room temperature. As shown in Figure 12, the apparent viscosity of the $PAM_{90}AA_{10}$ and $PAM_{100}MBA_{0.5}$ nanogel-stabilized crude oil/water Pickering emulsions remained almost constant at shear rate from 7.3 to 100 s^{-1}, which indicating a Newtonian behavior of the Pickering emulsions. Moreover, the apparent viscosity of the light oil and heavy oil significantly reduced from ~ 320 and 1400 cP to less than 10 cP, respectively. The results revealed the flow ability of crude oil could be improved by forming nanogel-stabilized o/w Pickering emulsions.

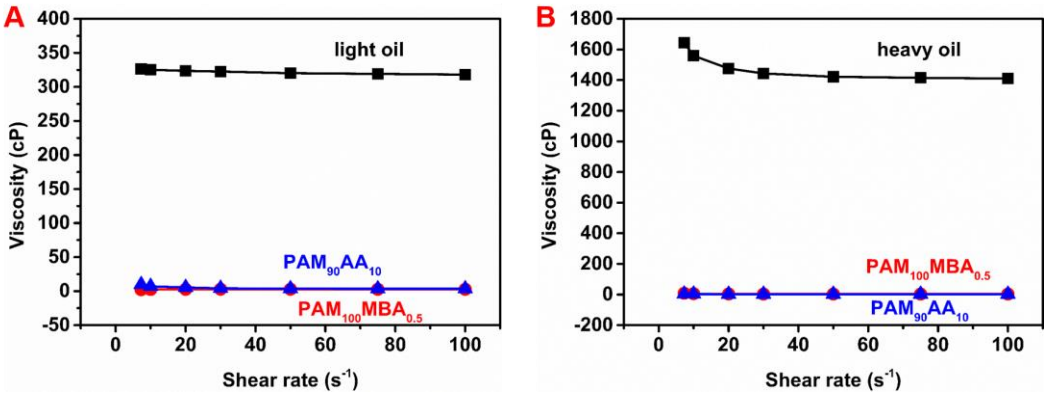

Figure 12. Viscosity of crude oil and corresponding Pickering emulsions.

3.8. ALKALINE-TRIGGERED DEMULSIFICATION OF PICKERING EMULSIONS

The demulsification of the o/w Pickering emulsion after producing from subterranean is a key factor for the following transportation and refining of crude oil. In this work, the demulsification process was investigated using the PAM nanogel-stabilized decane-, light oil-, and heavy oil-in-water Pickering emulsions. By adding 2 drops of 10

wt.% NaOH solution, the decane/water Pickering emulsion was markedly creaming and completely demulsified in 48 h (Figure 13). The light oil/water and heavy oil/water Pickering emulsions also creamed and demulsified with the trigger of alkaline at a smaller rate in comparison with the decane/water sample.

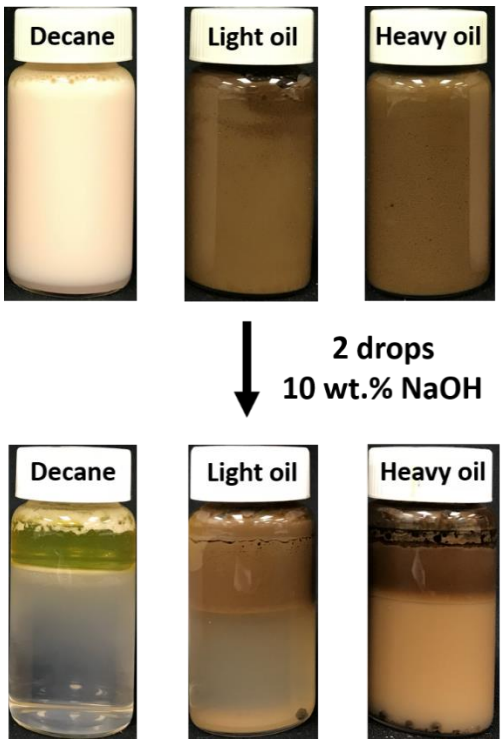

Figure 13. Demulsification of Pickering emulsions stabilized by nanogels.

The hydroxide (OH^-) ions in the aqueous solution could introduce negative charges to the PAM nanogels adsorbed at the oil-water interface, thus leading to the destabilization of the adsorbed nanogel layer. Moreover, the OH- ions helped the ionization of asphaltenes in the crude oil to form amphoteric surfactants[32], which prolong the demulsification of the Pickering emulsions. Interestingly, the insoluble solid contents in the crude oil was precipitated out during the demulsification, which could

potentially enhance the quality of crude oil. The alkaline-triggered demulsification experiment demonstrated the o/w Pickering emulsions can be quickly demulsified on demand.

4. CONCLUSIONS

In conclusion, the alkaline-demulsified Pickering emulsions stabilized by the stimuli-responsive PAM nanogels has been described. Stimulation PAM nanogels with NaOH hydrolyzed the acrylamide into carboxylate moieties containing in the polymeric networks, which would significantly increase the hydrodynamic diameter and reduce the zeta potential of PAM nanogels. The Pickering emulsions showed excellent stability in brines and acidic solutions that no separated oil phase had been observed 24 h after emulsion preparation. Based on the optical microscopy results, the average diameter of oil drops was no longer decreased above the critical nanogel concentration of 1000 mg/L. The stable Pickering emulsions could be prepared over a broad range of sonication period from 15 to 240s. Compared to alkanes/water Pickering emulsions, the stability of aromatic hydrocarbons/water Pickering emulsions was enhanced by the string-like nanogel structures. Rheological studies demonstrated the flow ability of crude oil was significantly enhanced by forming crude oil/water Pickering emulsions. The alkaline-triggered demulsification property of PAM nanogel stabilized Pickering emulsions suggests potential utility in the engineering applications.

ACKNOWLEDGEMENTS

The authors would like to express their grateful acknowledgement to the financial support from DOE under the contract of DE-FE0024558.

REFERENCES

[1] S. Schmidt, T. Liu, S. Rütten, K.-H. Phan, M. Möller, W. Richtering, Influence of microgel architecture and oil polarity on stabilization of emulsions by stimuli-sensitive core–shell poly (N-isopropylacrylamide-co-methacrylic acid) microgels: Mickering versus Pickering behavior?, Langmuir 27 (2011) 9801-9806.

[2] T. Ngai, S.H. Behrens, H. Auweter, Novel emulsions stabilized by pH and temperature sensitive microgels, Chemical communications (2005) 331-333.

[3] Z. Li, T. Ngai, Microgel particles at the fluid–fluid interfaces, Nanoscale 5 (2013) 1399-1410.

[4] E. Dickinson, Microgels—An alternative colloidal ingredient for stabilization of food emulsions, Trends in Food Science & Technology 43 (2015) 178-188.

[5] M. Destribats, M. Rouvet, C. Gehin-Delval, C. Schmitt, B.P. Binks, Emulsions stabilised by whey protein microgel particles: towards food-grade Pickering emulsions, Soft matter 10 (2014) 6941-6954.

[6] M. Veverka, T. Dubaj, E. Veverková, P. Šimon, Natural oil emulsions stabilized by β-glucan gel, Colloids and Surfaces A: Physicochemical and Engineering Aspects 537 (2018) 390-398.

[7] Y. Gong, A.M. Zhu, Q.G. Zhang, M.L. Ye, H.T. Wang, Q.L. Liu, Preparation of cell-embedded colloidosomes in an oil-in-water emulsion, ACS applied materials & interfaces 5 (2013) 10682-10689.

[8] W. Wang, A.H. Milani, Z. Cui, M. Zhu, B.R. Saunders, Pickering Emulsions Stabilized by pH-Responsive Microgels and Their Scalable Transformation to Robust Submicrometer Colloidoisomes with Selective Permeability, Langmuir 33 (2017) 8192-8200.

[9] Y. Gong, A.M. Zhu, Q.G. Zhang, Q.L. Liu, Colloidosomes from poly (N-vinyl-2-pyrrolidone)-coated poly (N-isopropylacrylamide-co-acrylic acid) microgels via UV crosslinking, RSC Advances 4 (2014) 9445-9450.

[10] Y. Zhou, J. Huang, W. Sun, Y. Ju, P. Yang, L. Ding, Z.-R. Chen, J.A. Kornfield, Fabrication of active surfaces with metastable microgel layers formed during breath figure templating, ACS applied materials & interfaces 9 (2017) 4177-4183.

[11] H. Chen, E.M. Nofen, K. Rykaczewski, L.L. Dai, Colloidal lattices of environmentally responsive microgel particles at ionic liquid–water interfaces, Journal of colloid and interface science 504 (2017) 440-447.

[12] S. Wiese, A.C. Spiess, W. Richtering, Microgel-Stabilized Smart Emulsions for Biocatalysis, Angew. Chem. 125 (2013) 604-607.

[13] J. Geng, J. Pu, L. Wang, B. Bai, Surface charge effect of nanogel on emulsification of oil in water for fossil energy recovery, Fuel 223 (2018) 140-148.

[14] J. Geng, H. Ding, P. Han, Y. Wu, B. Bai, The transportation and potential enhanced oil recovery mechanisms of nanogels in sandstone, Energy & Fuels (2018).

[15] Y. Wu, S. Wiese, A. Balaceanu, W. Richtering, A. Pich, Behavior of temperature-responsive copolymer microgels at the oil/water interface, Langmuir 30 (2014) 7660-7669.

[16] K. Du, E. Glogowski, T. Emrick, T.P. Russell, A.D. Dinsmore, Adsorption energy of nano-and microparticles at liquid− liquid interfaces, Langmuir 26 (2010) 12518-12522.

[17] Z. Li, T. Ming, J. Wang, T. Ngai, High internal phase emulsions stabilized solely by microgel particles, Angewandte Chemie 121 (2009) 8642-8645.

[18] M. Destribats, V. Lapeyre, M. Wolfs, E. Sellier, F. Leal-Calderon, V. Ravaine, V. Schmitt, Soft microgels as Pickering emulsion stabilisers: role of particle deformability, Soft Matter 7 (2011) 7689-7698.

[19] R.A. Gumerov, A.M. Rumyantsev, A.A. Rudov, A. Pich, W. Richtering, M. Möller, I.I. Potemkin, Mixing of Two Immiscible Liquids within the Polymer Microgel Adsorbed at Their Interface, ACS Macro Letters 5 (2016) 612-616.

[20] J. Sun, W. Wang, F. He, Z.-H. Chen, R. Xie, X.-J. Ju, Z. Liu, L.-Y. Chu, On-chip thermo-triggered coalescence of controllable Pickering emulsion droplet pairs, RSC Advances 6 (2016) 64182-64192.

[21] B. Brugger, J. Vermant, W. Richtering, Interfacial layers of stimuli-responsive poly-(N-isopropylacrylamide-co-methacrylicacid)(PNIPAM-co-MAA) microgels characterized by interfacial rheology and compression isotherms, Physical Chemistry Chemical Physics 12 (2010) 14573-14578.

[22] J. Tang, M.F.X. Lee, W. Zhang, B. Zhao, R.M. Berry, K.C. Tam, Dual responsive pickering emulsion stabilized by poly [2-(dimethylamino) ethyl methacrylate] grafted cellulose nanocrystals, Biomacromolecules 15 (2014) 3052-3060.

[23] A. Morse, S. Armes, K. Thompson, D. Dupin, L. Fielding, P. Mills, R. Swart, Novel Pickering emulsifiers based on pH-responsive poly (2-(diethylamino) ethyl methacrylate) latexes, Langmuir 29 (2013) 5466-5475.

[24] A.J. Morse, D. Dupin, K.L. Thompson, S. Armes, K. Ouzineb, P. Mills, R. Swart, Novel Pickering emulsifiers based on pH-responsive poly (tert-butylaminoethyl methacrylate) latexes, Langmuir 28 (2012) 11733-11744.

[25] R. Zolfaghari, A. Fakhru'l-Razi, L.C. Abdullah, S.S. Elnashaie, A. Pendashteh, Demulsification techniques of water-in-oil and oil-in-water emulsions in petroleum industry, Separation and Purification Technology 170 (2016) 377-407.

[26] M.-h. Kwok, T. Ngai, A confocal microscopy study of micron-sized poly (N-isopropylacrylamide) microgel particles at the oil–water interface and anisotopic flattening of highly swollen microgel, Journal of colloid and interface science 461 (2016) 409-418.

[27] B.P. Binks, R. Murakami, S.P. Armes, S. Fujii, Effects of pH and salt concentration on oil-in-water emulsions stabilized solely by nanocomposite microgel particles, Langmuir 22 (2006) 2050-2057.

[28] M. Destribats, M. Eyharts, V. Lapeyre, E. Sellier, I. Varga, V. Ravaine, V. Schmitt, Impact of pNIPAM microgel size on its ability to stabilize Pickering emulsions, Langmuir 30 (2014) 1768-1777.

[29] F. Yang, S. Liu, J. Xu, Q. Lan, F. Wei, D. Sun, Pickering emulsions stabilized solely by layered double hydroxides particles: The effect of salt on emulsion formation and stability, Journal of Colloid and Interface Science 302 (2006) 159-169.

[30] V.A. Lifton, Microfluidics: an enabling screening technology for enhanced oil recovery (EOR), Lab on a Chip 16 (2016) 1777-1796.

[31] V. Schröder, O. Behrend, H. Schubert, Effect of dynamic interfacial tension on the emulsification process using microporous, ceramic membranes, Journal of Colloid and Interface Science 202 (1998) 334-340.

[32] N. Li, G. Zhang, J. Ge, L. Zhang, X. Liu, J. Wang, Ultra-low interfacial tension between heavy oil and betaine-type amphoteric surfactants, Journal of Dispersion Science and Technology 33 (2012) 258-264.

SECTION

3. NANOGEL SYNTHESIS IN SUPERCRITICAL CO_2

CO_2 flooding is a proven enhanced oil recovery (EOR) technique in the United States with an estimated contribution of 4% of the national oil production. CO_2 flooding has attracted much attention in recent years, especially with the increasing need for carbon capture and storage. Primary objectives for a CO_2 EOR project in a given reservoir usually include pressure maintenance, improved displacement efficiency, and reduced residual oil saturation. One major impediment to effective CO_2 flooding is the reservoir conformance problem. The root cause of reservoir conformance problems is the strong heterogeneity of many reservoirs. One or more low permeability zones may impede fluid flow from high permeability zones to the less permeable oil-saturated zones. In addition, the large differences in viscosity and density between the injected supercritical CO_2 ($scCO_2$) and the formation oil often cause serious gravity override and/or viscous fingering, with CO_2 channeling through high permeability zones or fractures. Moreover, the heterogeneity has been aggravated in many mature reservoirs due to long term water or CO_2 flooding, which often cause minerals dissolution, sand production or un-intentioned hydraulic fracturing. In conclusion, CO_2 sweep efficiency is usually poor, due to the reservoir heterogeneity, unfavorable mobility ratio, and gravity segregation. The low sweep efficiency significantly limits both the CO_2 EOR and CO_2 storage efficiency in oil fields. The reservoir conformance control is a cost-effective method to significantly improve CO_2 sweep and storage efficiency.

Nanoparticle gels are nano-sized crosslinked polymeric particles that are able to swell tens to hundreds of times in water and deform under external forces. Although the nanoparticle gels have the same three-dimensional network with preformed particle gels, the small diameter renders nanoparticle gels to correct the conformance problems in the matrix of oil reservoirs. In order to endow nanoparticle gels the capacity to be used in the CO_2 flooding reservoirs, the polymeric networks of nanoparticle gels should not degrade and shrink under CO_2. Herein, we synthesized three novel nanoparticle gels that either resistant or response to CO_2 through emulsion and dispersion polymerization under $scCO_2$. We studied the effect of synthetic parameters and environmental factors on the size distributions and physicochemical properties of the nanoparticle gels. We also investigated the long-term stability of the synthesized nanoparticle gels under different temperatures. In our work, we found that the AMPS-based nanoparticle gel is much more resistant to salt, acid, and CO_2 than the HPAM nanoparticle gel. In addition, the CO_2-responsive nanoparticle gels were able to re-swell when contact with CO_2 that would be good candidates for conformance control in the CO_2 flooding reservoirs.

Nanoparticle gels, nano-sized crosslinked polymeric particles, are able to transport into the in-depth of oil reservoirs and perform matrix treatments. The nanoparticle gels are able to deform to transport through the narrow pore throats due to the elasticity of polymeric networks. The environmental stimulations, such as salinity, pH, and temperature can result in different responses of nanoparticle gels including swell, shrinkage, aggregate, and crosslink. In addition, nanoparticle gels are much easier to be modified for targeted applications with selected properties. Currently, the nanoparticle

gels are synthesized and prepared through physical and chemical methods to control the size of produced nanoparticle gels.

The physical methods including two main categories: synthesize the nanoparticle gels in a confined space and break the produced gel particles into nano range. The technical methods, such as using microfluidic model, micromolding, and spinning plate, mold the precursor of the nanoparticle gels into nano-sized and initiate the polymerization using heat and/or photo-initiation. On the other hand, the grinding machines are used to crash the gel particles into nanoparticle gels with the help of the corresponding solvents. However, no matter the methods of synthesize the nanoparticle gels in a confined space or the methods of break gel particles into nano ranges, the physical methods are time consuming that cannot be applied for the industry scale production.

In the chemical methods, the precursor of the nanoparticle gels are dispersed and stabilized in some certain solutions. The dispersion polymerization, emulsion polymerization, and suspension polymerization are the three methods widely used to prepare the polymeric nanoparticles and the nanoparticle gels. Based on the polymerization condition and system, emulsion polymerization and suspension polymerization also include microemulsion polymerization and miniemulsion polymerization. In emulsion polymerization, two immiscible phases are mixed together stabilized by the emulsifier. The monomers and crosslinkers are dissolved in the inner phase while the initiator is soluble in the outer phase (continuous phase). Free radicals are formed in the outer phase and transported into the isolated droplets of the inner phase to start the polymerization. Based on the type of inner phase, the emulsion polymerization

can be divided into emulsion polymerization (o/w) and reverse emulsion polymerization (w/o). The advantages of emulsion polymerization are that: the rapid polymerization enable the formation of a high molecular weight as well as a narrow molecular weight distribution of products, the viscosity of emulsion system is typically lower than other methods, and the produced heat is relatively easy to remove from the reactor. However, one of the disadvantages of emulsion polymerization is that the emulsifier will adsorb on the surface of the produced nanoparticle gels, which is hard to be removed.

Supercritical carbon dioxide ($scCO_2$) is a fluid state of carbon dioxide where it is held at or above its critical pressure and critical temperature. If the pressure and temperature are both increased from standard temperature and pressure to be at or above the critical point of carbon dioxide, it can adopt properties midway between a gas and liquid. More specifically, it behaves as a supercritical fluid above its critical temperature (304.25 K, 31.10 °C) and critical pressure (7.39 MPa, 1071 psi), expanding to fill its container like a gas but with a density like that of a liquid.

In addition to being an environmentally benign alternative to volatile organic and aqueous solvents, $scCO_2$ offers several advantages as solvents, such as low solution viscosity, an effectively inert solution medium (no detectable chain transfer to solvent), and tunable solvent strength. Other researchers' work has shown that CO_2 is an excellent medium for performing radical polymerization. In the recent decades, several kinds of radical polymerizations have been successfully carried out in $scCO_2$, including solution, dispersion, precipitation, and emulsion polymerization. Compared with conventional solvents, $scCO_2$ is a slightly polar solvent that has a polarizability similar in value to that of methane, which suggests that $scCO_2$ is indeed a very weak supercritical fluid solvent

for hydrophilic polymers and hydrogels. The quadrupole of CO_2 plays a dominant role in determining polymer solubility due to low polarizability of CO_2. The ability to dissolve polymers in CO_2 is depending on temperature and the polarity of polymers For instance, CO_2 is hard to dissolve poly(acrylic acid) even to 300 °C and 2750 bar. Introducing fluorine into polymer chains helps polymer dissolve in $scCO_2$ and a fluorinated copolymer (Teflon AF) can be dissolved in $scCO_2$ at temperature as low as 70 °C and pressure less than 600 bar.

The only polymers shown to have good solubility in pure CO_2 under mild conditions are certain amorphous fluoropolymers and silicones. While CO_2 is a weak solvent for non-polar polymers under most conditions since CO_2 quadrupolar interactions dominate the inter charge energy as the temperature is lowered, the introduction of a degree of polarity in the polymer chain tends to lead somewhat enhanced solubility, although it still need to use impractically high pressures and temperatures in order to dissolve non-fluorinated materials[3]. Poly(1H, 1H-perfluorooctylmethyl acrylate) (PFOA) is a successful stabilizer in the dispersion polymerization of poly(methyl methacrylate) (Figure 3.1). In addition to its use in dispersion polymerization, PFOA has been employed for the production of polymer microparticles by antisolvent precipitation in CO_2.

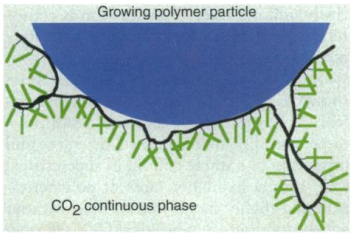

Figure 3.1 Schematic representation of stabilize mechanism of PFOA in $scCO_2$.

An anionic phosphate fluorosurfactants that enable significant water uptake within a continuous CO_2 phase though the formation of water-in-CO_2 microemulsions without the aid of a co-surfactant has been reported by Keiper's group. The cloud-point profiles of phosphate fluorosurfactants in CO_2 with various water loadings in their work can guide us to control the feeding ratio of different components and the condition during reactions.

Dispersion polymerization is a heterogeneous polymerization that all the monomers, crosslinkers, and initiators are dissolvable in the continuous phase. Dispersion polymerization is one of precipitation polymerizations, as polymerization starts, the produced polymer/gel does not prefer staying in the continuous phase and form precipitates. After precipitation, the polymerization proceeds by adsorption of monomer, crosslinker and free radical into the polymer/gel particles. Compared with precipitation polymerization in conventional solvent (alkane, benzene, etc.), polymerization in $scCO_2$ is more environment friendly and economically. Only by releasing the pressure, produced polymer/gels can be collected without further purification, such as centrifuging, washing, and dialyzing.

Acrylic acid is moderately soluble in supercritical carbon dioxide, while poly(acrylic acid) is insoluble. Therefore, it is possible to polymerize poly(acrylic acid) in $scCO_2$ via dispersion polymerization. It has reported that 1,1,2-trichloro-1,2,2-reifluoroethane was used as co-solvent in the dispersion polymerization of poly(acrylic acid) hydrogel under $scCO_2$ condition. And the morphology of the produced poly(acrylic acid) is in agglomerate state of small particles rather than separated uniformly spheres. Polyacrylamide-based hydrogel is a cost-effective conformance control agent in

petroleum industry. However, polyacrylamide-based hydrogel cannot stand acid conditions because of the hydrolysis of acrylamide into acrylic acid moieties, which cannot stand high salt concentration of formation water. Also, the mechanical strength of polyacrylamide-based hydrogel reduces a lot and can no longer provide efficient plugging when contact with CO_2. The stability of ionic hydrogel, such as poly(2-acrylamido-2-methylpropane sulfonic acid sodium salt)-based hydrogel, is much better than polyacrylamide-based hydrogel under acid condition. Moreover, aqueous solution containing ionic monomers forms more stable dispersion in $scCO_2$ compared with containing nonionic monomers.

Inspired by the unique properties of $scCO_2$, we have synthesized nanoparticle gels in the presence of $scCO_2$ through free radical polymerization in this work. In the emulsion polymerization, the fluorinated surfactants/ polymers were synthesized and utilized as emulsifier of the aqueous solution of monomers and crosslinkers. For the dispersion polymerization, no emulsifier or stabilizer was used throughout the reaction and monomers were stabilized by their affinity to $scCO_2$.

3.1. EXPERIMENTAL

All the materials and equipment used in the following experiments and the experimental procedures are listed as below. The nanoparticle gels were prepared through either suspension polymerization under ambient conditions or dispersion polymerization under supercritical carbon dioxide conditions. The simpler reactor was lab-made using stainless steel which could stand as high as 3500 psi. For safety consideration, the highest pressure used in our experiments are much less than 3500 psi.

3.1.1. Materials and Equipment. All chemicals and reagents were purchased from Sigma-Aldrich (St. Louis, MO) and used as received except further noted. Acrylamide (AM) was purified by recrystallization from acetone and dried under vacuum at 25 °C for one day. To prepare sodium acrylate in the lab scale, solid NaOH was added to a stirring solution of acrylic acid in methanol at room temperature. The reaction mixture was vigorously stirred for 1 h and the precipitate was isolated, washed with methanol and dried under vacuum at 25 °C for one day. To prepare sodium salt of 2-acrylamido-2-methylpropane sulfonic acid, the diluted NaOH solution was added into the aqueous solution of 2-acrylamido-2-methylpropane sulfonic acid under ice bath until the pH of the mixture became 7.

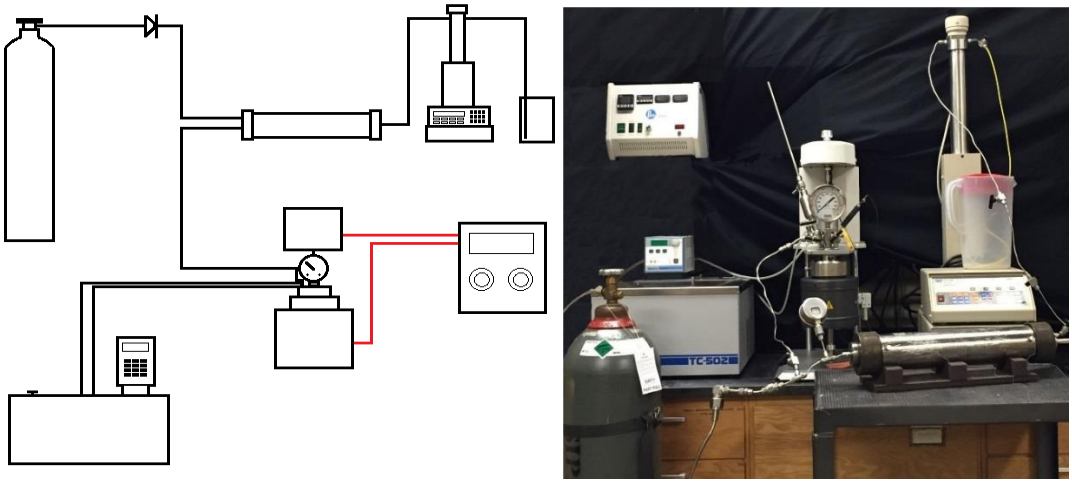

Figure 3.2. Schematic representation (left) and digital photo (right) of experimental apparatus of Parr for emulsion polymerization.

Three kinds of experimental apparatus were used for the synthesis of nanoparticle gels under $scCO_2$ conditions. The experimental apparatus of Parr for the emulsion polymerization mainly contains four parts: gas sources and pressure build-up system,

stirring and heating control system, water cooling system, and polymerization reactor. The schematic representation and photo of the experimental apparatus for polymerization in $scCO_2$ are shown in Figure 3.2.

Gas sources and pressure build-up system: the gas source used in our experiments was compressed CO_2 cylinder equipped with a siphon tube that with an original pressure at 800 psi. There is a check valve in the pipeline from the outlet of CO_2 gas cylinder to the accumulator to prevent the high pressure gas flow back into the CO_2 cylinder. The accumulator was connected with gas cylinder, reactor, and column pump. The piston made of stainless steel inside the accumulator can separate CO_2 gas and distilled water and transfer pressure at the same time. The rubber o-ring was replaced by Teflon o-ring because rubber o-ring was easily corroded under $scCO_2$ condition and can no longer provide sufficient sealing. To reach supercritical condition, the column pump was used to press compressed CO_2 into reactor in several cycles. Stirring and heating control: shearing in the main reactor was provided by an internal stirrer shaft driven by magnetically coupled motor. The reactor was sitting in a heating jacket, which can provide efficiently heat up to 150 °C. The stirring rate and temperature inside the reactor were controlled by the 4848 reactor controller via wires. Water cooling system: Brookfield TC-502 was used as the temperature controller for the water circulation and distilled water was used as the cycling coolant. The aim of water cooling system is to make sure the reaction is performed under mild temperature. Polymerization reactor: Parr 4560 Mini reactor was used for the polymerization. The volume of reactor is 300 mL and the highest pressure it can stand is 2000 psi. The closure type of this reactor is split-ring with 6 compression bolts and sealed by a flat, PTFE gasket. This reactor contains

pressure gauge, gas inlet, gas outlet, liquid inlet, stirring rod, fixed thermocouple, and cooling coil.

A simple reactor was designed and made in our lab to perform the dispersion polymerization in $scCO_2$ (Figure 3.3). The reactor contains pressure gauge, gas pipeline, and PTFE-coated magnetic stirrer. The reactor is able to hold pressure as high as 3500 psi and the safety pressure is below 3000 psi. The reacting temperature was controlled by oil bath (heat plate equipped with thermocouple). The gas source and pressure system is same with the experimental apparatus of Parr.

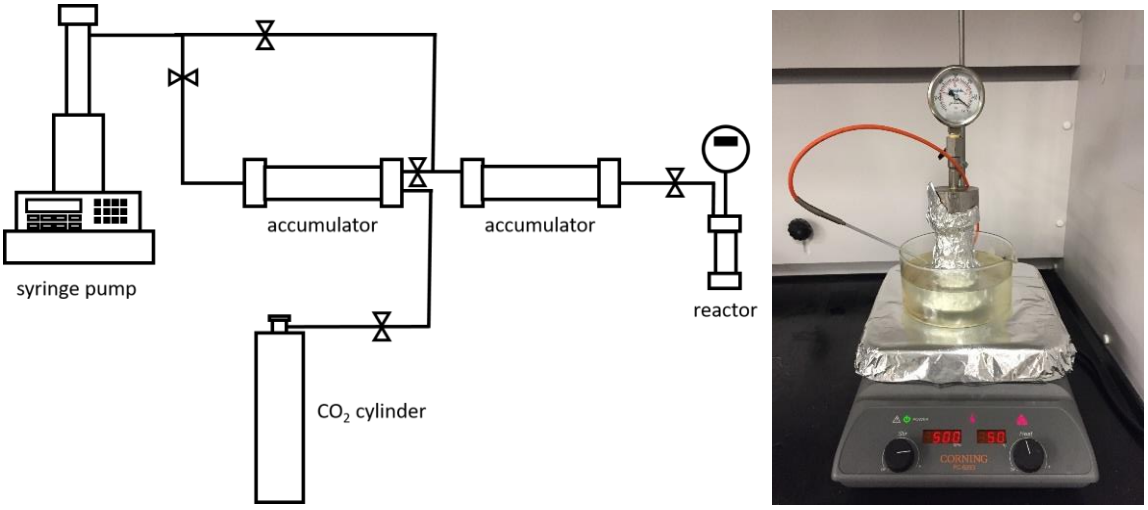

Figure 3.3. Schematic representation of experimental apparatus (left) and reactor in oil bath (right) for dispersion polymerization.

The visible experimental apparatus for dispersion polymerization contains four systems similar with the experimental apparatus of Parr (Figure 3.4). The main different between the visible experimental apparatus and that of Parr is that the reactor of visible experimental apparatus contains two transparent sapphire glass on the opposite side each assembled by six bolts. The reactor can work under as high as 8700 psi and 400 °C.

3.1.2. Poly(1h,1h-Perfluorooctylmethyl Acrylate) Synthesis. The poly(1H, 1H-perfluorooctylmethyl acrylate) (PFOA) was synthesized through solution polymerization. In a typical experiment, 5 g of 1H, 1H-perfluorooctylmethyl acrylate and 0.05 g 2,2'-azobis(2-methylpropionitrile) (AIBN) in 2 mL benzene were mixed sufficiently before heated up to 60 °C. The reaction was kept for 20 h to let the monomers fully reacted. After that, the wax-like polymer was washed by tetrahydrofuran to remove the unreacted monomers and initiators for three times.

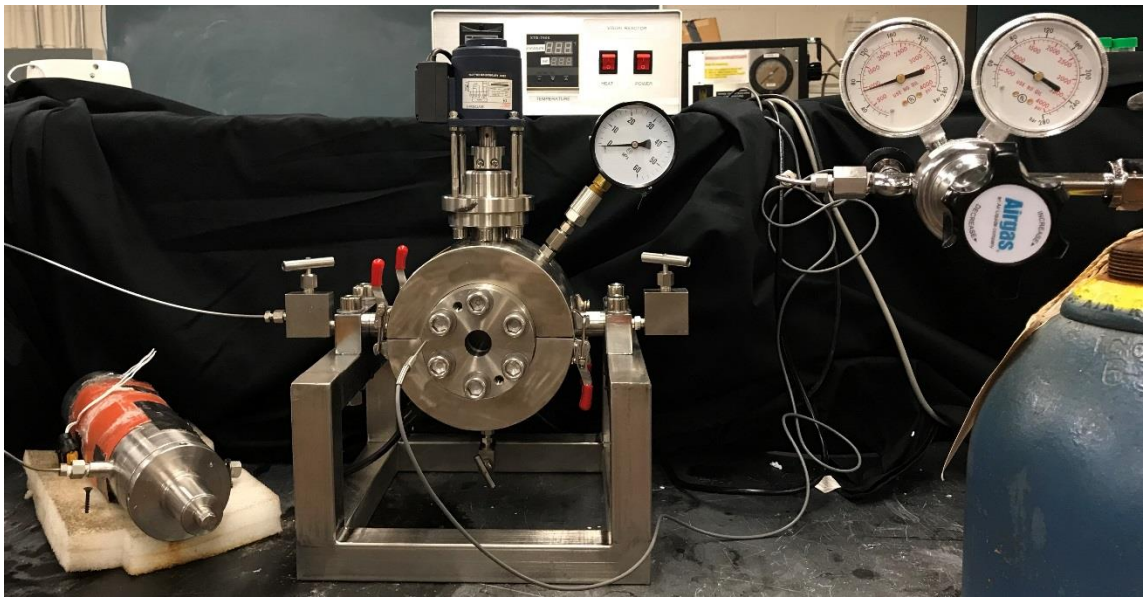

Figure 3.4. High pressure, high temperature experimental apparatus for nanoparticle gel synthesis.

The synthesized PFOA polymer was a white powder that would like to form aggregation under ambient condition. The PFOA polymer displayed a hydrophobic behavior when dispersed in water as the polymer itself turned to float at the surface of water rather than dissolve or disperse in water.

3.1.3. Phosphate Fluoro-surfactant Synthesis. The synthesis of bis-[2-(F-hexyl) ethyl] phosphate, sodium salt was based on the work of Keiper's group. The steps are listed as follow: a) 0.256 mL Phosphorous oxychloride was added to 16 mL diethyl ether (anhydrous); b) cool the mixture to 0 °C and then add the solution of 1.392 g triethyl amine, 8 mL diethyl ether and 2 g 1H, 1H, 2H, 2H-perfluorooctanol. Stirring over night; c) filtered and removed the solid precipitation. The precipitation was washed by diethyl ether for three times; d) using nitrogen to let diethyl ether & triethyl amine vaporize; e) the oil like liquid was collected and dissolved into acetonitrile (8 mL) with water (0.4 mL); f) isolated the lower phase and dissolved in 8 mL ethanol; g) dropt the mixture of 1.6 mL ethanol and 0.1824 g 50 wt.% NaOH solution, stirred overnight. h) filtered and vaporized ethanol, then dropped it into diethyl ether and centrifuged. After all the steps above, the white precipitation was collect for the following experiment.

3.1.4. Emulsion Polymerization of Nanoparticle Gels. The sodium salt of 2-acrylamido-2-methylpropane sulfonic acid-based nanoparticle gels and acrylamide-based nanoparticle gels were synthesized through emulsion polymerization in the presence of phosphate fluoro-surfactant. In a typical experiment, 0.8 g aqueous solution (63 wt.% acrylamide and 0.2 wt.% N,N'-methylenebis(acrylamide)), 0.82 g bis-[2-F-hexyl) ethyl] phosphate, sodium salt, and 0.002 g azobisisobutyronitrile were added into the reactor. Then the reactor was filled up with CO_2 and pressure was then raised to 1000 psi at 60 °C. The reaction was conducted under 800 rpm stirring for 24 h. After reaction, the nanoparticle gels was collected from the bottom of the reactor and precipitated and washed by acetone for three times to remove the unreacted monomers.

3.1.5. Dispersion Polymerization of Nanoparticle Gels. In a typical experiment, 30 mg AIBN and 2.4 mL aqueous solution containing 1.737 mol/L 2-acrylamido-2-methylpropane sulfonic acid sodium salt (AMPS-Na), and 0.0174 mol/L N,N'-methylene bis(acrylamide) (MBAA) were added into the 150 mL reactor with a magnetic stirrer. Then, compressed CO_2 was injected into reactor until the pressure reaches 1600 psi (3000 psi at 50 °C). After that, reactor was moved into 50 °C oil bath and the stirring rate was fixed at 500 rpm. The reaction took 8 hours before pressure releasing. Finally, product was washed by acetone three times and dried in vacuum oven. The synthetic parameters of dispersion polymerizations of poly(2-acrylamido-2-methylpropane sulfonic acid, sodium salt) nanoparticle gels are shown in Table 3.1.

Table 3.1. Synthetic parameters of dispersion polymerizations of nanoparticle gels.

Sample Name	Aqueous solution/ mL	AIBN/ mg	Stirring rate/ rpm	Temperature/ °C	Pressure/ psi
1	0.4 g AMPS-Na & 3 mg MBAA	6	500	50	3000
2	2.4	6	500	50	2550
3	2.4	6	500	50	2500
4	2.4	6	500	50	3000
5	2.4	6	500	50	2650
6	2.4	6	500	50	1200
7	2.4	12	500	50	2700
8	2.4	6	500	50	2600
9	4.8	12	500	50	2300
10	7.2	6	500	50	1350
11	7.2	18	500	50	1950
12	1.6	6	500	50	1350

3.1.6. Core-shell Nanoparticle Gels Synthesis. The core-shell nanoparticle gels were prepared through a semi-continuous suspension polymerization. In a typical experiment, the aqueous solution of hydrophilic monomers and crosslinkers were dissolved in distilled water and dispersed in oil phase contained emulsifiers. Then the initiator was added into the mixture to start the polymerization at 40 °C for 2 h. After that, the oleic solution contained hydrophobic initiator, monomers and crosslinkers was dropt into the precursor at a slow rate. At the same time, the system was heated up to 60 °C to start the formation of hydrophobic shell. After 4 h, the mixture was quenched by acetone and the precipitation was collected, washed and dried for the further characterizations.

3.1.7. Morphology and Size Distribution Studies. Scanning electron microscopy (SEM) images were collected on a Hitachi S-4700 FESEM microscope (Tokyo, Japan) operated at 15.0 kV to elucidate the microstructure of the nanoparticle gels. All images were captured of nanoparticle gels coated with Au/Pd prior to imaging. The size distribution of nanoparticle gels was examined by dynamic light scattering (DLS) (Malvern NanoSizer ZS90). The measurements were carried out at a scattering angle of 90° with the light source (He-Ne laser, 4.0 mW 633 nm) at 25 °C. Transmission electron microscopy (TEM) images were collected on Tecnai F20 using holey carbon film copper grids.

3.1.8. Nuclear Magnetic Resonance Analysis. ^{1}H and ^{19}F nuclear magnetic resonance (NMR) spectroscopy was conducted on a Varian (Palo Alto, CA) Inova 400 FT-NMR using D_2O as solvent and the residue peak at 4.80 ppm as an internal reference.

3.1.9. Rheological Studies. The rheological properties of the dispersions of nanoparticle gels were measured using a Brookfield DV3T rheometer. The samples were subject to rheological measurements at 25 °C using a SC-31 geometry.

3.1.10. Thermal Stability Studies. The long-term stability of nanoparticle gels were studied in 1 wt.% NaCl solution under varies of temperature with and without the presence of CO_2. The nanoparticle gel dispersions were placed into a small capless glass vail and put into high pressure vessel vertically as displayed in Figure 3.5. The high pressure vessel is able to stand as high as 3000 psi pressure at 100 °C, which is in the supercritical region of CO_2. The average diameter and size distribution of nanoparticle gels was monitored at different aging time.

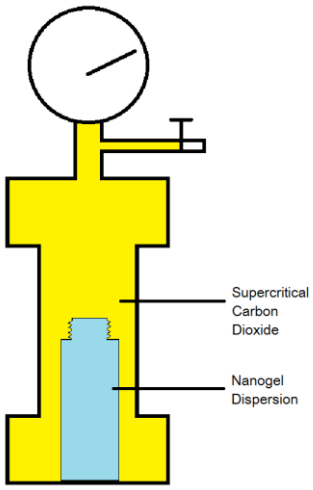

Figure 3.5. Schematic representation of high pressure vessel for thermal stability test.

The ampoules were used to investigate the long-term thermal stability of nanoparticle gels at the atmosphere pressure. The preparation process is as follow: the dispersions of nanoparticle gels were placed into ampoules and vacuumed using the

vacuum maniford with a liquid nitrogen trap (Figure 3.6). The ampoules were sealed till no more bubbles come out from the nanoparticle gel dispersions. Then the sealed ampoules were placed under different temperatures. The control samples were prepared in the absence of vacuum procedure.

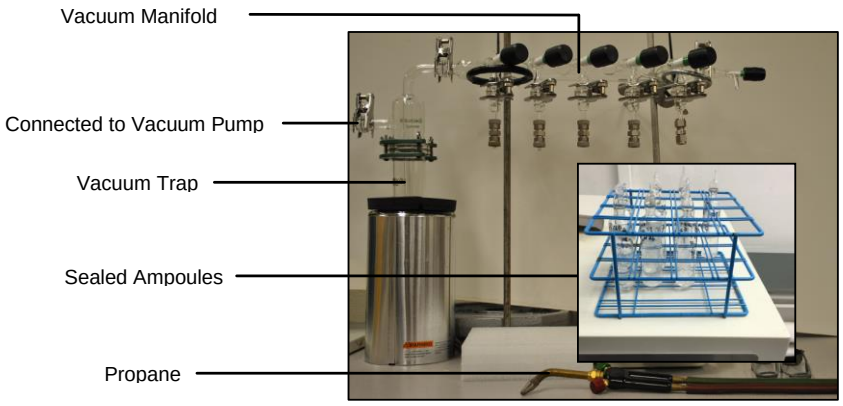

Figure 3.6. Experimental apparatus to seal ampoules for long-term thermal stability experiments.

3.2. RESULTS AND ANALYSIS

The nanoparticle gels were successfully synthesized through dispersion polymerization and suspension polymerization. By prepared suitable fluoro-surfactants, the polymeric nanoparticle gels can be prepared under supercritical carbon dioxide conditions. The nanoparticle gels with different physicochemical properties were designed and further characterized for their specific stimuli-responsive behaviors to the surrounding environments. Two kinds of CO_2-responsive nanoparticle gels were developed in our experiments by either introducing a labile crosslinker or core structure into the nanoparticle gels or applying a CO_2-responsive monomer which could protonated in the presence of CO_2.

3.2.1. Emulsion Polymerization in $scCO_2$. The only polymers shown to have good solubility in pure CO_2 under mild conditions are certain amorphous fluoropolymers and silicones. Herein, a kind of fluoropolymer, poly(1H, 1H-perfluorooctylmethyl acrylate) (PFOA) was used as the stabilizer in the emulsion polymerization of polyacrylamide-based nanoparticle gels. The mixture of 2 g acrylamide and 18 g water was added into a high pressure vessel with sapphire crystal glass on one side under $scCO_2$ condition (1500 psi, 50 °C). After added different amount of PFOA, the container was shook vigorously to investigate the stability of fluoropolymer stabilized emulsion. In our observation, the phase separate time increased with the amount of PFOA added into the emulsion system. When the concentration of PFOA in the emulsion system reached 16.7 wt.%, which is pretty high amount for conventional polymerization, the produced emulsion separated into two phases in less than 60 s. The PFOA is not able to stabilize aqueous solution containing hydrophilic/polar monomers at 1500 psi and 50 C. The reason that the PFOA failed to be a good stabilizer for aqueous solution of acrylamide might cause by the affinity between fluoropolymer backbones and aqueous was not sufficient and/or the hydrophilic segments were hindered by the fluorinated moieties that cannot emulsify aqueous solution in $scCO_2$.

In order to synthesis the nanoparticle gels with narrow size distribution, aqueous solution that contains monomer, crosslinker, and initiator need to be dispersed uniformly in $scCO_2$ that forming stable water-in-$scCO_2$ emulsions. Bis-[2-(F-hexyl) ethyl] phosphate, sodium salt is a kind of surfactant with hydrophilic head and CO_2-philic tail that can be used to stabilize water-in-$scCO_2$ emulsions. The chemical structure of synthesized surfactant was demonstrated by the nuclear magnetic resonance (NMR)

spectroscopy as shown in Figure 3.7. ^{1}H NMR spectra (in D_2O) of the phosphate fluorosurfactant showed three types of signals at chemical shifts of δ 4.1575-4.2086 (q, 4H; J_{HH}: 6.6 Hz, J_{HP}: 6.8 Hz; CH_2O), δ 2.5227-2.6505 (tt, 4H; J_{HH}: 6.6 Hz, J_{HF}: 19.2 Hz; CF_2CH_2), and δ 1.2560-1.2936. ^{19}F NMR showed five types of signals at chemical shifts: -82.5 (CF_2CF_3), -114.6 (CH_2CF_2), -123.0, -124.0, -124.8 (3*CF_2), -127.4 (CF_2CF_3). The NMR spectroscopy results demonstrated that the synthesized phosphate fluorosurfactant is bis-[2-(F-hexyl) ethyl] phosphate, sodium salt.

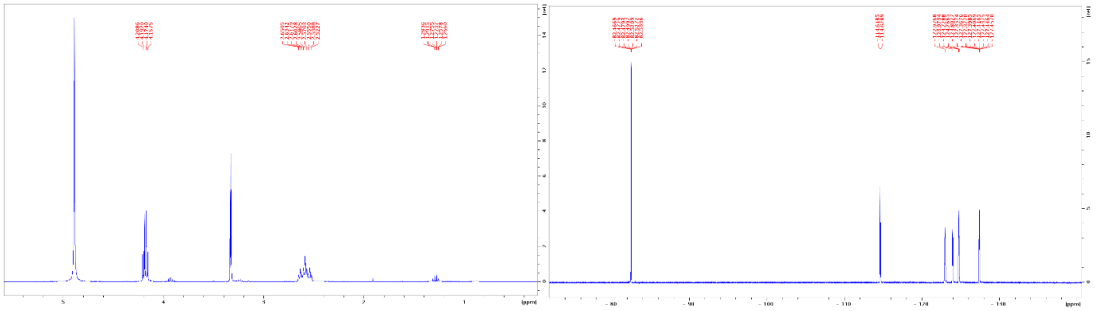

Figure 3.7. ^{1}H and ^{19}F NMR photos of phosphate fluorosurfactant (left: ^{1}H NMR of phosphate fluorosurfactant; right: ^{19}F NMR of phosphate fluorosurfactant).

The size distribution of produced nanoparticle gels was measured using dynamic light scattering (DLS) in distilled water (Figure 3.8) and the average diameter of nanoparticle gels produced by using phosphate fluorosurfactant as stabilizer is 473.8 nm after swelling. Scanning electron microscope (SEM) photo showed that the produced nanoparticle gels displayed a cubic instead of spherical appearance (Figure 3.8) and the size of these crystal-like cubes is much larger than the size measured by DLS. The different size of nanoparticle gels from DLS and SEM results indicated that the produced nanoparticle gels prefer aggregate in the poor solvents, like acetone, and will dispersed in their swollen state in the good solvents, like distilled water.

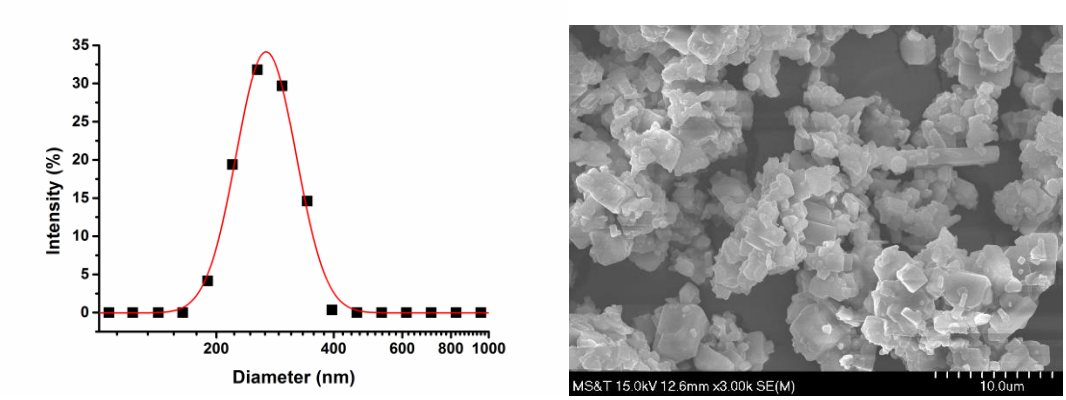

Figure 3.8. Size distribution (left) and SEM photo of nanoparticle gels (right) produced using phosphate fluorosurfactant.

3.2.2. Nanoparticle Gel Synthesis by Dispersion Polymerization. Acrylic acid is moderately soluble in $scCO_2$ whereas its polymer, poly(acrylic acid) is insoluble. Thus, it is possible to polymerize poly(acrylic acid) in $scCO_2$ via dispersion polymerization.

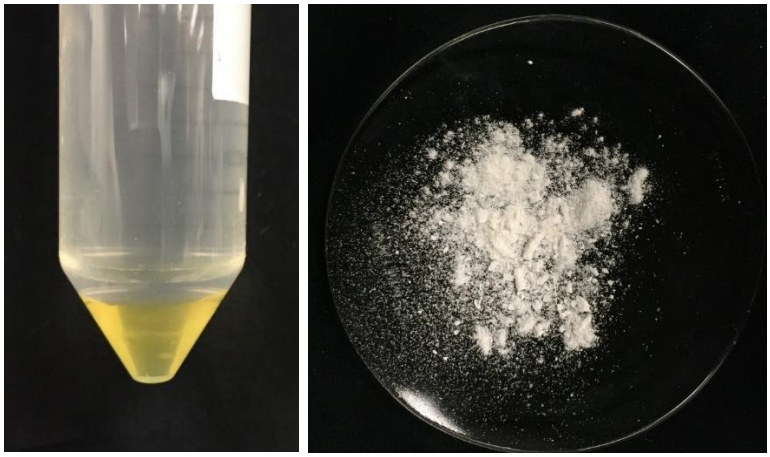

Figure 3.9. Photo of (left) aqueous solution after dispersion polymerization and (right) produced nanoparticle gels.

Herein, we synthesized nanoparticle gels using 2-acrylamido-2-methylpropane sulfonic acid sodium salt (AMPS-Na) through surfactant-free polymerization due to the similar properties between acrylic acid and AMPS. The dispersed aqueous solution after

dispersion polymerization was transparent and displayed a bright yellow color (Figure 3.9). After precipitated by acetone and dried in vacuum, the produced nanoparticle gels showed to be a white powder as shown in Figure 3.9.

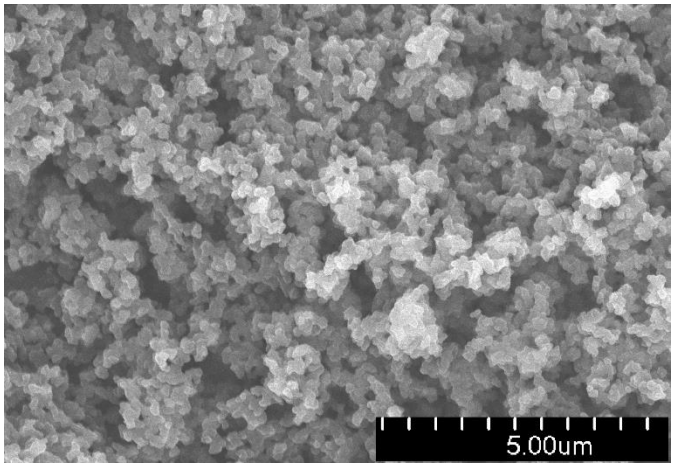

Figure 3.10. SEM image of nanoparticle gels produced through dispersion polymerization in $scCO_2$.

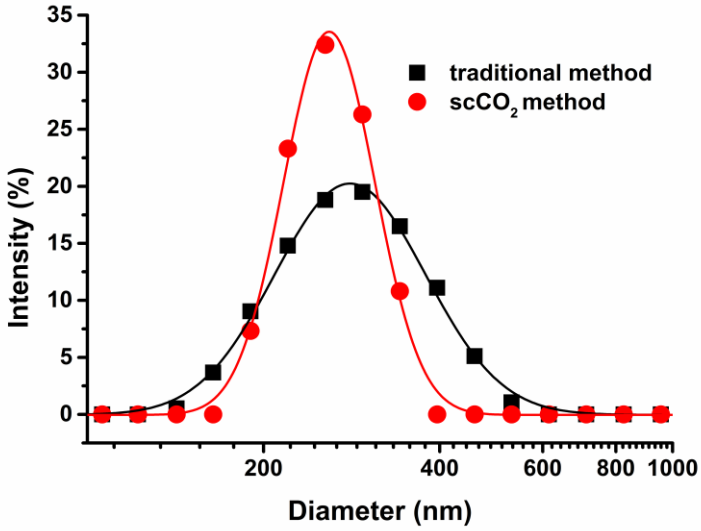

Figure 3.11. Particle size distribution of the nanoparticle gels with same composition synthesized through polymerization in organic solvent and in $scCO_2$.

The nanoparticle gels produced through dispersion polymerization showed a spherical appearance and the average diameter of the nanoparticle gels was ~50 nm as shown in Figure 3.10. The dispersion polymerization method contributed to the narrow size distribution and uniform size and appearance of produced nanoparticle gels.Compared with the nanoparticle gels synthesized in organic solvent, the nanoparticle gels produced using scCO2 has a narrower size distribution and a smaller particle size (Figure 3.11).

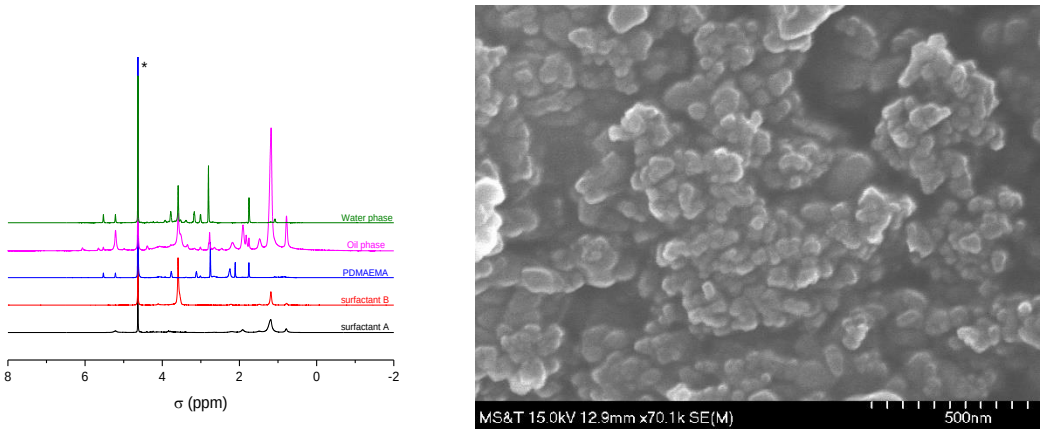

Figure 3.12. ^{1}H NMR photos of produced water phase, oil phase and pure contents (left) and SEM photo of produced CO_2 responsive nanoparticle gel.

The narrowed size distribution might be contributed by the density and viscosity of $scCO_2$. In conventional method (polymerization in organic solvent), the size of produced nanoparticle gels is related with the concentration and properties of emulsifier, the viscosity and density of surrounding solutions, reaction time, and reaction temperature, etc. However, in scCO2 dispersion polymerization, no emulsifier or stabilizer was used. The stability of polymeric nanoparticle gels was solely balanced by soluble parts and insoluble parts that changed as a function of reaction time. The

produced nanoparticle gels have a much narrower size distribution because the solubility of nanoparticle gels controlled the size much more precisely than the emulsifier and stabilizer.

3.2.3. CO_2-responsive Nanoparticle Gel Characterization. The 2-(dimethylamino) ethyl methacrylate (DMAEMA), a monomer that is able to protonated in acidic solutions, was used to prepare the nanoparticle gels that can swell when contact with CO_2. However, after emulsion polymerization, it's hard to tell the produced nanoparticle gels were contained in water phase or oil phase. NMR spectroscopy was used to characterize the water phase, oil phase, and feed chemicals to illustrate the soluble phase of produced nanoparticle gels (Figure 3.12).

The NMR spectroscopy showed that the DMAEMA signal was detected in both water phase and oil phase. However, the finger print peaks in water phase was quite sharp whereas the one in oil phase was considerably broader, which indicated that the unreacted DMAEMA monomer was remained in water phase while the produced polyDMAEMA nanoparticle gels were in oil phase. After extracted DMAEMA nanoparticle gels, the morphology of produced nanoparticle gels was examined using SEM and the average diameter of polyDMAEMA nanoparticle gels is around 50 nm (Figure 3.12).

3.2.4. Effect of Synthetic Factors on Nanoparticle Gels. The average diameter and size distribution of produced nanoparticle gels were influenced by the synthetic pressure, the initiator concentration, and the monomer concentration, and so on.

In order to investigate the effect of different parameters and control the size of produced nanoparticle gels, a series of experiments were conducted at different feeding ratios and under different conditions. Herein, the effect of initiator concentration,

synthetic pressure, monomer concentration, and reactor dimension on the properties of produced nanoparticle gels was discussed.

In our experiments, we found that the diameter of produced nanoparticle gels decreased with the initiator concentration and the decreasing trend turned to be neglectable when the concentration of initiator was above 5000 ppm (Figure 3.13).

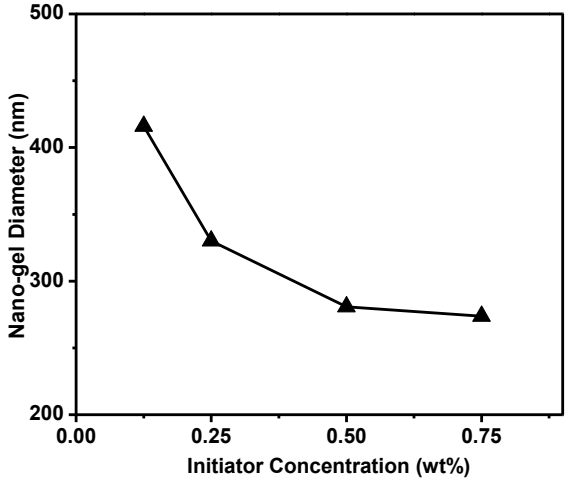

Figure 3.13. Diameter of swollen nanoparticle gels synthesized at different initiator concentration.

The initiator used for scCO2 polymerization was AIBN, an azo-initiator that insoluble in water. After heated up to 60 °C, AIBN started to decompose and produce free radicals and nitrogen gas. The rate of polymerization was dominated by the concentration of initiator transported from scCO2 to the aqueous solution as described in the following equation:

$$R_p = k_p[M]\sqrt{\frac{fk_i}{k_t}[I_2]} = k_p'[M][I_2]$$

where R_p is the rate of polymerization, k_p is the rate of propagation, [M] is the concentration of monomer, f is the friction of reactive initiator, k_i is the rate of initiation, k_t is the rate of termination, and $[I_2]$ is the concentration of initiator.

The diameter of produced nanoparticle gels is related to the rate of polymerization. In general, high concentration of initiator creates a large amount of free radicals in a short time. Each radical can start initiation and chain propagation to form a nanoparticle gel when meet with the monomers.

Due to the fixed monomer concentration, the higher the initiator concentration the fewer monomers involved in a single nanoparticle gel, which leads to a smaller diameter of produced nanoparticle gels. In addition, the diameter of produced nanoparticle gels is dominated by the affinity between the produced nanoparticle gels and solvent at high initiator concentration. Polymer chain starts to entanglement and fold that in consequence, precipitate from the solvent when reaches certain chain length. At that time, monomers, oligomers, and short polymer chains will attached to the precipitated polymer chains controlled by their polarities and further propagation. When the concentration of initiator is efficient to initiate enough monomers at the start of polymerization, very tiny amount of monomers will attached to the precipitated polymer chains and make the nanoparticle gels further growing. Thus, the diameter of nanoparticle gel will not further decreased with the initiator concentration.

The diameter of produced nanoparticle gels was also influenced by the synthetic pressure of $scCO_2$ during the polymerization as shown in Figure 3.14. When the pressure of $scCO_2$ below 2500 psi, the diameter of produced nanoparticle gels was higher than 800 nm and the produced solution was not stable compared with the sample synthesized at

3000 psi. The trend of diameter sudden changed when the pressure was above 2600 psi, which might cause by the properties of $scCO_2$ changed dramatically when the pressure was above 2600 psi at 60 °C.

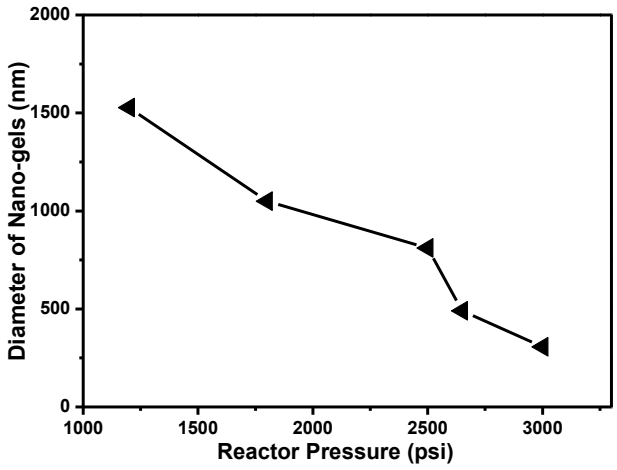

Figure 3.14. Diameter of the swollen nanoparticle gel synthesized under different pressures.

We can find out that the density of $scCO_2$ at 2500 psi is 0.658 g/cm^3 and 0.674 g/cm^3 at 2600 psi using the online calculator from the website of http://www.peacesoftware.de/einigewerte/co2_e.html. However, at 1200 psi, the density of $scCO_2$ is only 0.203 g/cm^3, which is insufficient to hold the produced nanoparticle gels with constant shear. Moreover, the viscosity of $scCO_2$ was significant lower compared with the organic solvents and water. At 3000 psi, the viscosity of $scCO_2$ reached 0.06 mPa•s. Considered the effect of surrounding solutions on the produced nanoparticle gels, low viscosity and high density of the $scCO_2$ contributed to a uniform size distribution of produced nanoparticle gels.

Herein, we investigated the effect of monomer concentration on the size of nanoparticle gels by controlling the amount of feeding monomer solution in the system. For a common understanding, the diameter of produced nanoparticle gels increased with volume of monomer solution because sufficient monomers could attach to the precipitated polymer chains and help the nanoparticle gels grow. However, in our experiments, the results showed that the diameter of produced nanoparticle gels did not increase proportionally with the volume of fed monomer solution (Figure 3.15). From the previous equation, we can know that the rate of polymerization is indirect proportion to monomer concentration.

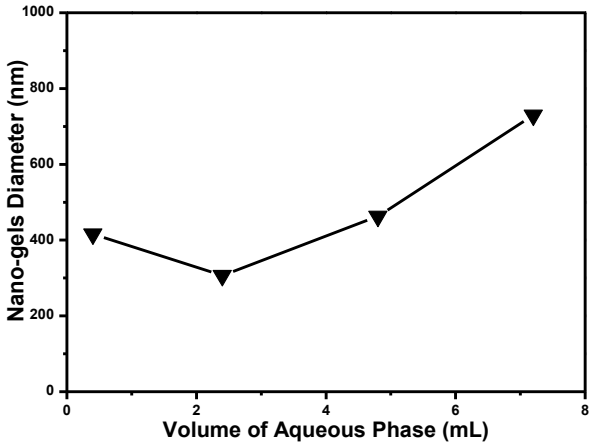

Figure 3.15. Diameter of the swollen nanoparticle gels synthesized with different volumes of monomer solution.

Although the increased concentration of monomer (volume of monomer solution) caused a faster polymerization rate and a bigger produced nanoparticle gel. Nevertheless, insufficient shear influenced the diameter of produced nanoparticle gels when the volume of monomer solution was less than 0.5 mL, which was too little compared with the size of

reactor and stirrer. Thus, when the amount of monomer solution was insufficient, the efficiency of shearing took the place to dominate the diameter of produced nanoparticle gels. Otherwise, the diameter of produced nanoparticle gels was proportional to the monomer concentrations.

The relationship between swelling ratio and crosslinking density, which was proportional to the crosslinker concentration, was studied and demonstrated by the Flory-Huggins equation:

$$Q^{\frac{5}{3}} = \frac{(\frac{i}{2V_u S^{\frac{1}{2}}})^2 + (\frac{1}{2} - x_1)/V_1}{V_E/V_0}$$

where Q is the degree of swelling, i/V_u is the charge density of polymer, S is the ionic strength of solution, $(1/2 - x_1)/V_1$ is the polymer-solvent affinity, V_E/V_0 is the crosslinking density.

In our experiments, we controlled the crosslinker to monomer ratio by mole to study the effect of crosslinker concentration on the average diameter of produced nanoparticle gels. The relationship between the average diameter of produced nanoparticle gels and the ratio of crosslinker to monomers follows power law as displayed in Figure 3.16. When the ratio of crosslinker to monomer was less than 0.07% mol/mol, the average diameter of produced nanoparticle gels was greatly influenced by the crosslinker concentration. For the point of the ratio of crosslinker to monomers was 0.05% mol/mol, the produced nanoparticle gels had loosely crosslinked polymeric network. With the increased crosslinking density, the polymeric network turned to be tighter and tighter. When the crosslinking density reached the critical point (0.09% mol/mol in our experiments), the network of polymer chains cannot further compact and

the diameter of corresponding nanoparticle gels became independent to the crosslinker concentrations.

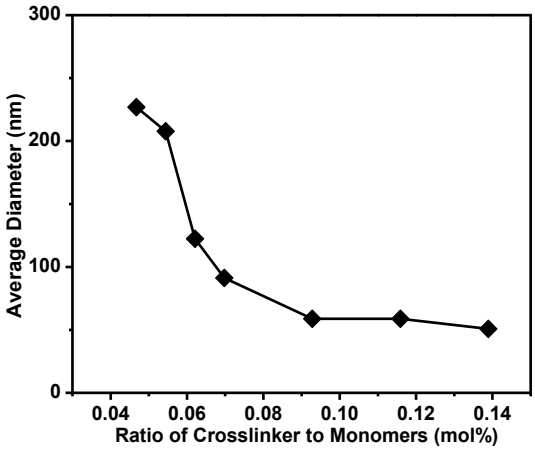

Figure 3.16. Diameter of swollen nanoparticle gels synthesized with different crosslinker concentrations.

In our experiments, we also studied the influenced of reactor capacity on the diameter of produced nanoparticle gels. Two reactors with the similar shape but different capacities were used to synthesize nanoparticle gels with controlled monomer solution volume. All the other parameters were controlled to be same during the reaction. The diameter of produced nanoparticle gels was same in the 50 and 300 mL reactor as shown in Figure 3.17. It can also be seen that the trend of diameter changing was same when the monomer solution volume changed. Considered the results of various monomer solution volumes, we found an interesting phenomenon that the diameter of produced nanoparticle gels kept constant even the ratio of $scCO_2$ to monomer solution changed. This was different with the conventional suspension polymerization, as we known that the ratio of surrounding solution to dispersed solution usually determined the size of result particles.

The capacity of reactor influenced the shear provided by the magnetic stirrer so that balanced the influenced the monomer concentration effect on the diameter of produced nanoparticle gels.

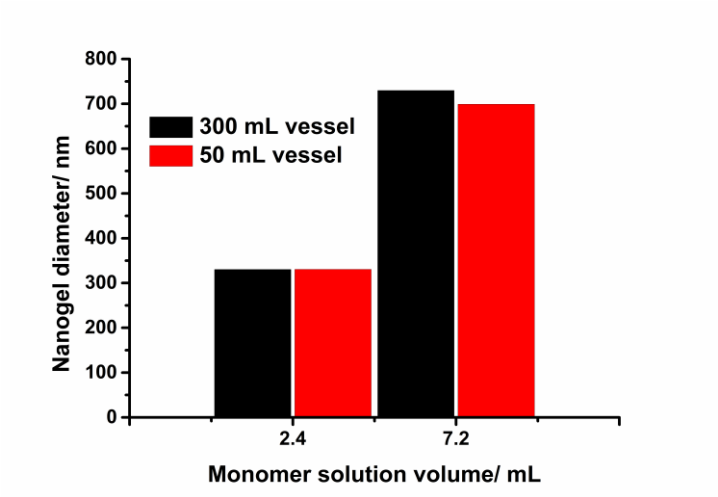

Figure 3.17. Diameter of swollen nanoparticle gels synthesized in different reactor.

3.2.5. Effect of Environmental Factors on Nanoparticle Gels. In order to perform successful nanoparticle gel treatment in the oil reservoirs that produced using CO_2 or $scCO_2$ flooding, the nanoparticle gels should maintain or increase their swelling ratio and strength when contacted with CO_2.

Herein, we prepared the partially hydrolyzed polyacrylamide (HPAM) nanoparticle gels as control sample because HPAM-based polymers and hydrogels are the most widely used conformance control agents in the oil industry. The AMPS nanoparticle gels, which were resistant to salt and acid, were prepared and compared with the HPAM nanoparticle gels. In addition, AMPS monomer was subjected in two of the CO_2-responsive nanoparticle gels to prevent the shrinkage of polymer chains in the presence of CO_2. Herein, a cationic monomer, DMAEMA was used to synthesize CO_2

responsive nanogels due to the protonation of tertiary amine moieties in acidic solutions. The physicochemical properties of the produced nanoparticle gels for the in-depth treatment were listed in Table 3.2.

Table 3.2. Physicochemical properties of the produced nanoparticle gels.

Nanoparticle gels	Functional component	Diameter before reswell	Diameter after reswell	Trigger	Reswelling rate
HPAM	Amine	360 nm	115 nm	N/A	N/A
AMPS	Sulfonic	220 nm	190 nm	N/A	N/A
Double crosslinker	Labile and stable crosslinker	100 nm	155 nm	Heat and CO_2	Slow
Core-shell	Labile hydrophobic shell and hydrophilic core	280 nm	5000 nm	Heat and CO_2	Fast
CO_2 responsive	Amine moieties	175 nm	245 nm	CO_2	Fast

Herein, the performance of AMPS nanoparticle gels that synthesized in $scCO_2$ was compared with HPAM nanoparticle gels, which has the same properties of the plugging agent used in the petroleum industry. The main composition of HPAM nanoparticle gels is partially hydrolyzed polyacrylamide with a 10% hydrolyzed degree by mole. In our experiments, we used 10% sodium acrylate and 90% acrylamide to prepare HPAM nanogel through the conventional emulsion polymerization.

Sodium chloride (NaCl) solutions of different salt concentrations from 0 to 2 wt.% were prepared to examine the effect of NaCl on the properties of AMPS and HPAM nanoparticle gels. The diameters of AMPS and HPAM nanoparticle gels in different NaCl solutions were measured by dynamic light scattering (DLS) as shown in Figure 3.18. From the figure we can conclude that both AMPS and HPMA nanoparticle gels

shrunk with the increased salt concentration. However, the AMPS nanoparticle gels were not as sensitive to NaCl concentrations as the HPAM nanoparticle gels. In detail, the diameter of AMPS nanoparticle gels only decreased at the NaCl concentrations from 0 to 0.25 wt.%. Then, the diameter became constant with the increased NaCl concentrations. Nevertheless, the HPAM nanoparticle gels kept shrinking until the salt concentration reached 0.5 wt.%. In addition, the ratio of shrinkage calculated by the volume of AMPS nanoparticle gels was 54.5%, which was much smaller than the 88.0% of the HPAM nanoparticle gels. The swelling behaviors of the AMPS and HPAM nanoparticle gels demonstrated that the AMPS nanoparticle gels were more salt tolerant compared with the HPAM nanoparticle gels.

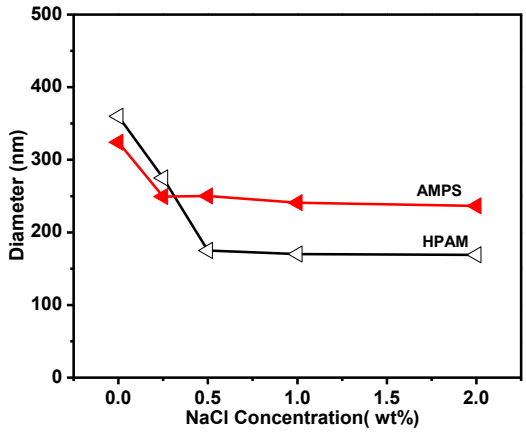

Figure 3.18. Diameter of the AMPS and HPAM nanoparticle gels in different NaCl solutions.

Swelling behavior is not the only parameter to characterize the salt resistance of nanoparticle gels. Besides shrinkage, nanoparticle gels can aggregate and form precipitations at high salt concentrations due to the reduction of electrostatic repulsion

among nanoparticle gels. Zeta potential was used to describe the charge of the slipping panel of nanoparticle gels that usually used to study the stability of dispersions of nanoparticle gels. A high zeta potential confers stability that the nanoparticle gel dispersions will resist aggregation. When the zeta potential is low, attractive forces may exceed the electrostatic repulsion and the dispersions turn to break and nanoparticle gels flocculate. Thus, nanoparticle gels with high zeta potentials, no matter positive or negative, are electrically stabilized while nanoparticle gels with low zeta potentials tend to coagulate or flocculate.

Zeta potential of the HPAM nanoparticle gels reduced dramatically when the NaCl concentration increased from 0 to 0.5 wt.% and tend to be constant when the salt concentration above 1 wt.% as shown in Figure 3.19. For the AMPS nanoparticle gels, the zeta potential did not change when salt concentration below 0.5 wt.% and started to decrease linearly with further increased salt concentration at a smaller slope than the one of HPAM nanoparticle gels. When the NaCl concentration reached 2 wt.%, the zeta potential of the AMPS nanoparticle gels was lower than 20 mV, which demonstrated that the AMPS nanoparticle gel dispersions was moderately stable in the NaCl solution. Furthermore, absolute zeta potential of the AMPS nanoparticle gels was higher than the one of HPAM nanoparticle gels at varies NaCl concentrations, which indicated that the dispersion of the AMPS nanoparticle gels was more stable in NaCl solutions than the dispersion of the HPAM nanoparticle gels.

Viscosity is an important parameter of nanoparticle gel dispersion because that the viscosity determined the mobility of nanoparticle gel dispersion. The viscosity of nanoparticle gel dispersions was measured at room temperature at a 6 s^{-1} shear rate to

simulate the flow condition of nanoparticle gels transport through the formation. The viscosity of nanoparticle gel dispersions in the absence of NaCl increased from 1.4 to 4.9 cP with the nanoparticle gel concentration as shown in Figure 3.20. According to the Einstein theory, the viscosity of nanoparticle gel dispersion was a linear function to the concentration. It is easy to find out that the trend of viscosity versus concentration curve started not following the linear trend at the concentration above 5000 ppm. The interaction among nanoparticle gels cannot be neglected above that concentration.

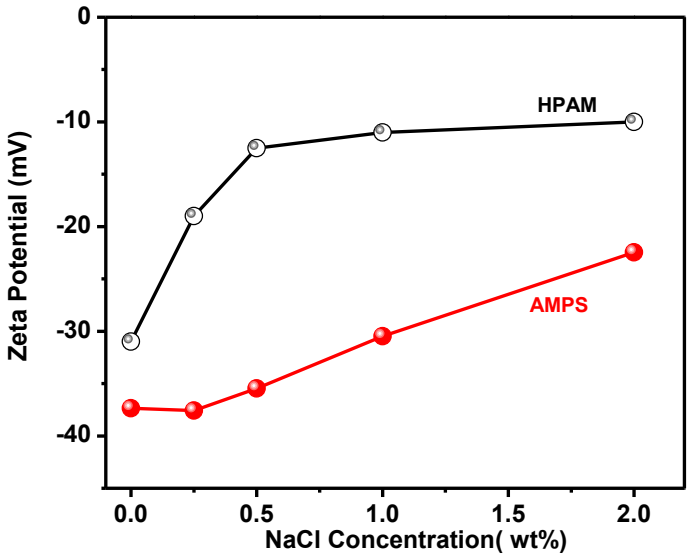

Figure 3.19. Zeta potential of the AMPS and HPAM nanoparticle gels in different NaCl solutions.

Therefore, the Einstein theory was no longer applicable in the concentrated nanoparticle gel dispersions. Moreover, the viscosity of nanoparticle gel dispersions increased with the salt concentration, which is contrary to the Einstein theory that viscosity of the dispersion was proportional to the volume friction of the dispersant. This

might cause by the interaction among the dispersed nanoparticle gels. Added salt not only made nanoparticle gels shrink, but also reduced the zeta potential of the nanoparticle gels, which decreased the stability of nanoparticle gel dispersion and increased the interaction among the nanoparticle gels. However, the influence of NaCl on the viscosity of nanoparticle gel dispersions was neglectable for the AMPS nanoparticle gels.

Same with salt, pH influence the swelling ratio of nanoparticle gels by changing the ionic strength of the solutions. In addition, the proton and hydroxide ion released by acid and alkaline could affect the swelling ratio as well as reduce the electrostatic repulsion among the nanoparticle gels.

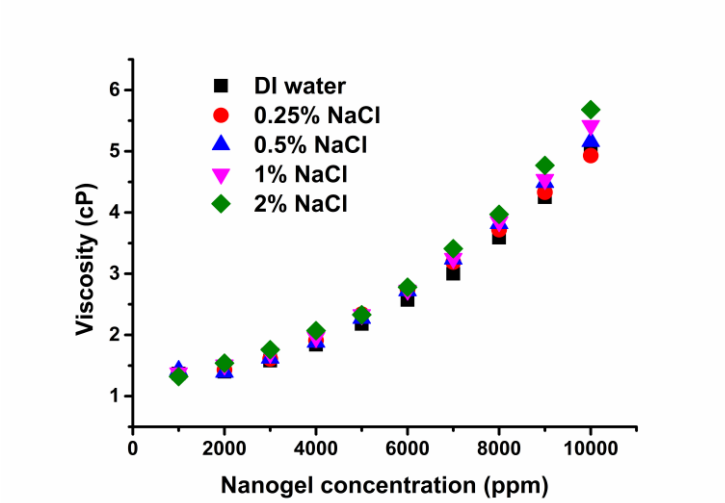

Figure 3.20. Viscosity of nanoparticle gel dispersions at different salt concentrations.

The salt effect was excluded in this experiment by controlled the ionic strength of pH solutions. The diameter of the AMPS nanoparticle gels was kept constant at pH varies from 3 to 9 as shown in Figure 3.21. However, for the HPAM nanoparticle gels, the diameter at pH 3 is two third of the diameter of at pH 7. The HPAM nanoparticle gels

also tended to degrade at high pH that the diameter of nanoparticle gels kept increasing and had no peak signals above 10 nm after soaked for 24 h. Thus, the AMPS nanoparticle gels were much more stable in both acidic and alkali solutions compared with the HPAM nanoparticle gels.

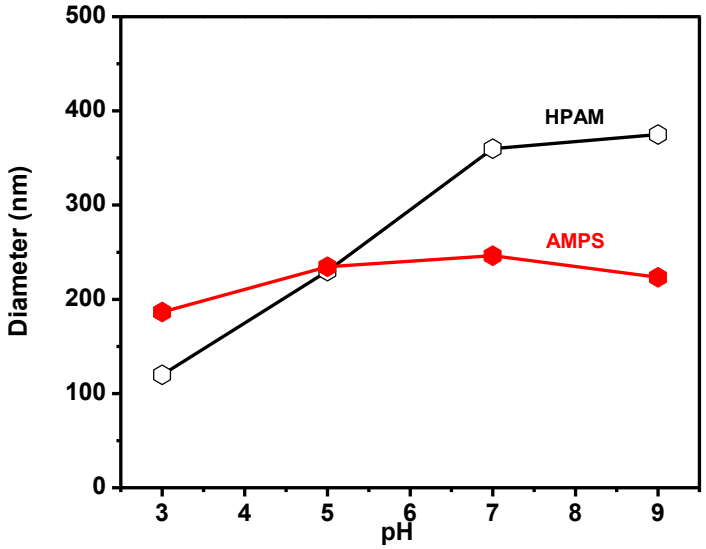

Figure 3.21. Diameter of the AMPS and HPAM nanoparticle gels in different pH solutions.

The double crosslinker and core-shell nanoparticle gels were synthesized and characterized at different temperature, salt concentration, and in the presence of CO_2 to investigate the response of nanoparticle gels to the stimulations. In order to deliver the nanoparticle gels to the in-depth formation, the size of the nanoparticle gel should be small enough before it reach the target zone and then start to swell and plug the water path. The reservoir temperature is usually higher than surface temperature so that the temperature could be used as a trigger for the second swelling of nanoparticle gels. In

addition, carbon dioxide produced carbonic acid slowly that can turn the pH of water to as low as 3 when contact with water, which could be another trigger for the second swelling of the nanoparticle gels. Thus, nanoparticle gels with double crosslinkers, both stable and labile (acid/ temperature triggered) crosslinkers can meet the requirement of the in-depth treatment. Herein, polyethylene glycol-200-diacrylate (PEG-200-DA) was subjected as the labile crosslinker of the double crosslinker and core-shell nanoparticle gels.

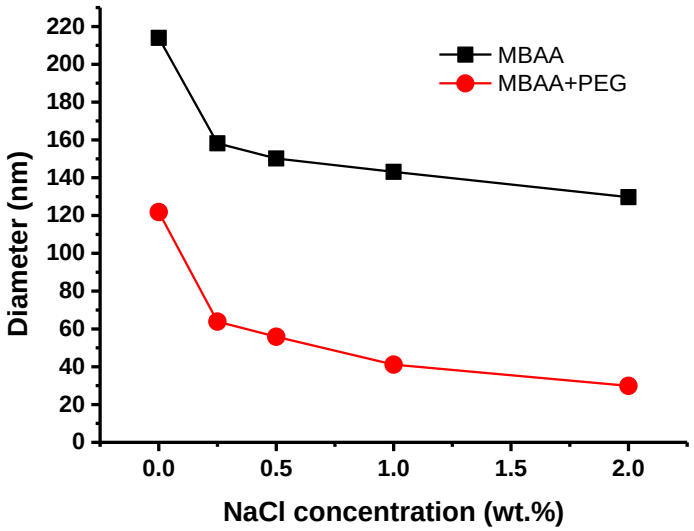

Figure 3.22. Diameter of the AMPS and double crosslinker nanoparticle gels at different NaCl concentrations.

The diameter of double crosslinker nanoparticle gels was smaller than the AMPS nanoparticle gels caused by the higher crosslinking density from the additional PEG-200-DA as shown in Figure 3.22. The diameter of the AMPS nanoparticle gels was 214 nm in distilled water while the double crosslinker nanoparticle gels was only 122 nm. The NaCl effect on the AMPS and nanoparticle gels was same because the swelling of both

nanoparticle gels were mainly dominated by the electrostatic repulsion among the sulfonic moieties on the polyAMPS chains.

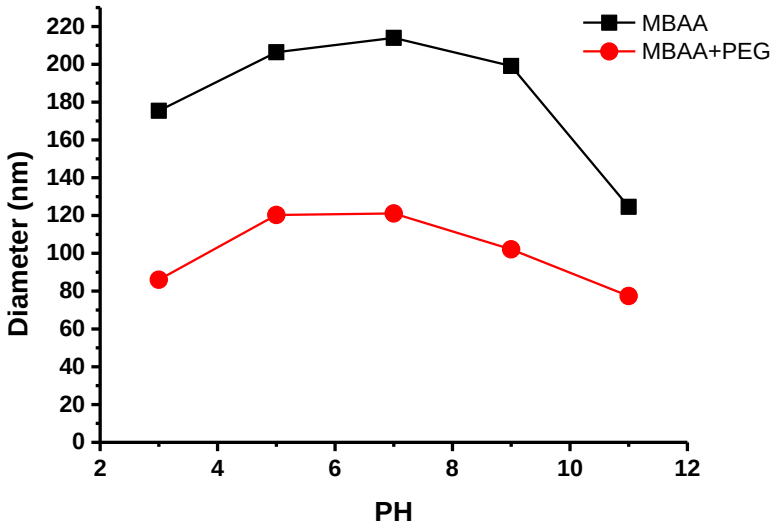

Figure 3.23. Diameter of the AMPS and double crosslinker nanoparticle gels at different pHs.

The effect of pH on the diameter of the double crosslinker nanoparticle gels was studied as the following procedure: the AMPS and double crosslinker nanoparticle gels were fully swelled in distilled water and then, transferred to solution with different pHs. After 10 min, the diameter of nanoparticle gels at different pHs was characterized using DLS. From Figure 3.23, the diameter of the AMPS and double crosslinker nanoparticle gels decreased at low or high pHs. In pH 3 solution, the diameter of double crosslinker nanoparticle gels was 86 nm, which was much smaller than the diameter in distilled water. The total ionic strength of the pH solutions was controlled same by added NaCl. However, the nanoparticle gels still showed shrinkage at both high and low pHs, which might cause by the proton and hydroxide ions could reduce the electrostatic repulsion

among polyAMPS chains much more than the sodium or chloride ions. Furthermore, the labile crosslinker contained in the double crosslinker nanoparticle gels did not hydrolyze and degrade in 10 min.

The core-shell nanoparticle gels, which consisted a hydrophilic core crosslinked by a stable crosslinker and a hydrophobic shell crosslinked by a labile crosslinker, were prepared through a semi-continuous emulsion polymerization. The hydrophobic shell hindered the shrinkage of polyAMPS chains in the solution with salt, acid, and alkaline.

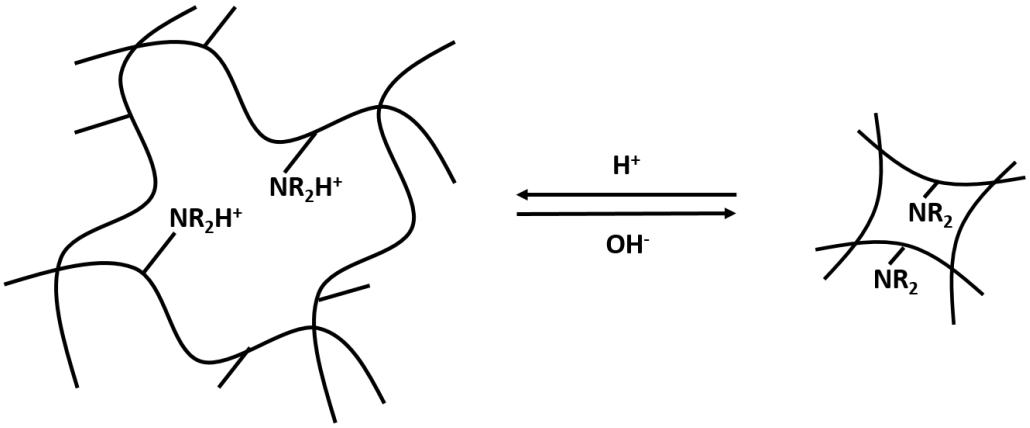

Figure 3.24. Scheme of pH stimulation of cationic nanogel.

The double crosslinker nanoparticle gels can second swell in the in-depth formation when the labile crosslinker degraded by temperature or CO_2. However, the slowly degrading rate of the labile crosslinker brought some uncertainty for the treatment in the oil field. Herein, we described a nanoparticle gel that was able to response to the stimulation (CO_2) in a short time.

When the CO_2 dissolved in the formation water, carbonic acid started to form and release the protons slowly. The cationic monomer, 2-(dimethylamino) ethyl methacrylate (DMAEMA) protonated in acidic solutions and produced extra electrostatic repulsions

among the polymer chains. The size of DMAEMA nanoparticle would response to the pH value of the surrounding solutions by the protonation and deprotionation of tertiary amine in the polymer chains (Figure 3.24).

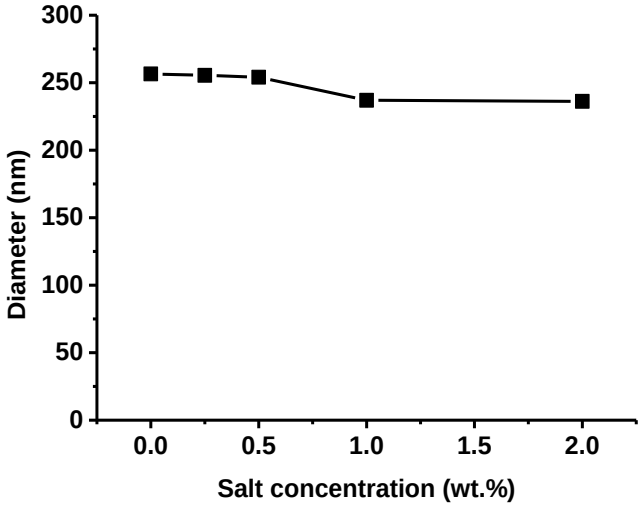

Figure 3.25. Average diameter of the CO_2 responsive nanoparticle gels at different NaCl concentrations.

NaCl solutions with different concentrations from 0 to 2 wt.% were prepared to examine the effect of salt concentration on the average diameter of the CO_2 responsive nanoparticle gels, which was examined by DLS at room temperature. The average diameter of the CO_2 responsive nanoparticle gels did not changed with the increased NaCl concentrations as shown in Figure 3.25. The salt tolerant properties of the CO_2 responsive nanoparticle gels due to the tertiary amine moieties on the polyDMAEMA chains. Different to the HPAM and AMPS nanoparticle gels, the polymeric network of the CO_2 responsive nanoparticle gels was neutral charged in the pH 7 solutions. The swelling ratio of the CO_2 responsive nanoparticle gels was controlled by the affinity between the polyDMAEMA chains and the solvent.

The CO_2 responsive properties of the CO_2 responsive nanoparticle gels was measured by purging CO_2 into the dispersion of nanoparticle gels. The diameter of the CO_2 responsive nanoparticle gels was measured respect to the time of the CO_2 purging. The diameter of the CO_2 responsive nanoparticle gels increased from 175 to 245 nm after 10 min CO_2 purging. Also, the diameter of the CO_2 responsive nanoparticle gels kept constant at ~245 nm with further CO_2 purging as shown in Figure 3.26. The CO_2 responsive nanoparticle gels was sensitive to acid environment because the reaction rate of protonation of the tertiary amine moieties was very fast in the solution. After protonated, the electrostatic repulsion among the tertiary amine groups contained in the polyDMAEMA chains greatly increased. The repulsion force made the CO_2 responsive nanoparticle gels continuously swell until reached the equilibrium swelling ratio.

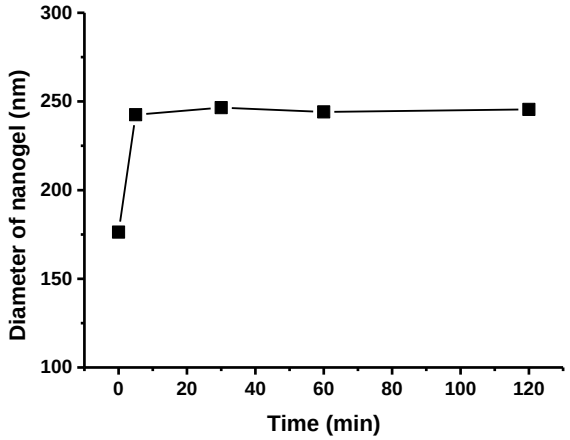

Figure 3.26. Diameter of the CO_2 responsive nanoparticle gels in brine after CO_2 purging.

The effect of CO_2 on the CO_2 responsive nanoparticle gels can also been detected by measuring zeta potential of the nanoparticle gels. The zeta potential of the CO_2 responsive nanoparticle gels before CO_2 purging was ~3 mV and increased to ~14 mV

after 10 min CO_2 purging as shown in Figure 3.27. Zeta potential of the CO_2 responsive nanoparticle gels increased with the time of CO_2 purging, from 14 to 19 mV, which indicated further protonated of the polyDMAEMA chains. In addition, this CO_2 responsive of the PAETAC polymeric network is very sensitive to the environmental stimulation that the polymeric network quickly response to the CO_2 purging in 5 minutes.

3.2.6. Thermal Stability of Nanoparticle Gels. Thermal stability is an important parameter to evaluate the application of the nanoparticle gels under the reservoir conditions.

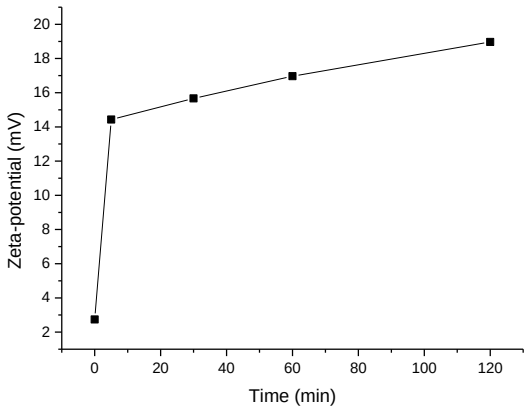

Figure 3.27. Zeta potential of the CO_2 responsive nanoparticle gels in brine after CO_2 purging.

To perform successfully nanoparticle gel treatments, the nanoparticle gels should stand the reservoir temperature without fully degradation. Herein, the diameter of double crosslinker nanoparticle gels changed respect to time of labile crosslinker under different temperature as shown in Figure 3.28. As shown in the figure, the diameter of double crosslinker nanoparticle gels was not changed under 25 and 40 °C. However, for the

double crosslinker nanoparticle gels at 60 ℃, the diameter slowly increased after 2 months, which indicated the labile crosslinker consisted in the nanoparticle gels started to degrade. Moreover, the diameter of double crosslinker nanoparticle gels at different temperatures was slightly difference at the beginning of experiments. The diameter of double crosslinker nanoparticle gels was 130, 122, and 100 nm at 25, 40, and 60 ℃, respectively. This phenomenon might cause by the dispersity of nanoparticle gels was higher at high temperature considered that the Brownian movement of dispersant was proportional to the surrounding temperature. Therefore, the higher temperature lead to a smaller diameter of the nanoparticle gels.

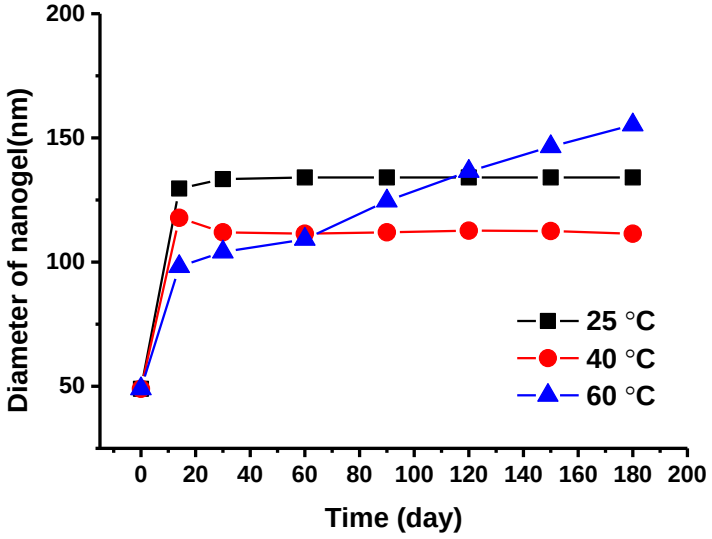

Figure 3.28. Diameter of double crosslinker nanoparticle gels under different temperature of long term measurement.

CO_2 can dissolve in and react with water to produce carbonic acid. The pH value of the CO_2 saturated water can become as low as 4.2 under room condition and around 3 under the formation condition. As mentioned before, the acidic solution were able to

accelerate the degradation of labile crosslinker in the double crosslinker nanoparticle gels. It is necessary to know the effect of CO_2 on the diameter of double crosslinker nanoparticle gels. The double crosslinked nanoparticle gels were dispersed in 1 wt.% NaCl solution saturated with CO_2 and stand at 60 °C for one month and measured the size distribution. The control sample was dispersed in 1 wt.% NaCl solution in the absence of CO_2.

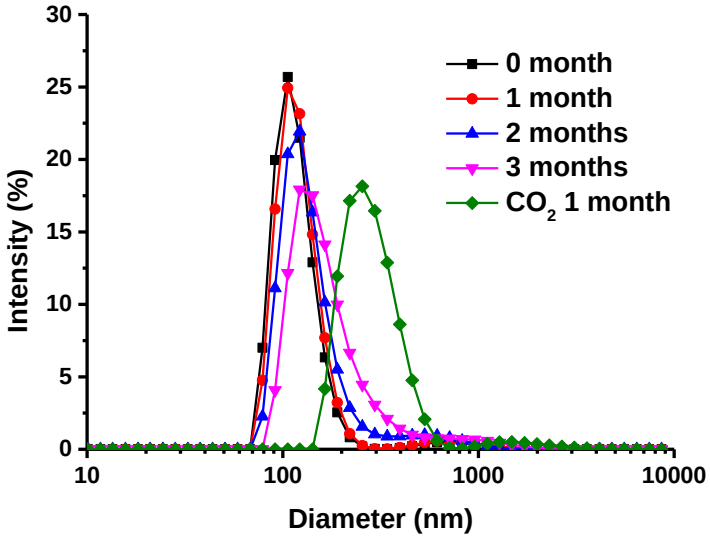

Figure 3.29. Size distribution of the double crosslinker nanoparticle gels at 60 °C.

From the size distribution of double crosslinker nanoparticle gels (Figure 3.29), the CO_2 affected the diameter of double crosslinker nanoparticle gels much more than temperature. The intensity peak of size distribution shifted from 110 to 300 nm after 30 days stimulation in the CO_2 saturated NaCl solution whereas did not shift in the absence of CO_2. This result demonstrated the degradation of ester groups in the double crosslinker nanoparticle gels was much faster in the presence of proton as demonstrated in Figure

3.30. Considered the formation condition that using CO2 to enhance oil recovery, the double crosslinker nanoparticle gels can transported to the in-depth formation and re-swell with the stimulation of temperature (slow rate) and CO2 (fast).

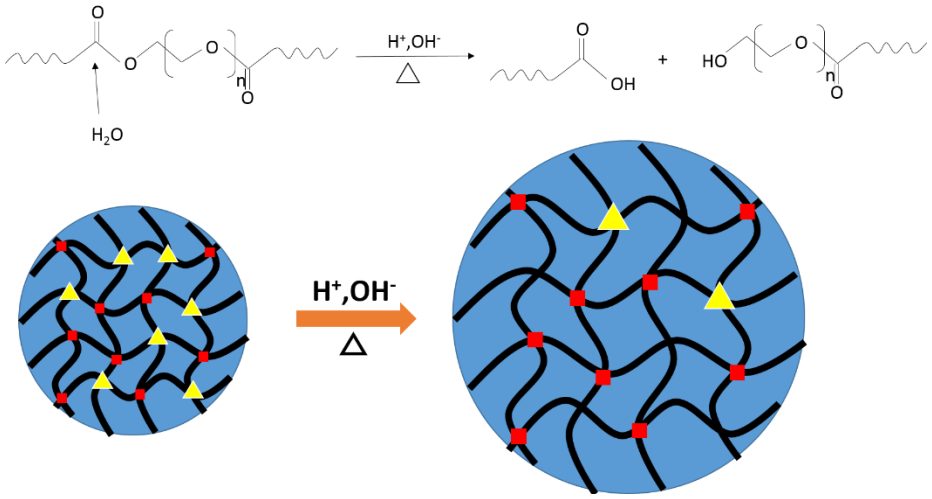

Figure 3.30. Schematic representation of the labile crosslinker degradation in water. H^+, OH^-, and heat can catalyze the degradation of polyethylene glycol diacrylate crosslinker.

Thermal stability of the CO_2 responsive nanoparticle gels was an important property for the performance on the in-depth treatment, especially under the CO_2 condition. The CO_2 responsive nanoparticle gel dispersions were placed in the high pressure vessel for the long term stability experiment in the presence of $scCO_2$ (Figure 3.31). The diameter of the CO_2 responsive nanoparticle gels at 25 °C was ~240 nm for more than 1 year while the diameters at 40 and 60 °C was almost the same with the one at 25 °C. The three dimension network of the CO_2 responsive nanoparticle gels was formed by the thermostable crosslinker, which can stand as high as 90 °C in the presence of $scCO_2$ for one year. The CO_2 responsive nanoparticle gels showed an excellent thermal stability under $scCO_2$ condition based on our experiment results.

Inspired by the swelling delayed nanoparticle gels, we prepared the core shell nanoparticle gels that formed by a hydrophilic core and a hydrophobic shell. Different with double crosslinker nanoparticle gels, we used a semi-continuous polymerization to synthesize the core shell nanoparticle gels. The crosslinked hydrophilic core was synthesized with a high monomer concentration and a low crosslinker to monomer ratio. Therefore, the synthesized core can swell tens to hundred times when contact with water. Then, a labile crosslinker was subjected to crosslink the hydrophobic monomers and form the shell structure.

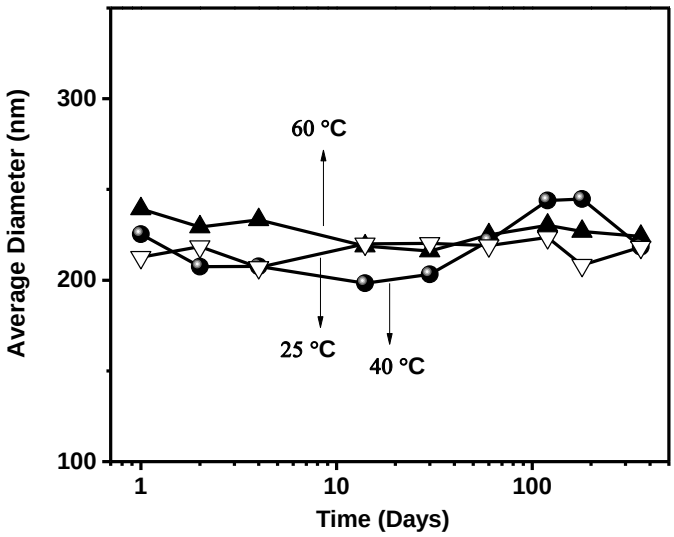

Figure 3.31. Diameter of the CO_2 responsive nanoparticle gels at different temperature in scCO_2.

The long term stability experiments was conduct as the core shell nanoparticle gels were dispersed in 1 wt.% NaCl solutions saturated with CO_2, and then, the samples were aged at 60 °C for different time before measured the size distribution as shown in Figure 3.32. The average diameter of the core shell nanoparticle gels measured immediately was ~280 nm. After aged for 7 days, the hydrophobic shell of around 17%

core shell nanoparticle gels broke under the acid and temperature stimulations. After aged for 14 days, the percentage of degraded shell did not increase. However, after 1 month, the percentage of degraded shell dramatically increased to 70% and kept increasing to 80% after 4 months. Compared with the double crosslinker nanoparticle gels, the diameter of core shell nanoparticle gels did not increase gradually. Two main peaks of core shell nanoparticle gels appeared at 300 and 5000 m, which were the diameters of core shell nanoparticle gels and the swelled cores.

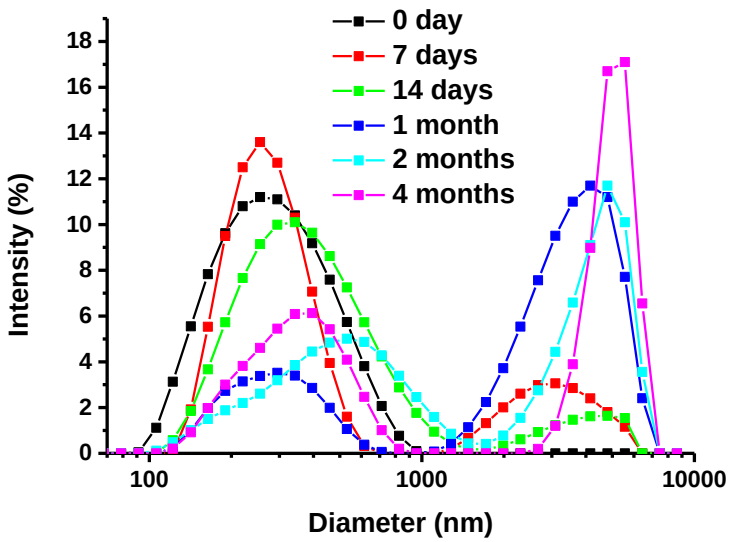

Figure 3.32. Size distribution of the core shell nanoparticle gels in NaCl solution saturated with CO_2.

3.3. SUMMARY

In our experiments, four series of nanoparticle gels were synthesized and characterized in the presence of CO_2. The double crosslinker nanoparticle gels were AMPS based nanoparticle gels contained both labile and stable crosslinkers that were able to second swell stimulated by heat and acidic solution. After injected into the

reservoirs, the double crosslinker nanoparticle gels could transport through the matrix and form efficient plugging triggered by the formation temperature and/or CO_2. For the in-depth treatment, the swelling delayed time should be controlled to let nanoparticle gels transported to the in-depth. Based on our experimental results, the double crosslinker nanoparticle gels can be controlled to start their second swelling after 30 days at 60 °C while 2 days at 80 °C. Therefore, the double crosslinker nanoparticle gels were applicable for the in-depth treatment in the reservoirs with low temperature. Another swelling delayed nanoparticle gels with core shell structures were designed to control the second swell time of the nanoparticle gels. The core shell nanoparticle gels contained two parts: a hydrophilic core that can fully swell in several minutes in water and a hydrophobic shell that prevented water penetrated to the core. The degradation rate of the hydrophobic shell was dominated by the thickness of shell. When placed at the target zone, at where the hydrophobic shell fully broke, the core shell nanoparticle gels could fully swell and form efficiently plugging. Similar with the double crosslinker nanoparticle gels, the core shell nanoparticle gels cannot be used in the reservoirs with the formation temperature higher than 80 °C.

The CO_2 responsive nanoparticle gels, DMAEMA-based nanoparticle gels that were not sensitive to the temperature and salinity, can second swell in the presence of CO_2. The CO_2 responsive nanoparticle gels reached the maximum swelling ratio in 5 min when contact with CO_2. The CO_2 responsive nanoparticle gels could be applied for the in-depth treatment in the high temperature reservoirs in the combination with CO_2 flooding.

4. CONCLUSION

In summary, four major goals were achieved in this dissertation through the study of nanogels behavior at the oil-water ineterface and in the porous medium. The application of nanogels has a profound effect on the oil-water interfacial properties and the fluid transportation in porous medium, which is a promising chemical for enhanced oil recovery.

In the first paper, three nanogels with different surface charges have been synthesized through suspension polymerization. The physicochemical properties of the synthesized nanogels were elucidated by dynamic light scattering, scanning electron microscopy, and transmission electron microscopy. In comparison with nanosilica, no precipitation was observed in the nanogel dispersions at 1 wt.% NaCl concentration. The polymeric nanogels markedly decreased the oil-water interfacial tension. Moreover, the o/w emulsion stabilized by neutral charged nanogels remained more than 90 % of its original volume at 25 °C for 30 days while emulsion treated with nanosilica fully phase separated in 5 minutes after homogenization. Furthermore, neutral-charged nanogel was able to stabilize oil-in-water emulsion to remain 82 % of its original volume at 65 °C after 48 h. The surface charge effect on the oil-water interfacial reduction and o/w emulsion stabilization properties of nanogels was systematically studied.

In the second paper, the nanogels used in chemical enhanced oil recovery has been described. Compared to dispersed nanoparticle system, the viscosity of nanogels presented an exponential relationship with concentration, which indicated percolation among nanogels. Rheological studies demonstrated the nanogels' ability to be easily injected into the matrix in reservoirs. The contact angle of sandstone showed slightly

decrease upon the hydrophilicity of adsorbed nanogels, and the sandstone had a larger contact angle after adsorbed cationic nanogels. The kinetic of nanogel adsorption was controlled by the surface charge of sandstone and nanogel as demonstrated by static and dynamic adsorption measurements. The nanogels showed good plugging efficiency in 1 wt.% NaCl solution. In addition, it has been demonstrated that the nanogels had the ability to emulsify residual oil and enhance displacing efficiency. The second brine injection, which simulated post water flooding, demonstrated that nanogels could efficiently divert brine flow to enhance sweep efficiency.

In the third paper, the oil-water interfacial tension reduction and o/w emulsion stabilization ability of nanogels were investigated at various salinities. Decane and crude oil was subjected in this study to illustrate the influence of oil type on the performance of nanogels. The swelling ratio and zeta potential of ionic nanogels were significantly influenced by the NaCl concentration while the swelling ratio and zeta potential of neutral charged nanogels were independent to the NaCl concentration. The salt ions can help to reduce the oil-water interfacial tension and accelerate the creaming process of emulsions stabilized by nanogels. In addition, the interfacial tension kinetic and emulsion stability were affected by the oil types. The crude oil/water emulsion was more stable than the decane/water emulsion.

In the fourth paper, the alkaline-demulsified Pickering emulsions stabilized by the stimuli-responsive PAM nanogels has been described. Stimulation PAM nanogels with NaOH hydrolyzed the acrylamide into carboxylate moieties containing in the polymeric networks, which would significantly increase the hydrodynamic diameter and reduce the zeta potential of PAM nanogels. The Pickering emulsions showed excellent stability in

brines and acidic solutions that no separated oil phase had been observed 24 h after emulsion preparation. Based on the optical microscopy results, the average diameter of oil drops was no longer decreased above the critical nanogel concentration of 1000 mg/L. The stable Pickering emulsions could be prepared over a broad range of sonication period from 15 to 240s. Compared to alkanes/water Pickering emulsions, the stability of aromatic hydrocarbons/water Pickering emulsions was enhanced by the string-like nanogel structures. Rheological studies demonstrated the flow ability of crude oil was significantly enhanced by forming crude oil/water Pickering emulsions.

The nanogels are promising candidates that help reduce the oil-water interfacial tension and recover residual oil. The produced oil/water Pickering emulsion can be effectively demulsified using alkaline at surface condition that suggests the applications in petroleum engineering.

5. SUGGESTED FUTURE WORK

In our experiments, we found that some of the residual oil was produced out from the sandstone core in o/w emulsion state during the nanogel flooding. This observation indicated that nanogels could emulsify residual oil during their transportation in the sandstone core. As this phenomenon hasn't been reported by any researchers before, it is important to investigate this shear-induced emulsification in porous medium. Capillary tube model and microfluidic model could be applied to investigated the shape change of residual oil during the emulsify procedure.

In addition, further studies on the nanogel distribution in the porous medium are suggested. In our experiment, we have found that the ability of nanogels in pressure increase and oil recovery was dramatically influenced by the nanogel distribution in the sandstone core. The nanogels displayed the disproportionate permeability reduction property that it reduced the relative water permeability while not affected the relative oil permeability. CT scanning was suggested to elucidate the distribution of nanogel, oil, and water in the porous medium.

BIBLIOGRAPHY

[1] X. Kong, M. Ohadi, Applications of micro and nano technologies in the oil and gas industry-overview of the recent progress, Abu Dhabi international petroleum exhibition and conference, Society of Petroleum Engineers, 2010.

[2] Z. Hua, M. Lin, Z. Dong, M. Li, G. Zhang, J. Yang, Study of deep profile control and oil displacement technologies with nanoscale polymer microspheres, Journal of colloid and interface science 424 (2014) 67-74.

[3] A. Mehranfar, M.H. Ghazanfari, Investigation of the microscopic displacement mechanisms and macroscopic behavior of alkaline flooding at different wettability conditions in shaly glass micromodels, Journal of Petroleum Science and Engineering 122 (2014) 595-615.

[4] A.Z. Pich, H.J.P. Adler, Composite aqueous microgels: an overview of recent advances in synthesis, characterization and application, Polymer international 56 (2007) 291-307.

[5] J.K. Oh, R. Drumright, D.J. Siegwart, K. Matyjaszewski, The development of microgels/nanogels for drug delivery applications, Progress in Polymer Science 33 (2008) 448-477.

[6] J.B. Thorne, G.J. Vine, M.J. Snowden, Microgel applications and commercial considerations, Colloid and Polymer Science 289 (2011) 625.

[7] M. Abdulbaki, C. Huh, K. Sepehrnoori, M. Delshad, A. Varavei, A critical review on use of polymer microgels for conformance control purposes, Journal of Petroleum Science and Engineering 122 (2014) 741-753.

[8] B.R. Saunders, B. Vincent, Microgel particles as model colloids: theory, properties and applications, Advances in colloid and interface science 80 (1999) 1-25.

[9] O.J. Cayre, N. Chagneux, S. Biggs, Stimulus responsive core-shell nanoparticles: synthesis and applications of polymer based aqueous systems, Soft Matter 7 (2011) 2211-2234.

[10] E.M. Ahmed, Hydrogel: Preparation, characterization, and applications: A review, Journal of advanced research 6 (2015) 105-121.

[11] L. Yang, J.S. Chu, J.A. Fix, Colon-specific drug delivery: new approaches and in vitro/in vivo evaluation, International journal of pharmaceutics 235 (2002) 1-15.

[12] Q. Chen, L. Zhu, C. Zhao, Q. Wang, J. Zheng, A robust, one‐pot synthesis of highly mechanical and recoverable double network hydrogels using thermoreversible sol‐gel polysaccharide, Advanced materials 25 (2013) 4171-4176.

[13] J. Ma, B. Fan, B. Liang, J. Xu, Synthesis and characterization of Poly (N-isopropylacrylamide)/Poly (acrylic acid) semi-IPN nanocomposite microgels, Journal of colloid and interface science 341 (2010) 88-93.

[14] S. Jin, M. Liu, F. Zhang, S. Chen, A. Niu, Synthesis and characterization of pH-sensitivity semi-IPN hydrogel based on hydrogen bond between poly (N-vinylpyrrolidone) and poly (acrylic acid), Polymer 47 (2006) 1526-1532.

[15] L. Chen, J. Gong, Y. Osada, Novel thermosensitive IPN hydrogel having a phase transition without volume change, Macromolecular rapid communications 23 (2002) 171-174.

[16] J.E. Wong, A.K. Gaharwar, D. Müller-Schulte, D. Bahadur, W. Richtering, Dual-stimuli responsive PNiPAM microgel achieved via layer-by-layer assembly: Magnetic and thermoresponsive, Journal of colloid and interface science 324 (2008) 47-54.

[17] M. Bradley, B. Vincent, G. Burnett, Uptake and Release of Anionic Surfactant into and from Cationic Core− Shell Microgel Particles, Langmuir 23 (2007) 9237-9241.

[18] R. Saito, H. Kotsubo, K. Ishizu, Core-shell type polymer microspheres prepared from poly (styrene-b-methacrylic acid)—1. Synthesis of microgel, European polymer journal 27 (1991) 1153-1159.

[19] Y. Chen, J.E. Gautrot, X. Zhu, Synthesis and Characterization of Core− Shell Microspheres with Double Thermosensitivity, Langmuir 23 (2007) 1047-1051.

[20] C. Dagallier, H. Dietsch, P. Schurtenberger, F. Scheffold, Thermoresponsive hybrid microgel particles with intrinsic optical and magnetic anisotropy, Soft Matter 6 (2010) 2174-2177.

[21] M. Lattuada, T.A. Hatton, Synthesis, properties and applications of Janus nanoparticles, Nano Today 6 (2011) 286-308.

[22] T. Isojima, M. Lattuada, J.B. Vander Sande, T.A. Hatton, Reversible clustering of pH-and temperature-responsive Janus magnetic nanoparticles, Acs Nano 2 (2008) 1799-1806.

[23] M. Lattuada, T.A. Hatton, Preparation and controlled self-assembly of Janus magnetic nanoparticles, Journal of the American Chemical Society 129 (2007) 12878-12889.

[24] N. Glaser, D.J. Adams, A. Böker, G. Krausch, Janus particles at liquid− liquid interfaces, Langmuir 22 (2006) 5227-5229.

[25] N.A. Al-manasir, A.-L. Kjøniksen, K. Zhu, B. Nyström, Effect of Surfactant Addition, Temperature, and Solvent conditions on Functional Microgels for Enhanced Oil recovery Applications, Kuwait International Petroleum Conference and Exhibition, Society of Petroleum Engineers, 2009.

[26] G. Fethi, K. Kaddour, M. Tesconi, B. Alberto, C. Carlo, G.G. Angelo, El Borma-Bright Water-tertiary method of Enhanced Oil Recovery for a mature field, SPE Production and Operations Conference and Exhibition, Society of Petroleum Engineers, 2010.

[27] X. Zhang, X. Wang, L. Li, S. Zhang, R. Wu, Preparation and swelling behaviors of a high temperature resistant superabsorbent using tetraallylammonium chloride as crosslinking agent, Reactive and Functional Polymers 87 (2015) 15-21.

[28] C. Huh, S.K. Choi, M.M. Sharma, A rheological model for pH-sensitive ionic polymer solutions for optimal mobility control applications, SPE annual technical conference and exhibition, Society of Petroleum Engineers, 2005.

[29] V.K. Thakur, M.R. Kessler, Self-healing polymer nanocomposite materials: A review, Polymer 69 (2015) 369-383.

[30] K. Haraguchi, K. Uyama, H. Tanimoto, Self‐healing in Nanocomposite Hydrogels, Macromolecular rapid communications 32 (2011) 1253-1258.

[31] S. Huang, L. Yang, M. Liu, S.L. Phua, W.A. Yee, W. Liu, R. Zhou, X. Lu, Complexes of polydopamine-modified clay and ferric ions as the framework for pollutant-absorbing supramolecular hydrogels, Langmuir 29 (2013) 1238-1244.

[32] W. Li, M. Liu, H. Chen, J. Xu, Y. Gao, H. Li, Phenylboronate‐diol crosslinked polymer/SWCNT hybrid gels with reversible sol–gel transition, Polymers for Advanced Technologies 25 (2014) 233-239.

[33] J. Liu, G. Song, C. He, H. Wang, Self‐healing in tough graphene oxide composite hydrogels, Macromolecular rapid communications 34 (2013) 1002-1007.

[34] D.Y. Wu, S. Meure, D. Solomon, Self-healing polymeric materials: a review of recent developments, Progress in Polymer Science 33 (2008) 479-522.

[35] J. Pu, B. Bai, A. Alhuraishawy, S. Thomas, Y. Chen, X. Sun, A Novel Re-Assembly Preformed Polymer Particle Gel RPPG and Re-Assembling Characteristics under Extreme Heterogeneous Reservoir Conditions, SPE Annual Technical Conference and Exhibition, Society of Petroleum Engineers, 2018.

[36] H. Yang, L. Hu, C. Chen, Y. Gao, X. Tang, X. Yin, W. Kang, Synthesis and plugging behavior of fluorescent polymer microspheres as a kind of conformance control agent in reservoirs, RSC Advances 8 (2018) 10478-10488.

[37] Z. Li, T. Ming, J. Wang, T. Ngai, High internal phase emulsions stabilized solely by microgel particles, Angewandte Chemie 121 (2009) 8642-8645.

[38] S. Uchiyama, K. Kimura, C. Gota, K. Okabe, K. Kawamoto, N. Inada, T. Yoshihara, S. Tobita, Environment‐Sensitive Fluorophores with Benzothiadiazole and Benzoselenadiazole Structures as Candidate Components of a Fluorescent Polymeric Thermometer, Chemistry–A European Journal 18 (2012) 9552-9563.

[39] C. Gota, K. Okabe, T. Funatsu, Y. Harada, S. Uchiyama, Hydrophilic fluorescent nanogel thermometer for intracellular thermometry, Journal of the American Chemical Society 131 (2009) 2766-2767.

[40] M. Destribats, V. Lapeyre, E. Sellier, F. Leal-Calderon, V. Schmitt, V. Ravaine, Water-in-oil emulsions stabilized by water-dispersible poly (N-isopropylacrylamide) microgels: understanding anti-Finkle behavior, Langmuir 27 (2011) 14096-14107.

[41] X.C. i Solvas, Droplet microfluidics: recent developments and future applications, Chemical Communications 47 (2011) 1936-1942.

[42] H. Zhang, E. Tumarkin, R.M.A. Sullan, G.C. Walker, E. Kumacheva, Exploring microfluidic routes to microgels of biological polymers, Macromolecular rapid communications 28 (2007) 527-538.

[43] R.K. Shah, J.W. Kim, D.A. Weitz, Janus supraparticles by induced phase separation of nanoparticles in droplets, Advanced Materials 21 (2009) 1949-1953.

[44] T. Nisisako, T. Torii, T. Takahashi, Y. Takizawa, Synthesis of monodisperse bicolored janus particles with electrical anisotropy using a microfluidic Co‐Flow system, Advanced Materials 18 (2006) 1152-1156.

[45] Z. Nie, W. Li, M. Seo, S. Xu, E. Kumacheva, Janus and ternary particles generated by microfluidic synthesis: design, synthesis, and self-assembly, Journal of the American Chemical Society 128 (2006) 9408-9412.

[46] J. Thiele, S. Seiffert, Double emulsions with controlled morphology by microgel scaffolding, Lab on a Chip 11 (2011) 3188-3192.

[47] H.M. Shewan, J.R. Stokes, Review of techniques to manufacture micro-hydrogel particles for the food industry and their applications, Journal of Food Engineering 119 (2013) 781-792.

[48] J. Yeh, Y. Ling, J.M. Karp, J. Gantz, A. Chandawarkar, G. Eng, J. Blumling Iii, R. Langer, A. Khademhosseini, Micromolding of shape-controlled, harvestable cell-laden hydrogels, Biomaterials 27 (2006) 5391-5398.

[49] J.P. Rolland, B.W. Maynor, L.E. Euliss, A.E. Exner, G.M. Denison, J.M. DeSimone, Direct fabrication and harvesting of monodisperse, shape-specific nanobiomaterials, Journal of the American Chemical Society 127 (2005) 10096-10100.

[50] K. McAllister, P. Sazani, M. Adam, M.J. Cho, M. Rubinstein, R.J. Samulski, J.M. DeSimone, Polymeric nanogels produced via inverse microemulsion polymerization as potential gene and antisense delivery agents, Journal of the American Chemical Society 124 (2002) 15198-15207.

[51] L. Etchenausia, E. Deniau, A. Brûlet, J. Forcada, M. Save, Cationic Thermoresponsive Poly (N-vinylcaprolactam) Microgels Synthesized by Emulsion Polymerization Using a Reactive Cationic Macro-RAFT Agent, Macromolecules 51 (2018) 2551-2563.

[52] S. Copelli, M. Barozzi, N. Petrucci, V.C. Moreno, Modeling and Process Optimization of a Full-Scale Emulsion Polymerization Reactor, Chemical Engineering Journal (2018).

[53] R. Arshady, A. Ledwith, Suspension polymerisation and its application to the preparation of polymer supports, Reactive Polymers, Ion Exchangers, Sorbents 1 (1983) 159-174.

[54] D. Horák, M. Kryštůfek, J. Spěváček, Effect of reaction parameters on the dispersion polymerization of 1 - vinyl - 2 - pyrrolidone, Journal of Polymer Science Part A: Polymer Chemistry 38 (2000) 653-663.

[55] J. DeSimone, E. Maury, Y.Z. Menceloglu, J. McClain, T. Romack, J. Combes, Dispersion polymerizations in supercritical carbon dioxide, Science 265 (1994) 356-359.

[56] A.Y. Malkin, A.I. Isayev, Rheology, Concepts, methods and applications. ChemTec Publisching, Toronto Google Scholar (2006).

[57] X.-S. Wu, Y. Luo, G.-W. Chu, Y.-C. Xu, L. Sang, B.-C. Sun, J.-F. Chen, Visual Study of Liquid Flow in a Spinning Disk Reactor with a Hydrophobic Surface, Industrial & Engineering Chemistry Research (2018).

[58] Y. Senuma, J.G. Hilborn, High speed imaging of drop formation from low viscosity liquids and polymer melts in spinning disk atomization, Polymer Engineering & Science 42 (2002) 969-982.

[59] Y. Senuma, C. Lowe, Y. Zweifel, J. Hilborn, I. Marison, Alginate hydrogel microspheres and microcapsules prepared by spinning disk atomization, Biotechnology and bioengineering 67 (2000) 616-622.

[60] N. Sheridon, E. Richley, J. Mikkelsen, D. Tsuda, J. Crowley, K. Oraha, M. Howard, M. Rodkin, R. Swidler, R. Sprague, The gyricon rotating ball display, Journal of the society for information display 7 (1999) 141-144.

[61] S. Gouin, Microencapsulation: industrial appraisal of existing technologies and trends, Trends in food science & technology 15 (2004) 330-347.

[62] Y. Senuma, J.G. Hilborn, Key parameters for monodispersed polymer microspheres with spinning disk atomization, Material Research Innovations 3 (1999) 42-49.

[63] H. Peng, N. Wang, D. Wang, X. Ling, Experimental study on the critical characteristics of liquid atomization by a spinning disk, Industrial & Engineering Chemistry Research 55 (2016) 6175-6185.

[64] M. Mishra, Handbook of encapsulation and controlled release, CRC Press2015.

[65] W. Zhao, R.W.N. Nugroho, K. Odelius, U. Edlund, C. Zhao, A.-C. Albertsson, In situ cross-linking of stimuli-responsive hemicellulose microgels during spray drying, ACS applied materials & interfaces 7 (2015) 4202-4215.

[66] B.B. Lee, B.R. Bhandari, T. Howes, Air extrusion system for ionotropic alginate microgel particle formation: a review, Chemical Engineering & Technology 39 (2016) 2355-2369.

[67] X. Li, N. Anton, C. Arpagaus, F. Belleteix, T.F. Vandamme, Nanoparticles by spray drying using innovative new technology: The Büchi Nano Spray Dryer B-90, Journal of Controlled Release 147 (2010) 304-310.

[68] J. Thiele, M. Windbergs, A.R. Abate, M. Trebbin, H.C. Shum, S. Förster, D.A. Weitz, Early development drug formulation on a chip: Fabrication of nanoparticles using a microfluidic spray dryer, Lab on a Chip 11 (2011) 2362-2368.

[69] Z. Hua, M. Lin, J. Guo, F. Xu, Z. Li, M. Li, Study on plugging performance of cross-linked polymer microspheres with reservoir pores, Journal of petroleum science and engineering 105 (2013) 70-75.

[70] Z. Chen, T.P. Schuman, J. Geng, B. Bai, Water‐free synthesis of temperature‐sensitive polyacrylamide microgels and pore modeled oil recovery performance, Journal of Applied Polymer Science 134 (2017).

[71] M. Lin, G. Zhang, Z. Hua, Q. Zhao, F. Sun, Conformation and plugging properties of crosslinked polymer microspheres for profile control, Colloids and Surfaces A: Physicochemical and Engineering Aspects 477 (2015) 49-54.

[72] J. Pu, J. Geng, P. Han, B. Bai, Preparation and salt-insensitive behavior study of swellable, Cr3+-embedded microgels for water management, Journal of Molecular Liquids (2018).

[73] Z. Shao, A.S. Negi, C.O. Osuji, Role of interparticle attraction in the yielding response of microgel suspensions, Soft Matter 9 (2013) 5492-5500.

[74] D.Ö. Kiminta, P. Luckham, S. Lenon, The rheology of deformable and thermoresponsive microgel particles, Polymer 36 (1995) 4827-4831.

[75] S.P. Meeker, R.T. Bonnecaze, M. Cloitre, Slip and flow in soft particle pastes, Physical Review Letters 92 (2004) 198302.

[76] J.R. Seth, M. Cloitre, R.T. Bonnecaze, Influence of short-range forces on wall-slip in microgel pastes, Journal of Rheology 52 (2008) 1241-1268.

[77] S. Biggs, G. Spinks, Atomic force microscopy investigation of the adhesion between a single polymer sphere and a flat surface, Journal of adhesion science and technology 12 (1998) 461-478.

[78] P. Paik, K. Kar, D. Deva, A. Sharma, Measurement of mechanical properties of polymer nanospheres by atomic force microscopy: effects of particle size, Micro & Nano Letters 2 (2007) 72-77.

[79] S. Schmidt, M. Zeiser, T. Hellweg, C. Duschl, A. Fery, H. Möhwald, Adhesion and mechanical properties of PNIPAM microgel films and their potential use as switchable cell culture substrates, Advanced Functional Materials 20 (2010) 3235-3243.

[80] S.M. Hashmi, E.R. Dufresne, Mechanical properties of individual microgel particles through the deswelling transition, Soft Matter 5 (2009) 3682-3688.

[81] O. Tagit, N. Tomczak, G.J. Vancso, Probing the Morphology and Nanoscale Mechanics of Single Poly (N‐isopropylacrylamide) Microgels Across the Lower‐Critical‐Solution Temperature by Atomic Force Microscopy, Small 4 (2008) 119-126.

[82] S. Tan, R.L. Sherman, W.T. Ford, Nanoscale compression of polymer microspheres by atomic force microscopy, Langmuir 20 (2004) 7015-7020.

[83] G. Dupuis, R.S. Al-Maamari, A.A. Al-Hashmi, H.H. Al-Sharji, A. Zaitoun, Mechanical and thermal stability of polyacrylamide-based microgel products for EOR, SPE International Symposium on Oilfield Chemistry, Society of Petroleum Engineers, 2013.

[84] Y. Qiu, M. Wei, J. Geng, F. Wu, Successful Field Application of Microgel Treatment in High Temperature High Salinity Reservoir in China, SPE Improved Oil Recovery Conference, Society of Petroleum Engineers, 2016.

[85] G. Chauveteau, R. Tabary, C. Le Bon, M. Renard, Y. Feng, A. Omari, In-depth permeability control by adsorption of soft size-controlled microgels, SPE European Formation Damage Conference, Society of Petroleum Engineers, 2003.

[86] G. Chauveteau, A. Omari, R. Tabary, M. Renard, J. Veerapen, J. Rose, New size-controlled microgels for oil production, SPE international symposium on oilfield chemistry, Society of Petroleum Engineers, 2001.

[87] C. Cozic, D. Rousseau, R. Tabary, Novel insights into microgel systems for water control, SPE Production & Operations 24 (2009) 590-601.

[88] D. Rousseau, G. Chauveteau, M. Renard, R. Tabary, A. Zaitoun, P. Mallo, Rheology and transport in porous media of new water shutoff/conformance control microgels. Paper SPE 93254 presented at the SPE international symposium on oilfield chemistry, Houston; 2–4 February 2005.

[89] G. Chauveteau, R. Tabary, N. Blin, M. Renard, D. Rousseau, R. Faber, Disproportionate permeability reduction by soft preformed microgels, SPE/DOE Symposium on Improved Oil Recovery, Society of Petroleum Engineers, 2004.

[90] C. Yao, X. Xu, D. Wang, G. Lei, S. Xue, J. Hou, L.M. Cathles, T.S. Steenhuis, Research and application of micron-size polyacrylamide elastic microspheres as a smart sweep improvement and profile modification agent, SPE Improved Oil Recovery Conference, Society of Petroleum Engineers, 2016.

[91] C. Dai, Y. Liu, C. Zou, Q. You, S. Yang, M. Zhao, G. Zhao, Y. Wu, Y. Sun, Investigation on matching relationship between dispersed particle gel (DPG) and reservoir pore-throats for in-depth profile control, Fuel 207 (2017) 109-120.

[92] H. Yang, W. Kang, H. Wu, Y. Yu, Z. Zhu, P. Wang, X. Zhang, B. Sarsenbekuly, Stability, rheological property and oil-displacement mechanism of a dispersed low-elastic microsphere system for enhanced oil recovery, RSC Advances 7 (2017) 8118-8130.

[93] M.O. Elsharafi, B. Bai, Effect of strong preformed particle gel on unswept oil zones/areas during conformance control treatments, EAGE Annual Conference & Exhibition incorporating SPE Europec, Society of Petroleum Engineers, 2013.

[94] A.K. Alhuraishawy, X. Sun, B. Bai, M. Wei, A. Imqam, A. Almansour, Improve Plugging Efficiency in Fractured Sandstone Reservoirs by Mixing Different Preformed Particles Gel Size, SPE Kingdom of Saudi Arabia Annual Technical Symposium and Exhibition, Society of Petroleum Engineers, 2017.

[95] A.M. Almohsin, B. Bai, A.H. Imqam, M. Wei, W. Kang, M. Delshad, K. Sepehrnoori, Transport of nanogel through porous media and its resistance to water flow, SPE Improved Oil Recovery Symposium, Society of Petroleum Engineers, 2014.

[96] J. Geng, H. Ding, P. Han, Y. Wu, B. Bai, Transportation and Potential Enhanced Oil Recovery Mechanisms of Nanogels in Sandstone, Energy & Fuels 32 (2018) 8358-8365.

[97] J. Geng, J. Pu, L. Wang, B. Bai, Surface charge effect of nanogel on emulsification of oil in water for fossil energy recovery, Fuel 223 (2018) 140-148.

[98] J. Geng, P. Han, B. Bai, Experimental Study on Charged Nanogels for Interfacial Tension Reduction and Emulsion Stabilization at Various Salinities and Oil Types, SPE Asia Pacific Oil and Gas Conference and Exhibition, Society of Petroleum Engineers, 2018.

[99] N.S. Lenchenkov, M. Slob, E. van Dalen, G. Glasbergen, C. van Kruijsdijk, Oil Recovery from Outcrop Cores with Polymeric Nano-Spheres, SPE Improved Oil Recovery Conference, Society of Petroleum Engineers, 2016.

[100] G. Lei, L. Li, H.A. Nasr-El-Din, New gel aggregates to improve sweep efficiency during waterflooding, SPE Reservoir Evaluation & Engineering 14 (2011) 120-128.

[101] A. Zaitoun, R. Tabary, D. Rousseau, T.R. Pichery, S. Nouyoux, P. Mallo, O. Braun, Using microgels to shut off water in a gas storage well, International Symposium on Oilfield Chemistry, Society of Petroleum Engineers, 2007.

[102] Y. Qiu, M. Wei, B. Bai, C. Mao, Data analysis and application guidelines for the microgel field applications, Fuel 210 (2017) 557-568.

[103] J.M. Griffin, Novel microgel suspensions: rheological, mechanical and adhesion properties and their filtration behaviour, (2007).

VITA

Jiaming Geng was born in Shandong, China. He received his bachelor of Petroleum Engineering degree in 2013 from China University of Petroleum (East China). He joined to continue his study and received his Master of Science in Petroleum Engineering from the Missouri University of Science and Technology in December 2015. Then he began his Ph.D. at Missouri University of Science and Technology in Dr. Baojun Bai's research group and received his Ph.D. degree in Petroleum Engineering in December 2018.